

Copyright
by
Tony Zifeng Tang
2024

The Dissertation Committee for Tony Zifeng Tang

Certifies this is the approved version of the following dissertation:

**Novel Biomarkers within Extracellular Vesicles for the
Identification of Traumatic Brain Injury**

Committee:

Dr. Bartosz Szczesny, PhD
Supervisor, Chair

Dr. Massoud Motamedi, PhD

Dr. Maria Micci, PhD

Dr. Yingxin Zhao, PhD

Dr. Stefan Bossmann, PhD

**Novel Biomarkers within Extracellular Vesicles for the
Identification of Traumatic Brain Injury**

by

Tony Zifeng Tang, B.S., M.S.

Dissertation

Presented to the Faculty of the Graduate School of Biomedical Sciences of

The University of Texas Medical Branch

in Partial Fulfillment

of the Requirements

for the Degree of

Doctor of Philosophy

The University of Texas Medical Branch

January, 2024

Dedication

I dedicate this entire PhD training and experience to my parents, Peter Tang and Tina Du; my brother Ethan Tang; and last but not least, my fiancée and future soon-to-be wife Jana DeJesus. Thank you, Mom and Dad, for your unconditional love through the best and worst of times; it is always reassuring to have your support no matter how difficult of a period of life I am going through. Thank you, Ethan, for help and empathy when I reach out to talk; you have always made time for me even when life gets busy for you. Finally, thank you to the love of my life Jana DeJesus who has been there for me daily to pick me up when I am down and cheer me on when I win. This degree symbolizes a body of work that has tested my limits in every aspect of life; it is difficult to put into words the amount of effort and time this journey has taken to shape me into not only a more well-rounded scientist, but an overall better person. I am proud to say I have accomplished this major milestone in my career, and I will never forget the memories I made throughout the process.

Acknowledgements

I want to thank my mentor Dr. Bartosz Szczesny for his guidance and mentorship. Thank you for your time, patience, and efforts throughout my time in your lab. I am aware that sometimes I can be a challenge to manage with my strong opinions and ways of doing things. Thank you for the opportunity to work with you when I decided to switch labs midway through my PhD training. I am so incredibly thankful I landed in your lab with this interesting project. Additionally, I would like to acknowledge several more individuals that have supported me throughout my time here:

- Lab members and fellow graduate students Ryan McCauley and Christina Payne: thank you both for keeping me company day in and day out. I will always remember our entertaining conversations about life; having good friends who can relate and share in the suffering makes things more tolerable knowing we are not alone in this journey. I wish the both of you the best of luck in your training and futures.
- Dr. Massoud Motamedi: thank you for your mentorship and guidance as an extra voice in my training. I've always valued your input on my projects and beyond. Additional thanks for the many letters of support you have written for me; I am sure they played a role in the awards and scholarship decisions I have received over the years.
- Collaborators Dr. Bala Natarajan, Dr. Yuanyi Zhang, Deepesh Agarwal and Aabila Tharzeen: thank you for your hard work in this project. This

manuscript would not have been possible without your expertise and contributions analyzing the data. Thank you for the constant updates and meetings we were progressing in the write up of the paper.

- Committee members Drs. Maria Micci, Yingxin Zhao, and Stefan Bossmann: thank you for your time and input on my training. I am well aware of the additional responsibilities and time commitment of serving on a dissertation committee on top of each of your day-to-day responsibilities.
- Drs. Tracy Toliver-Kinsky, Katalin Modis, and Elizabeth Hileman: thank you both for your kindness and always taking the time to talk to me. I am grateful for your support and constant words of encouragement, especially towards the end of my training as I started looking for career placement opportunities.
- Dr. Igor Patrikeev, Jamal Saada, and Gabor Toro: thank you for working with me and assisting in my experiments in your own individual ways. Special mention to Dr. Patrikeev for his efforts in helping me with the CT imaging.
- Drs. Owen Hamill, Ping Wu, and Debby Moncrief in the Neuroscience Graduate Program for their continued support and guidance throughout my training process. Special mention to Debby for her hard work in coordinating events, paperwork, classwork, and overall general support for the students.
- Dr. Fabio Bucchieri in the Department of Biomedicine, Neuroscience and Advanced Diagnostics at the University of Palermo in Italy for his support in the UNIPA collaboration program.

- My fellow graduate students in the Neuroscience Graduate Program for all the positive interactions throughout the years. Best of luck in all your respective career paths and journeys!

Finally, thank you to everyone who has given me words of encouragement. Your support in tough times have been helpful in overcoming the challenges of this PhD training.

Novel Biomarkers within Extracellular Vesicles for the Identification of Traumatic Brain Injury

Tony Zifeng Tang, PhD

The University of Texas Medical Branch, **2024**

Supervisor: Dr. Bartosz Szczesny, PhD

Traumatic brain injury (TBI) is defined by the National Institute of Neurological Disorders and Stroke (NINDS) as "...external physical forces cause damage to the brain, whether from impact, penetrating objects, blast waves or rapid movement of the brain within the skull". According to the most recent CDC data, there were roughly 214,000 TBI-related hospitalizations and 70,000 TBI-related deaths in 2021. The current diagnosis of TBI includes a neurological exam such as Glasgow Coma Scale (GCS) and imaging tests (CT, MRI). However, these modalities have several limitations, including inter-rater reliability, inconsistencies in diagnosis, and lack of predictive prognosis, all of which highlights the complex pathophysiology of this disease process. Thus, there is an urgent need for identification of novel methods for an early detection and quantitative monitoring of TBI. In this project, we investigated extracellular vesicles (EVs) in blood plasma as a potential source

of novel TBI biomarkers. Key characteristics of EVs, including the protection of the packaged cargo that reflects processes occurring in the cell of origin and their ability to cross the blood-brain-barrier (BBB), make them a highly valuable source of biomarkers. We subjected 10–12-week-old C57BL/6J male mice to moderate/severe TBI using the pre-clinical, closed head, weight drop model followed by EVs isolation from blood plasma at multiple time points post injury. We detected time-dependent qualitative and quantitative changes in the biophysical properties of EVs. Furthermore, we discovered TBI induced changes in specific EVs subpopulations of microglia/macrophage CD11b⁺ and astrocyte ACSA-2⁺ vesicles post-injury. These temporal dynamics of EVs are also reflected in both mitochondrial DNA content, nuclear DNA content, and brain-derived cellular markers NFL, GFAP, and Iba1. Additionally, we combined a global mass spectrometry proteomics approach with biostatistical analysis and computational Graph Neural Network (GNN)-based modeling to discover a panel of potential novel biomarkers for the detection and severity of TBI. Lastly, we confirmed the dynamic release of mtDNA and its fragments in EVs from neurons using an in-vitro TBI model and EVs derived from glucose oxidase stressed retinal pigment epithelial cells, respectively. Together, our findings indicate that a combination of DNA quantity, SAA, and CFD proteins in EVs may be used as diagnostic tools for the rapid, accurate assessment of TBI detection and its sequelae.

TABLE OF CONTENTS

List of Tables	xiii
List of Figures	xiv
List of Abbreviations	xvii
Chapter 1 Traumatic Brain Injury	21
1.1 Types and severity of TBI	23
1.2 Preclinical animal models of TBI	29
1.3 Pathophysiology of TBI	41
1.4 Current diagnosis of TBI	54
Chapter 2 Extracellular Vesicles	61
2.1 Biogenesis of EVs	63
2.2 Contents of EVs	66
2.3 EVs isolation techniques	74
2.4 EVs characterization techniques	81
2.5 Therapeutic and diagnostic applications of EVs	86
2.6 EVs in TBI pathology	91
2.7 EVs biomarkers in TBI	95
Chapter 3 Gap in Knowledge and Project Design	102
Chapter 4 Methods and Materials	106
4.1 Preclinical weight drop model of TBI	106
4.2 Neurological Severity Score	107
4.3 CT imaging and quantification of total brain parenchymal volume	108
4.4 Blood plasma harvest	108

4.5 Isolation of EVs from mouse plasma	109
4.6 Characterization of biophysical properties of EVs with NTA	110
4.7 Transmission electron microscopy imaging of EVs	110
4.8 Analysis of DNA content within EVs	111
4.9 Targeted immunoblotting analysis of EVs	112
4.10 Global mass spectrometry of isolated EVs	113
4.11 Biostatistical analysis of proteomics	115
4.12 Computational analysis of proteomics	116
4.13 Culturing and propagation of rat hippocampal neural stem cells	117
4.14 In-vitro rapid stretch injury model	117
4.15 Culturing and propagation of human retinal pigment epithelial cells	118
4.16 Glucose oxidase (GOx) induced oxidative stress on cells	118
4.17 Analysis of mtDNA in GOx-induced EVs released by ARPE-19 cells	118
Chapter 5 Results	121
5.1 Characterization of weight drop model reveals moderate to severe TBI	121
5.2 TBI induced changes in biophysical Properties of Circulating EVs and EVs subpopulations	125

5.3 Elevated DNA content within EVs in the acute phase post injury	130
5.4 Targeted immunoblotting for temporal alterations of neuronal, microglial, and astrocytic markers in circulating EVs post injury	133
5.5 EVs Proteomics and Biostatistical Analysis identify several novel promising TBI biomarkers	135
5.6 Computational Evaluation of EVs Proteomics for identification of TBI-specific biomarkers	140
5.7 Cultured neurons subjected to <i>in-vitro</i> model of TBI release EVs containing mtDNA	144
5.8 Analysis of DNA content in EVs released from glucose oxidase treatment of ARPE-19 cells	146
Chapter 6 Summary, Discussion, Limitations, and Future Directions	149
6.1 Summary	149
6.2 Discussion	149
6.3 Limitations	158
6.4 Future directions	160
Bibliography	166
Vita	194

List of Tables

Table 1.1 Summary of preclinical TBI models	40
Table 1.2 GCS-E Amnesia scale	55
Table 2.1 Summary of EVs isolation techniques	81
Table 5.1 Summary of biophysical properties of EVs as measured by NTA	128
Table 5.2 Proteins significantly changed in EVs after TBI	139
Table 5.3 List of ranked potential biomarkers broken down per time point	142

List of Figures

Figure 1.1: Diffuse axonal injury (DAI) from blunt force trauma	24
Figure 1.2: Blast TBI	27
Figure 1.3 Different types of penetrating TBI	28
Figure 1.4 Weight drop injury device	31
Figure 1.5 Schematic of pneumatic controlled CCI system	34
Figure 1.6 Schematic of shock tube blast TBI model	36
Figure 1.7 Fluid percussion injury model	37
Figure 1.8 Secondary mechanisms of injury across different phases	42
Figure 1.9 The effects of chronic inflammation in TBI	44
Figure 1.10 Astrogliosis in TBI	45
Figure 1.11 Serotonergic brainstem projections into all areas of the brain	47
Figure 1.12 Alterations of dopamine after TBI	49
Figure 1.13 Intrinsic and extrinsic pathways of cellular apoptosis	51
Figure 1.14 Necrotic cell death	52
Figure 1.15 Mitochondrial dysfunction	53
Figure 1.16 Glasgow Coma Scale	55
Figure 1.17 CT and MRI scans of the brain	59
Figure 2.1 Schematic of EVs release into the extracellular space	65

Figure 2.2 DNA origins and unknown packaging mechanisms	69
Figure 2.3 Summary of cargo and composition in EVs	74
Figure 2.4 Example of a DUC protocol	76
Figure 2.5 Basic principles of size exclusion chromatography	79
Figure 2.6 Schematic of nanoparticle tracking analysis (NTA)	83
Figure 2.7 Fluid-based TBI biomarkers	97
Figure 3.1 Graphical abstract of the main project	105
Figure 4.1 Preclinical weight drop mouse model of TBI	107
Figure 5.1 NSS assessment of preclinical TBI weight-drop model	121
Figure 5.2 CT images of animals at each time point	123
Figure 5.3 Characterization of TBI by CT imaging measurements	124
Figure 5.4 NTA of circulating EVs in blood plasma post injury	127
Figure 5.5 NTA data of particles in precleared plasma	127
Figure 5.6 TBI induces changes in EVs subpopulations	128
Figure 5.7 Representative TEM images of EVs isolated by UC	129
Figure 5.8 DNA levels are elevated in the acute phase post injury	131
Figure 5.9 mtDNA is predominantly found in EVs	132
Figure 5.10 Preferential release of mtDNA over nuDNA	132

Figure 5.11 TBI induced circulating EVs do not contain S100 β , NSE, UCH-L1 and Tau proteins	134
Figure 5.12 Dynamics of brain-derived markers in EVs post injury	134
Figure 5.13 EVs proteins matched in databases	136
Figure 5.14 Pearson correlation coefficient heat map	136
Figure 5.15 Potential targets from biostatistical analysis of proteomics	138
Figure 5.16 Computational analysis of EVs proteomics	141
Figure 5.17 Validation of proposed SAA and CFD markers for TBI	144
Figure 5.18 RSI causes acute mtDNA release in EVs from neurons	146
Figure 5.19 ARPE-19 derived EVs contain large fragments of mtDNA	148

List of Abbreviations

TBI	Traumatic brain injury
mTBI	Mild traumatic brain injury
CT	Computed tomography
MRI	Magnetic resonance imaging
DAI	Diffuse axonal injury
SAH	Sub arachnoid hemorrhage
pTBI	Penetrating traumatic brain injury
bTBI	Blast traumatic brain injury
PTSD	Post traumatic stress disorder
WDI	Weight drop injury
CCI	Controlled cortical impact
FPI	Fluid percussion injury
NSS	Neurological severity score
BBB	Blood brain barrier
DAMPs	Damage associated molecular patterns
TNF	Tumor necrosis factor
AD	Alzheimer's disease
PD	Parkinson's disease
ALS	Amyotrophic lateral sclerosis
FTD	Frontotemporal dementia
HD	Huntington's disease
APP	Amyloid precursor protein
ECF	Extracellular fluid
CSF	Cerebrospinal fluid
5-HT	5-hydroxytryptamine
DRN	Dorsal raphe nucleus
SERT	Serotonin transporter

VTA	Ventral tegmental area
NA	Nucleus accumbens
TS	Tourette's syndrome
DAT	Dopamine transporter
AIF	Apoptosis inducing factor
APAF-1	Apoptotic protein-activating factor 1
PARP	Poly ADPribose polymerase
ROS	Reactive oxygen species
mPTP	Mitochondrial permeability transition pore
ZBP1	Z-binding protein 1
GCS	Glasgow Coma Scale
EPO	Erythropoietin
CEPO	Carbamylated erythropoietin
MSC	Marrow stromal cells
QoL	Quality of life
GCS-E	Glasgow Coma Scale Extended
FOUR	Full Outline of UnResponsiveness
fMRI	Functional magnetic resonance imaging
EVs	Extracellular vesicles
ISEV	International Society for Extracellular Vesicles
MVE	Multivesicular endosomes
PEVs	Pathogenic extracellular vesicles
BEVs	Biological extracellular vesicles
EEVs	Engineered extracellular vesicles
ESCRT transport	Endosomal sorting complex responsible for
ssDNA	Single stranded DNA
mtDNA	Mitochondrial DNA
dsDNA	Double stranded DNA

nuDNA	Nuclear DNA
mRNA	Messenger RNA
miRNA	Micro RNA
ncRNA	Non-coding RNA
tRNA	Transfer RNA
MISEV	Minimal Information for the Studies of EVs
DUC	Differential ultracentrifugation
PEG	Polyethylene glycol
MF	Microfluidic
SEC	Size exclusion chromatography
NTA	Nanoparticle tracking analysis
MS	Mass spectrometry
TEM	Transmission electron microscopy
SP-IRIS imaging	Single particle interferometric reflectance
PK	Pharmacokinetic
PD	Pharmacodynamic
EEG	Electroencephalogram
CEA	Carcinoembryonic antigen
CA125	Cancer antigen 125
SCC-Ag	Squamous cell carcinoma antigen
PD-L1	Programmed death ligand 1
TLR4	Toll-like receptor 4
HER-2	Human epidermal growth factor receptor 2
RGCs	Retinal ganglion cells
AMD	Age-related macular degeneration
A β	Amyloid beta
PET	Positron emission tomography
OCT	Optical coherence tomography

UCH-L1	Ubiquitin C-terminal hydrolase L1
GFAP	Glial fibrillary acidic protein
NFL	Neurofilament light
NSE	Neuron specific enolase
S100 β	S100 calcium binding protein
BTI	Brain Trauma Indicator
ROI	Region of interest
FC	Fold change
PPI	Protein-protein interaction
GNN	Graph Neural Network
ANOVA	Analysis of variance
FDR	False discovery rate
SAA	Serum amyloid A
CFD	Complement factor D
CBG	Corticosteroid-binding globulin
VWF	von Willebrand factor
Hp	Haptoglobin
Apo	Apolipoproteins
Orm	Alpha-1-acid glycoproteins
Thbs	Thrombospondin
Serpina	Antitrypsin
MSC	Mesenchymal stem cell

Chapter 1. Traumatic Brain Injury

Traumatic brain injury, or TBI, is one of the leading causes of morbidity and mortality in the world. Here in the United States of America, this type of neurotrauma has been estimated to be directly responsible in ~2.5 million TBI-related Emergency Department visits (PREVENTION, 2019a), ~214,000 hospitalizations, and ~70,000 deaths (PREVENTION, 2020) in recent years. The cost of TBI-related disability and care ranges from approximately \$60 to \$220 billion dollars per year. In addition to the monetary costs associated with TBI, more severe cases impacts the patient's quality of life; the burden is further shared on those immediate family members who often must provide continuous life-long care for the affected patient. Although we have seen a decrease in cases of TBI-related deaths over the last decade (PREVENTION, 2020), TBI remains a common cause of morbidity and mortality to both the adult and pediatric populations. This apparent decrease may be partly due to increased preventative measures like awareness and education, but there remains much unknown about symptoms, prognosis, and overall complex pathophysiology of the disease process. Another possible explanation could be due to acute or asymptomatic cases of mild TBI where qualifying cases never reach hospitalization (i.e. concussions, mild TBI); thus, the true prevalence count is underestimated (LEVIN, 2013; PREVENTION, 2019a). However, repetitive mild TBI cases may lead to long term pathologies such as neurodegeneration and chronic traumatic encephalopathy (CTE).

TBI is non-discriminatory as it affects both the young and old. However, certain age groups, sex, ethnicities, socioeconomic status, and military personnel

are more prone to suffer these types of injuries. The elderly, classified as age 75 and above, accounts for about 32% of TBI-related hospitalizations and 28% of TBI-related deaths (PREVENTION, 2019a). Furthermore, TBI has been shown to occur more frequently in young adult males (BIEGON, 2021; FROST; FARRER; PRIMOSCH; HEDGES, 2013), presumably through risky behaviors that are commonly exhibited during the adolescent development stages. Males are twice as likely to suffer a TBI-related hospitalization than their female counterparts, and three times more likely to be involved in a TBI-related death. However, although males are more prone to injury incidences, females who suffer a TBI exhibit more unfavorable outcomes (GUPTE; BROOKS; VUKAS; PIERCE *et al.*, 2019). Studies have postulated that brain anatomy, biomarkers, pharmacological pathways, and cellular processes can be affected by biological sex (GUPTE; BROOKS; VUKAS; PIERCE *et al.*, 2019). Also, active-duty military personnel and veterans are among the most affected groups. Between 2000-2021, more than 450,000 service members were diagnosed with a TBI, as military conflicts often result in significantly increased risks to blast TBI (DEFENSE, 2022) (LINDQUIST; LOVE; ELBOGEN, 2017). Unsurprisingly, studies have linked military patients experiencing co-occurring health conditions such as post-traumatic stress disorder (PTSD) and depression before and/or after TBI ((LINDQUIST; LOVE; ELBOGEN, 2017) (MAC DONALD; JOHNSON; WIERZECZOWSKI; KASSNER *et al.*, 2017) (O'NEIL; CARLSON; STORZBACH; BRENNER *et al.*, 2013).

The abovementioned epidemiological characteristics are only part of the complicated issues revolving around TBI, as there are many other challenges that

greatly affect the prevalence, treatment, and overall recovery from injury of TBI patients. A number of factors that contribute to the varying degrees of success in overall patient recovery include the type of TBI injury along with its severity, and the complex pathophysiology of the disease.

1.1 Types and severity of TBI

TBI can be broadly divided into two categories: non-penetrating and penetrating. Within these categories, the severity of the injury is classified as mild, moderate, or severe. While the mechanism of injury may be drastically different between the two categories, oftentimes the symptoms and resulting pathophysiologies have significant overlap. Furthermore, the subsequent outcomes and pathologies are greatly influenced by the severity of the injury.

Non-penetrating TBI

The most common type of TBI is from closed head blunt force trauma, resulting in mild TBI (mTBI). Sometimes mTBI is also referred to as concussions, where the most prevalent mechanism of injury is from falls, motor vehicle accidents and sports like football where the brain is violently jarred in the skull, resulting in diffuse axonal injury (DAI) (PREVENTION, 2019b). DAI is the consequence of shearing or tearing of the axons of nerve cells in the subcortical and white matter tissues from the sudden and rapid rotational force on the brain, resulting in compromising axonal transport and degradation of axonal cytoskeleton, thus ultimately inhibiting the transmission of electrochemical signals from one neuron to another. Furthermore, compromised blood flow due to disrupted blood

vasculature results in subarachnoid hemorrhage (SAH), edema, and ischemia in and around the site of impact (**Figure 1.1**). Unsurprisingly, insult to the brain by blunt forces resulting in DAI leads to a multitude of symptoms, ranging from behavioral to cognitive and even motor skills impairment. The most frequently reported symptoms immediately after a mTBI include dizziness, nausea, vomiting, sleepiness and fatigue (PREVENTION, 2019c); long term symptoms of learning impairment, memory loss, difficulty concentrating on tasks, and general motor or cognitive decline have also been reported (PREVENTION, 2020).

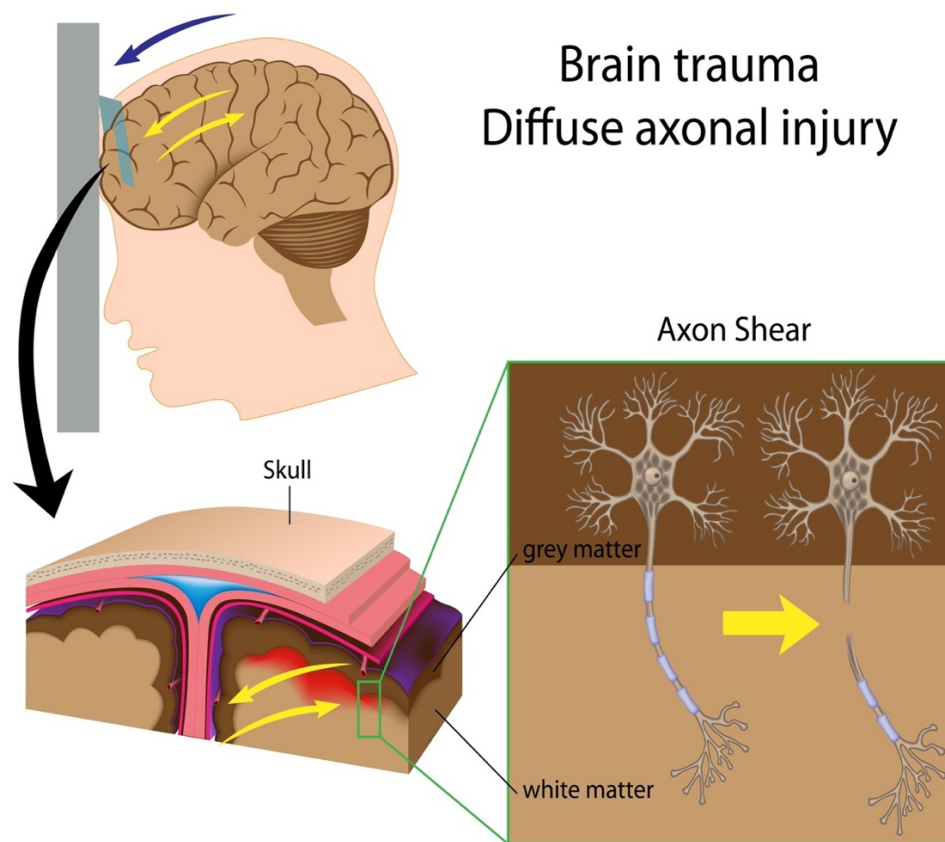


Figure 1.1: Diffuse axonal injury (DAI) from blunt force trauma. The sudden and often violent impact from falls, motor vehicle accidents, and collisions in sports (i.e. football) results in the damaged or severed axonal connections. This disruption may cause a variety of symptoms ranging from memory loss to behavioral changes. Reproduced with permission from (SCOTLAND, 2023).

More forceful impacts lead to upgraded severities of moderate and severe TBI, which include all the aforementioned symptoms and more serious outcomes, including death or permanent disabilities. Studies have shown moderate and severe TBI patients suffer from worsening headaches, loss of vision, seizures, slurred speech and comatose-like symptoms (DEVELOPMENT, 2020; STROKE, 2020). The area of impact, particularly the depth of destruction deep into the white matter, is a key characteristic of moderate and severe TBI (KINNUNEN; GREENWOOD; POWELL; LEECH *et al.*, 2011). While mTBI may affect the outermost layers of the white matter immediately bordering the grey matter, more serious cases of injury can adversely affect the deeper tissues, resulting in specific or worsening symptoms compared to mTBI (KINNUNEN; GREENWOOD; POWELL; LEECH *et al.*, 2011).

Another TBI category related to mTBI is blast TBI (bTBI). In the late 20th and early 21st centuries, the high prevalence of military personnel casualties stemming from warfare has garnered attention and subsequently been touted as its own category of injury. This type of TBI is defined as energy from explosive shock waves that are transmitted through the skull and into the brain, causing a series of subsequent injuries that are unique to bTBI (VLAHOS NICHOLAS, 2021). These injuries are complex and often deemed “invisible injuries” due to the lack of clear external injury on physical examinations and initial routine medical imaging diagnosis. This is because unlike closed head TBI and penetrating TBI, the exact mechanisms of injury due to transmission of pressure waves through bodily tissue are not well characterized. The initial primary injury occurs directly from the

explosion that produces pressure waves which causes a rapid change in pressure and compresses the brain, resulting in barotrauma (**Figure 1.2**) (VLAHOS NICHOLAS, 2021). Accompanied injuries are associated with the blast waves causing penetrating injuries from shrapnel, violent physical displacement of the individual into nearby structures or surfaces, and long-term illnesses like thermal and chemical burns, toxin inhalation and radiation exposure (VLAHOS NICHOLAS, 2021) (CERNAK; NOBLE-HAEUSSLEIN, 2010); (RISDALL; MENON, 2011). The kinetic energy from the primary blast wave causes temporary deformation of the brain, creating widespread DAI that affects both grey and white matter. Common pathophysiologies including neuronal cell death, axonal injury, compromised BBB functionality, contusions and cerebral edemas have all been reported (CERNAK; NOBLE-HAEUSSLEIN, 2010). One important clinical outcome that is much more prevalent in bTBI compared to the other types of injuries is the association with post-traumatic stress disorder (PTSD) (RISDALL; MENON, 2011). Not only has bTBI been shown to induce PTSD in a preclinical rat model of bTBI (ELDER; DORR; DE GASPERI; GAMA SOSA *et al.*, 2012), but is also associated with the symptom severity of PTSD (BORINUOLUWA; AHMED, 2023). In addition to PTSD, blast severity was also associated with depressive and neurobehavioral symptoms beyond the initial diagnosis (MARTINDALE; ORD; RULE; ROWLAND, 2021). It is worth noting that bTBI and PTSD have the unique context of psychological distress due to the combat environment as a factor in influencing the interplay between the two, thus ultimately affecting the long-term outcomes for patient recovery.

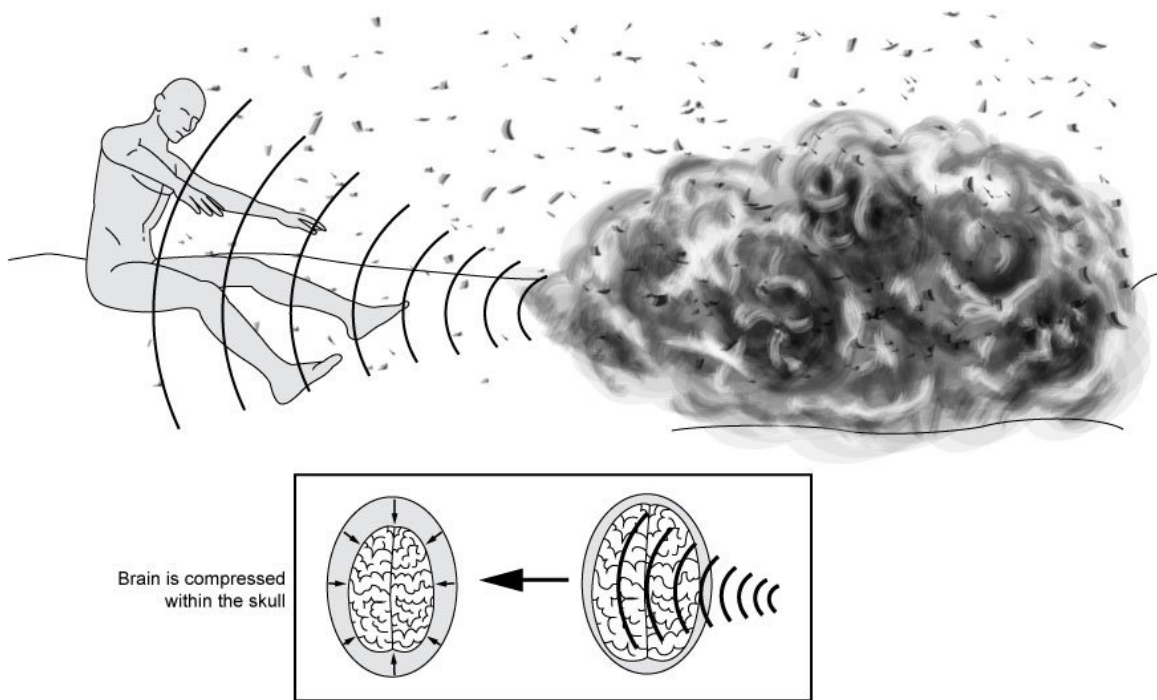


Figure 1.2: Blast TBI. bTBI from an explosive device causes shock waves (pressure waves) due to the sudden and often violent displacement of air around the object. These pressure waves are transmitted through the skull and into the brain, compressing the organ and causing DAI over a widespread area. bTBI is also associated with other mechanisms of injuries from the explosive device such as shrapnel, burns, and physically thrown back from the origin of explosion. Reproduced with permission from (STOLER, 2021).

Penetrating TBI

Penetrating TBI (pTBI) is defined as when a foreign body penetrates the skull and traverses through the layers of the dura and finally into the brain parenchyma (**Figure 1.3**). (NG; LEE, 2019). Similar to closed head injuries, intracranial hemorrhaging, edema, ischemia and other blood vasculature problems can be seen in pTBI. DAI is also prominent often due to the force and velocity of the penetrating projectile bruising the tissue layers in and around the injury site. The kinetic energy of the object is projected onto the tissues, causing the hallmark

pathophysiology of axonal shearing. A key difference of pTBI is that invasion of the fast-moving projectile (i.e. bullets, nails, rods, shrapnel, knives, etc) causes a physical cavity within the brain parenchyma, resulting in exacerbation of the injury symptoms. In many cases, skull fragments are also lodged within the brain parenchyma which may cause further damage and complicate the removal of the skull fragments during surgical intervention, depending on their location. Additionally, permanent loss of brain matter is common, along with increased chances of infection due to the invasive foreign object lodged within the skull for extended periods of time. Because of the invasive nature of pTBI, acute symptoms such as respiratory function, hypotonia, tachycardia, and cerebrospinal fluid leakage are observed from critically affected patients (BLACK; HANKS; WOOD; ZAFONTE *et al.*, 2002). The severity of symptoms from pTBI depends on the projectile size, speed, and location of penetration, with higher mortality rates associated with objects penetrating past the midline and stopping within regions of the brain that control essential functions like breathing (i.e. posterior fossa) (STROKE, 2020)(NG; LEE, 2019)

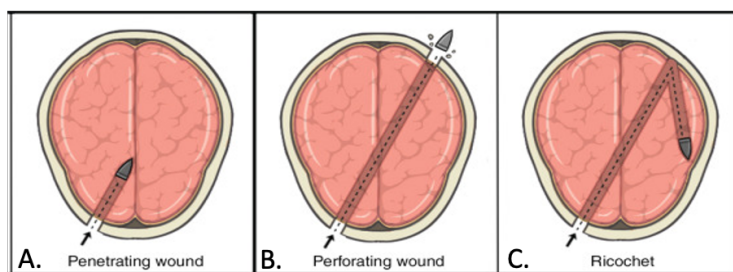


Figure 1.3: Different types of penetrating TBI. A. Penetrating TBI by projectiles like a bullet may become lodged within the brain resulting in an increased risk of infection. B. A perforating wound in which the projectile enters from one location, traverses through the brain parenchyma, and exits in a different location. C. Ricochet of projectile within the skull will change the original pathway and redirect the object in a different direction. Adapted and reproduced with permission from (VLAHOS NICHOLAS, 2021).

1.2 Preclinical animal models of TBI

Advancements in TBI research have relied heavily on preclinical animal models to understand the many different aspects of each type of injury and subsequent disease processes. Often times pre-clinical models provide the initial insight into the various mechanisms of TBI and the disease process, giving researchers a starting point. The most prominently studied models include weight drop injury (WDI), controlled cortical impact (CCI), shock tube blast for bTBI, and fluid percussion injury (FPI). Each model has subsequently been scaled and modified to accommodate for a variety of animals (i.e. mouse, rat, ferret, rabbit, pig, etc) and adjustments made to fine tune the severity, injury location and other parameters that ultimately affect downstream pathophysiology. Certain pre-injury manipulations may be required depending on the model used. For example, CCI requires a pre-injury craniectomy to expose the cortex tissue, and researchers must consider restrained or unrestrained options for the animal's head position. Most, if not all, of the injury models require the animals to be subjected to anesthesia for better handling of the animal and ethical considerations. Hardware and software calibrations are essential to the consistency and reproducibility of the injury, as any slight alterations to either aspect can drastically change the pathophysiology and subsequent outcomes. Subsequent behavioral testing like Neurological Severity Score, novel object recognition, and Morris water maze are common assays to quantify the severity of the injury along with the associated neurological deficits. Preclinical animal models have served as the foundation for

many translational therapeutics and treatments for TBI and are essential in the advancement of this scientific field.

Weight drop injury

The most widely used weight drop injury (WDI) model was first pioneered by Feeney et al. in 1981, but it was Marmarou et al. in 1994 that adapted and popularized the closed head WDI model seen today. Briefly, a plexiglass tubing with an inner diameter of 19 mm, outer diameter of 25 mm and overall height of 4 or more meters was attached to a metal ring stand with clamps. At the bottom is a foam bed foundation where the rat was laid prone with its head directly underneath the opening of the plexiglass tubing and secured in place by two belts. Prior to induction of WDI, the animal was anesthetized, the scalp was shaved, and a midline incision was performed to expose the periosteum covering the vertex. A steel 'helmet' of 10 mm in diameter and 3 mm in thickness was placed between the coronal and lambdoid sutures of the skull of the animal's unrestrained head. The injury was performed by dropping a brass weight between 50-500 grams from a predetermined height within the plexiglass tubing and striking the steel helmet, thus ultimately impacting the exposed skull (**Figure 1.4**). The animal was immediately removed from the device and monitored for recovery. The authors reported a severe TBI when 450- and 500-gram weights dropped from a height of 2 m with a mortality rate of 50%. The severity was lowered to a moderate TBI when the height was reduced to 1 m (MARMAROU; FODA; VAN DEN BRINK; CAMPBELL *et al.*, 1994). Skull fractures were noticeably higher in the most severe injury group (500 g, 2 m) with a rate of 31%. This prevalence decreased when the

weight was lowered to 450 g and eliminated all together in combination when dropped from 1 m (MARMAROU; FODA; VAN DEN BRINK; CAMPBELL *et al.*, 1994). The main cause of mortality from severe TBI was due to respiratory depression followed by hypotension (MARMAROU; FODA; VAN DEN BRINK; CAMPBELL *et al.*, 1994).

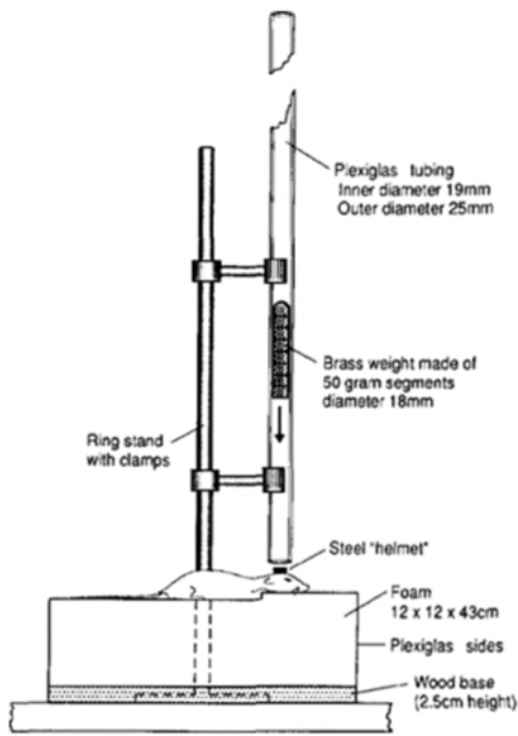


Figure 1.4: Weight drop injury device. The original WDI device pioneered by Marmarou *et al.* in 1994.. Weights of 450-500 grams were dropped from 1 meter or 2 meters directly onto the steel disc for the induction of a moderate or severe injury, respectively. Reproduced with permission from (MARMAROU; FODA; VAN DEN BRINK; CAMPBELL *et al.*, 1994).

There are some key differences between Feeney and Marmarou's respective models. Firstly, a craniectomy was performed in the Feeney model to expose the cortex, allowing the free-falling weight to directly impact the brain matter. The size of the hole should be large enough for the weight to strike without colliding with the edges of the skull, thus reducing the chances of skull fractures.

Furthermore, Feeney's model did not include the steel disc, but rather relied directly on the weight with different sized impactor tips that coincided with the diameter of injury. Hemorrhages in the white matter are observed immediately after injury leading to the development of necrotic tissue about 24 hours later (FEENEY; BOYESON; LINN; MURRAY *et al.*, 1981). The last prominent iteration of WDI is the Shohami model. Unlike the Feeney and Marmarou models, this version does not require a craniectomy or the use of a steel disc. Instead, a midline incision through the scalp is made to expose the skull, and the injury is directly induced by rounded free-falling rods. Modifications to the tip of the rod creates a blunt force trauma on an exposed skull that is directly opposite to the more invasive and penetrating mechanism of the Feeney model (XIONG; MAHMOOD; CHOPP, 2013) The authors reported BBB disruption, cerebral edema, focal contusions, and cerebral hemorrhaging in mice (CHEN; CONSTANTINI; TREMBOVLER; WEINSTOCK *et al.*, 1996). Additionally, the inflammatory response was significantly upregulated with increases in prostaglandins in the ipsilateral region 18 hours to 10 days post injury and immunostaining revealed activated microglia and astrocytes 1 week post TBI (ALBERT-WEIßENBERGER; VÁRRALLYAY; RASLAN; KLEINSCHNITZ *et al.*, 2012). Behavioral testing showed severely compromised behavioral functions immediately post injury with spontaneous and gradual recovery over time, although some motor deficits were still noticeable 30 days post TBI (CHEN; CONSTANTINI; TREMBOVLER; WEINSTOCK *et al.*, 1996). It is worth noting the progressive injury adaptations of each WDI version from direct impact onto exposed brain matter (Feeney) to steel helmet (Marmarou)

and finally round free falling rods (Shohami). The WDI models primarily produce a diffuse injury representing blunt force trauma to the head commonly seen in motor vehicle crashes, falls, and sports injuries where the brain is violently jarred within the skull. We will use an unrestricted mouse model of WDI for our project as described in more detail in **Chapter 4, sub-chapter 4.1**. However, other models like CCI have shown advantages in replicating pathophysiology that WDI models may not consistently represent.

Controlled cortical impact

CCI is a well characterized model originally developed in the 1980s and remains a popular choice among researchers due to its reproducibility and specificity of injury parameters (OSIER; DIXON, 2016) (ALLURI; SHAJI; DAVIS; THARAKAN, 2018) (DIXON; CLIFTON; LIGHTHALL; YAGHMAI *et al.*, 1991). Briefly, CCI uses a pneumatic or electromagnetic powered piston to deliver the injury to the exposed dura after a craniectomy. The model uses a stereotaxic system with that holds the head of the anesthetized animal in place (**Figure 1.5**). Several key advantages to CCI are the precise location, impactor diameter, impactor velocity, depth and dwell time can all be controlled, thus greatly enhancing the consistency and reproducibility of the effects (ROMINE; GAO; CHEN, 2014). For example, previous studies have shown a velocity of 3 m/s that penetrates the dura at a depth of 1 mm with a diameter tip of 3 mm induces a moderate TBI in mice (ROMINE; GAO; CHEN, 2014). The authors noted the presence of subdural hematomas, BBB disruption, cortical contusions/tissue loss, and secondary injuries like apoptosis, inflammation and oxidative stress

(CAMPOLO; AHMAD; CRUPI; IMPELLIZZERI *et al.*, 2013). These pathophysiologies are consistent with ones found in WDI models, although CCI has a much less prevalence of skull fractures (OSIER; DIXON, 2016). Both CCI and WDI models can produce both diffuse and focal injuries in the forms of blunt force trauma to a closed skull or pTBI through a craniectomy, respectively.

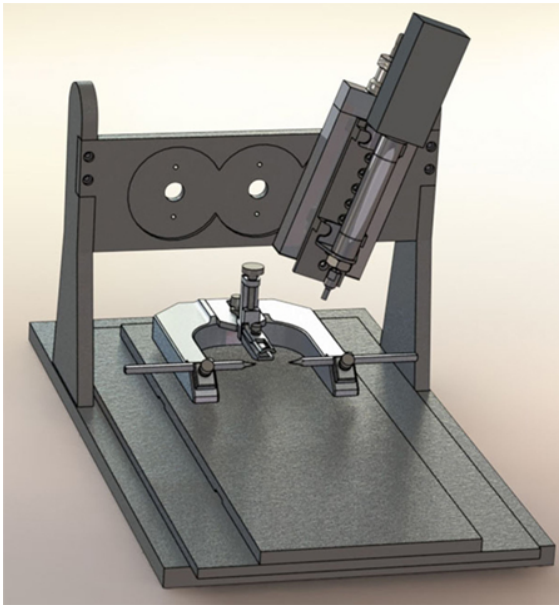


Figure 1.5: Schematic of pneumatic controlled CCI system. Stereotaxic frame with rods holds the anesthetized animal's head in place. CCI can be performed with or without a craniectomy depending on the type of TBI desired. The location, velocity, tip diameter, depth of injury and dwell time of piston can all be mechanically programmed and controlled, resulting in a high degree of consistency. Reproduced with permission from (OSIER; DIXON, 2016).

Blast injury

The shock tube blast TBI (bTBI) model has been used to characterize the effects of explosive injuries to the heads of military personnel deployed in combat areas. The shock tube model produces energy waves by releasing compressed gas through a tube to simulate the detonation of an explosive device without any

pre-surgery manipulations. Briefly, the source gas is pumped into a driver section where it is compressed and separated from the transition and test sections by membranes. Upon disruption of the membranes, the blast injury occurs when the rapidly expanding gas propagates through the transition section and into the test section where the animal is placed as a planar shock wave (KURIAKOSE; SKOTAK; MISISTIA; KAHALI *et al.*, 2016). The number, thickness, length of test section, placement of animal are all factors that influence the severity and duration of the blast injury (**Figure 1.6**). Furthermore, adaptations to the orientation of the animal, the use of head restraints and the end conditions of the blast tube (open vs. closed) play integral roles in the injury outcomes. Regardless of the modifications to the bTBI models, many of the cognitive and behavioral deficits resulting from the adapted blast injuries overlap with one another. The commonly reported symptoms from military personnel are retrograde and anterograde amnesia, decreased executive function, and increased risk of dementia development (TABER; WARDEN; HURLEY, 2006) (HICKS; FERTIG; DESROCHER; KOROSHETZ *et al.*, 2010) (BARNES; KAUP; KIRBY; BYERS *et al.*, 2014). bTBI remains the most technically challenging type of injury to model due to its high degree of physics involved. The Friedlander waveform requires deep understanding of how energy waves are generated and propagated through the test tube, thus researchers must calculate the exact amount of gas pressure needed to produce the desired effects. Other considerations like the type of material the chambers are constructed from will also impact how the energy waves

are propagated. Despite its technically challenging nature, bTBI remains the most unique of the pre-clinical models due to its mechanism of injury (energy wave

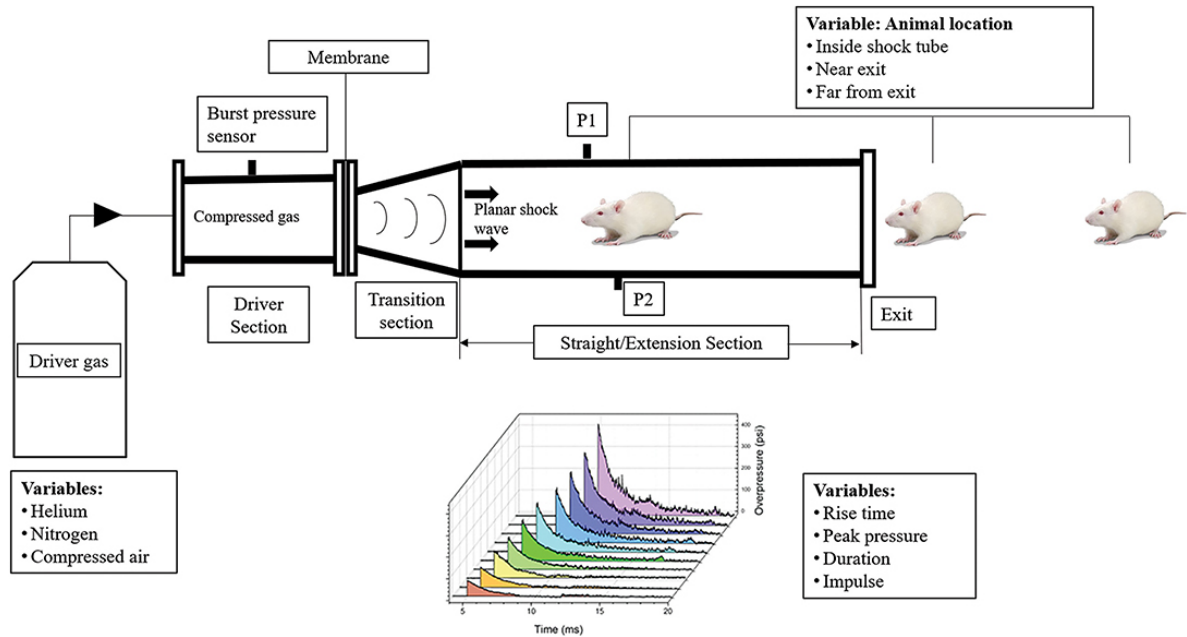


Figure 1.6: Schematic of shock tube blast TBI model. The gas chamber can be filled with different types of gases. Following entry into the driver section, the gas is compressed until the membrane(s) are breached due to pressure, resulting in the sudden and violent release of energy through the transition section and finally into the test section housing the animal. Variables like rise time, maximum pressure, duration of injury and impulse can be calculated using software to measure the severity of the injury. Reproduced with permission from (KURIAKOSE; SKOTAK; MISISTIA; KHALI *et al.*, 2016).

forms) as all previously mentioned models require a physical injury mechanism to induce damage.

Fluid percussion injury

Fluid percussion injury (FPI) harnesses the power of a fluid-based injury to diffuse (midline FPI) or mixed (lateral FPI) injuries to the exposed dura. Established in the late 1980's using rats, FPI is produced by applying a rapid fluid pulse (~20 msec) directly onto the dura surface, causing a brief deformation of the brain (DIXON; LYETH; POVLISHOCK; FINDLING *et al.*, 1987). Briefly, the FPI set up

requires a pendulum swing with a metal hammer at the end, which strikes the plunger cap at the end of the fluid cylinder, creating a pressure force that concentrates through the transducer housing before being released through a narrow Luer-Lock needle-like device. The energy of the pressure force is detected by a transducer and the signal is amplified to the connected oscilloscope (**Figure 1.7**).

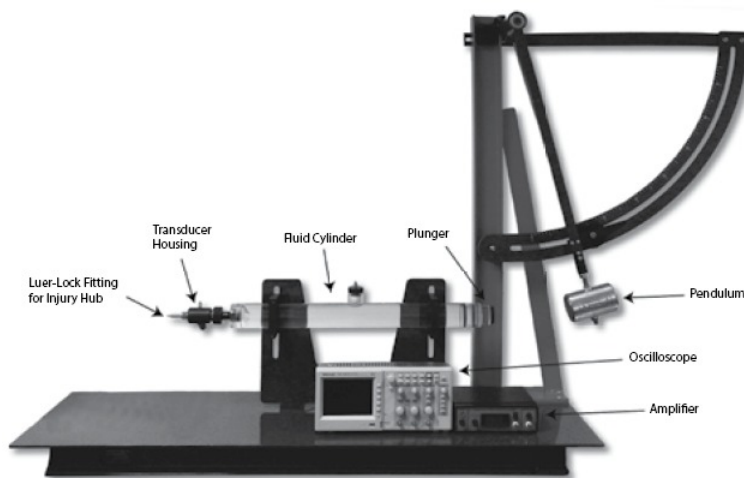


Figure 1.7: Fluid percussion injury model. A pendulum with a metal hammer strikes the plunger tip of the fluid cylinder. This creates a pressure force through the fluid that is concentrated through the transducer and finally released through a Luer-Lock mechanism directly onto the exposed dura of the animal. Stereotaxic equipment to hold and manipulate the head of the animal is not shown. Reproduced with permission from (KOBESSY, 2015).

A craniotomy is required before the induction of the injury. A midline injury targets the sagittal suture that is halfway between the lambda and bregma sutures; this type of injury produces a primarily diffuse injury. Conversely, a lateral FPI targets the parietal cortex, resulting in a mixed pathophysiology of focal and diffuse injury. Both forms of FPI have been shown to produce pathophysiologies like white-gray matter hemorrhaging, tissue necrosis, axonal damage, and mitochondrial dysfunction that are also seen in other preclinical injury models and in human TBI

patients (CORTEZ; MCINTOSH; NOBLE, 1989); (DIXON; LIGHTHALL; ANDERSON, 1988). The severity of FPI can be modulated by adjusting the force of the pendulum and the location of the injury. Appropriate recovery procedures including hydration packs, fluid injections with sterile saline, and careful monitoring in the immediate hours and days following injury may be needed to ensure survival of each animal. FPI is not without its own set of challenges as air bubbles and inconsistent pressure pulses from the pendulum have been reported as confounding variables in the injury process. However, with proper technique and adjustments, these issues can be fixed relatively easily requiring no special equipment.

Behavioral testing

Regardless of which TBI model is used, a common follow up experiment involves behavioral testing to define the severity of the injury with the neurological deficits. Characterizing the motor and cognitive deficiencies allows researchers to associate behavioral data with secondary mechanisms of injury, thus correlating the timing of these deficits with the disease progression. Some prominent examples of these paradigms include Neurological Severity Score, novel object recognition, and Morris water maze. These paradigms have been designed and adapted mostly for the use of rodents, but can be modified to suit the needs of the researchers.

Neurological Severity Score (NSS) is comprised of 11 different tests that gauges mostly the motor functions of the animal. Briefly, these tests range from open circle exit, straight walk, forelimb/hindlimb paw grasp, beam walk/balance,

and round stick balance. The order in which these individual tests are performed is increasingly difficult in nature, thus it is researchers can easily gauge the neurological deficits within the first few tests (KHALIN; JAMARI; RAZAK; HASAIN *et al.*, 2016). Failure to successfully perform an individual test results in a score of 1 point, thus the higher the NSS score, the more severe the injury and neurological deficits. NSS score of 1-4 denotes a mild, 5-7 for moderate, and 8-11 for severe TBI. Unsurprisingly, higher rates of mortality are correlated with severe TBI scores.

Novel object recognition (NOR) is a relatively fast and efficient approach for testing different phases of learning and memory in mice. Originally described in 1988 by Ennaceur and Delacour, the test has been adapted to fit the needs of researchers (ENNACEUR; DELACOUR, 1988). Briefly, the NOR test can be done over 3 days: habituation day, training day, and testing day. During habituation, the mice are allowed to explore the arena without any objects present. For training, the mice are exposed and familiarized to a single small object (i.e. cone, box, circle) before testing. For testing day, the familiar object is placed in the same arena as a novel object, and the mice are allowed to freely explore both. Because mice have an innate preference for novelty, the mice should recognize the familiar object and spend most of its time exploring the novel object. This preference does not require positive or negative reinforcement or long training regimes. This allows researchers to examine short-term and long-term memory based on their experimental procedures (LUEPTOW, 2017). Animals that have undergone a TBI would show impaired working memory, and thus may not be able to clearly distinguish the familiar versus novel objects in the paradigm.

The Morris water maze (MWM) is a learning and memory test, which assays for these traits in rodents by their ability to swim in an open arena to locate a submerged escape platform from a specific start position (VORHEES; WILLIAMS, 2006). Briefly, the mice acquire spatial learning by using distal cues to navigate a direct path to the submerged platform when starting from different, random locations around the perimeter of the tank. These locations are commonly denoted as N, S, E and W. By learning the location of each point, each animal should be able to orient themselves appropriately and swim to find the submerged platform to successfully complete the test. After TBI, animals may not be able to remember or orient themselves appropriate to reach the platform, thus suggesting impaired spatial recall and memory. Although these are the most common types of behavioral tests, there are other tests such as Y-maze, open field testing, and Barnes maze that similarly assess the motor and cognitive functions of animals post TBI.

	Mechanism	Gross pathophysiology	Pros	Cons
Weight drop injury (WDI)	<ul style="list-style-type: none"> • Craniectomy (Feeney) followed by direct impact onto brain matter • Steel disc (Marmarou) placed on top of skull • Free falling rods (Shohami) impacting skull 	<ul style="list-style-type: none"> • Diffuse axonal injury (DAI) • Skull fractures • White matter necrosis • Cerebral edema 	<ul style="list-style-type: none"> • May not need pre-surgery manipulations • Simplistic design • Adaptable • Cost efficient 	<ul style="list-style-type: none"> • High mortality rate (severe TBI) • Less refined than more sophisticated injury models

Controlled cortical impact (CCI)	<ul style="list-style-type: none"> • Pneumatic or electromagnetic powered piston directly onto exposed dura. 	<ul style="list-style-type: none"> • Subdural hematomas • Compromised BBB • Cortical contusions • Cortical tissue loss 	<ul style="list-style-type: none"> • High reproducibility • High specificity of injury parameters 	<ul style="list-style-type: none"> • May require pre-surgery manipulations • Time consuming
Shock tube blast TBI	<ul style="list-style-type: none"> • Energy waves produced through compressed gas 	<ul style="list-style-type: none"> • Compression shearing of brain tissue • Cortical contusions • Micro-hemorrhaging • Axonal injury 	<ul style="list-style-type: none"> • Most accurate form of blast TBI • Highly customizable • No pre-surgery manipulations required 	<ul style="list-style-type: none"> • Technically challenging • Variability (i.e. tube material, chambers, position of animal, driver gas)
Fluid percussion injury (FPI)	<ul style="list-style-type: none"> • Rapid fluid pulse directly onto exposed dura 	<ul style="list-style-type: none"> • DAI • White-gray matter hemorrhaging • Tissue necrosis • Axonal injury 	<ul style="list-style-type: none"> • Severity and location of injury can be fine tuned • Adaptable to lateral injuries 	<ul style="list-style-type: none"> • Air bubbles in pendulum • Inconsistent pressure pulses

Table 1.1: Summary of preclinical TBI models. Each model has different mechanisms of injury, resulting in various gross pathophysiologies. Furthermore, each model has their respective upsides and drawbacks, which needs to be take into consideration when choosing type of injury.

1.3 Pathophysiology of TBI

TBI has been proposed as not just a singular event, but a phasic, disease process (MASEL; DEWITT, 2010). The two main phases can be discerned between the primary mechanism of injury through the initial mechanical tissue damage, followed by secondary mechanisms of injury like neuroinflammation, neuromodulator dysfunction, cell death (apoptosis/necrosis), mitochondrial dysfunction (**Figure 1.8**). The initial insult to the brain is often sudden and violent in nature, from different mechanisms such as blunt force trauma, rotational/twisting acceleration (i.e. motor vehicle accidents), or penetrating objects. Blunt force trauma causes acute damage such as diffuse axonal injury (DAI), often resulting

in widespread destruction to the brain's white matter. Furthermore, the sudden rotational/twisting acceleration causes shearing forces that can damage axonal connections, leading to breakdown in communication between individual neural cells and/or in more severe cases, entire regions of the brain.

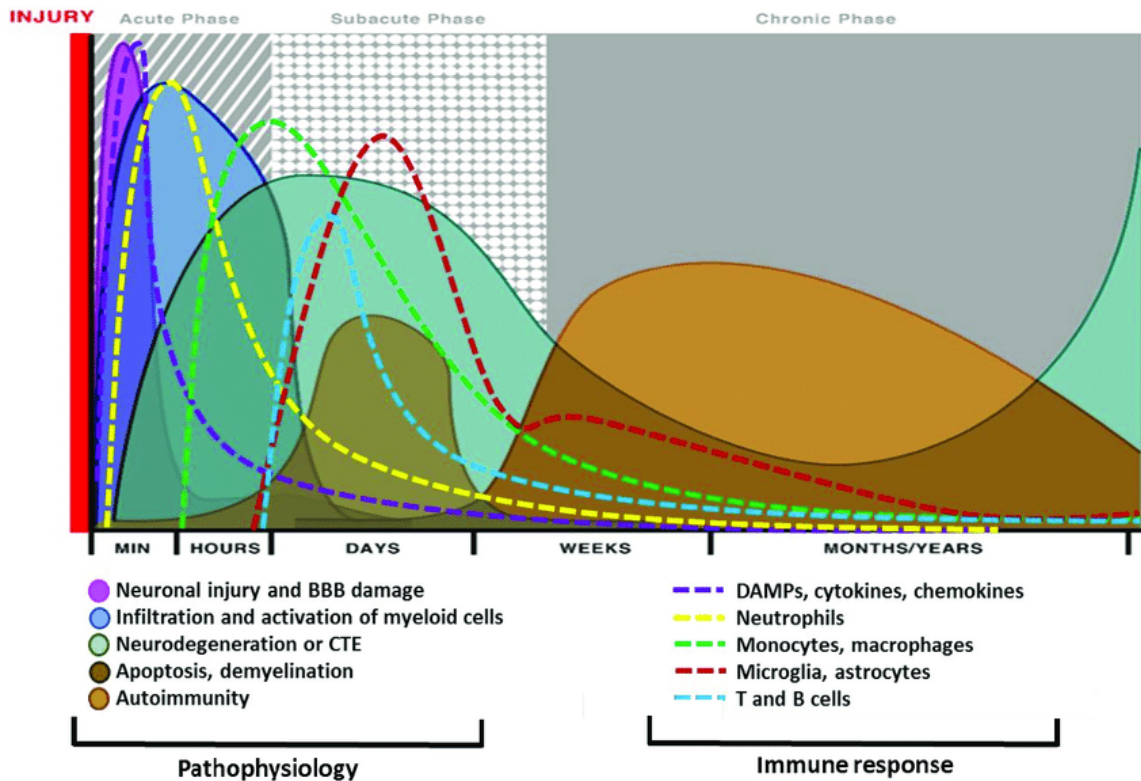


Figure 1.8: Secondary mechanisms of injury across different phases. After the primary insult to the skull, secondary injuries initiates as the patient begins recovery. Prominent secondary mechanisms of injury include neuroinflammation, cellular apoptosis/necrosis, and mitochondrial dysfunction. Reproduced with permission from (JARRAHI; BRAUN; AHLUWALIA; GUPTA *et al.*, 2020).

Penetrating projectiles often results in necrotic cell death, especially when the foreign objects creates significant cavitation of brain tissue.

Following the primary phase of injury, the secondary injuries commence as the patient begins recovery. Head injuries often result in compromisation of brain

vasculature, as highlighted by the blood-brain barrier (BBB) breakdown, a structure that is essential in mediating the movement of molecules and fluids between the circulatory system and the brain itself. Failure to regulate micronutrients, neuromodulators, and water contributes to the rise of neuroinflammation, neuromodulator dysfunction, apoptosis, mitochondrial dysfunction, and other physiological processes are prevalent (STROKE, 2020).

Neuroinflammation

Neuroinflammation is the general term for the inflammatory response after TBI. The resident microglia immune cells drives this inflammatory response, with the pro-inflammatory M1 to anti-inflammatory M2 phenotype transitions promoting various aspects of the neuroinflammatory process. Pro-inflammatory signals such as damage-associated molecular patterns (DAMPs) and the upregulation of tumor necrosis factor (TNF), IL-6, and IL-1 β act as beacons to further enhance the injury-initiated neuroinflammation response while simultaneously, pro- and anti-inflammatory cytokines are competing to prolong or terminate the inflammatory response, respectively (**Figure 1.9**) (CSUKA; MORGANTI-KOSSMANN; LENZLINGER; JOLLER *et al.*, 1999) (FRUGIER; MORGANTI-KOSSMANN; O'REILLY; MCLEAN, 2010). Interestingly, recent transcriptomic studies have suggested microglia display a broader transcriptional range than M1 and M2 depending on their environment. Thus, the often times conflicting molecular signals induced by TBI damage may result in microglia displaying a mixed expression of M1 and M2 associated markers, especially in the acute phase (HICKMAN; KINGERY; OHSUMI; BOROWSKY *et al.*, 2013). However, as the disease

progresses, the M2-like markers expression decreases while M1-like markers are still prominent, indicating that the pro-inflammatory action of microglia in the sub-acute and chronic phases exacerbates the detrimental neuroinflammatory effects.

Additionally, supporting cells such as astrocytes are affected as well. Specifically, reactive astrogliosis is the astrocytes-specific response to the TBI. Reactive astrogliosis is the process by which astrocytes respond to TBI damages through adaptive changes in gene expression, morphology, and function (BURDA; BERNSTEIN; SOFRONIEW, 2016). This strength of the response is reflective of the severity of TBI, as mild or moderate injuries can result in neuroinflammation, BBB disruption, and axonal injury (**Figure 1.10A**). In turn, these secondary mechanisms can all drive specific forms of astrogliosis. It is worth noting that hypertrophic reactive astrocytes are heterogeneously mixed with viable neural cells in the injured areas. In more severe cases, astrocytes proliferate and form astroglial scars around the injury site to restrict the intense neuroinflammatory response.

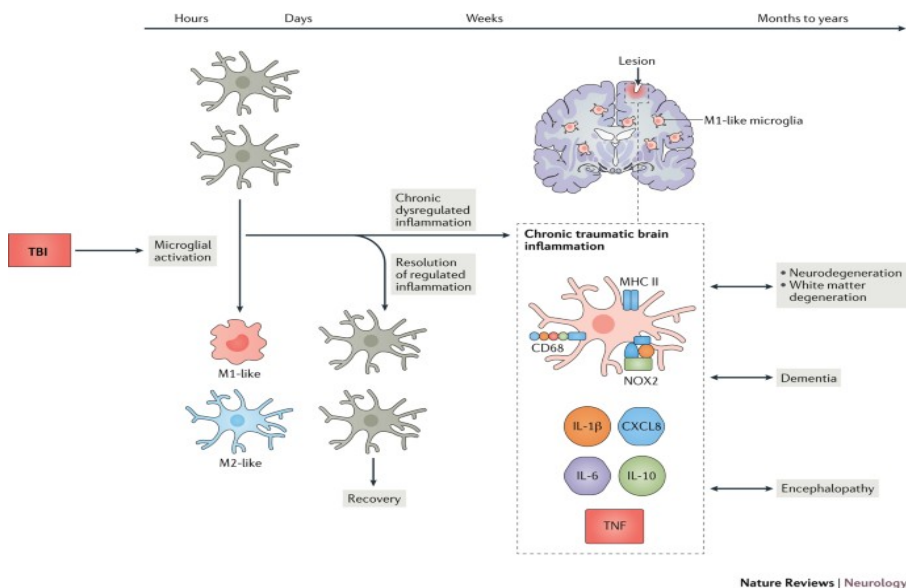


Figure 1.9: The effects of chronic inflammation in TBI. Acute microglial activation into M1-like and M2-like phenotypes are initially beneficial to recovery. However, long term neuroinflammation and microglial activation increases the likelihood for the advancement of neurodegeneration, dementia, and encephalopathy.. Reproduced with permission from (SIMON; MCGEACHY; BAYIR; CLARK *et al.*, 2017).

Adjacent to the scars are the above mentioned features that taper with distance from the injury site (**Figure 1.10B**)

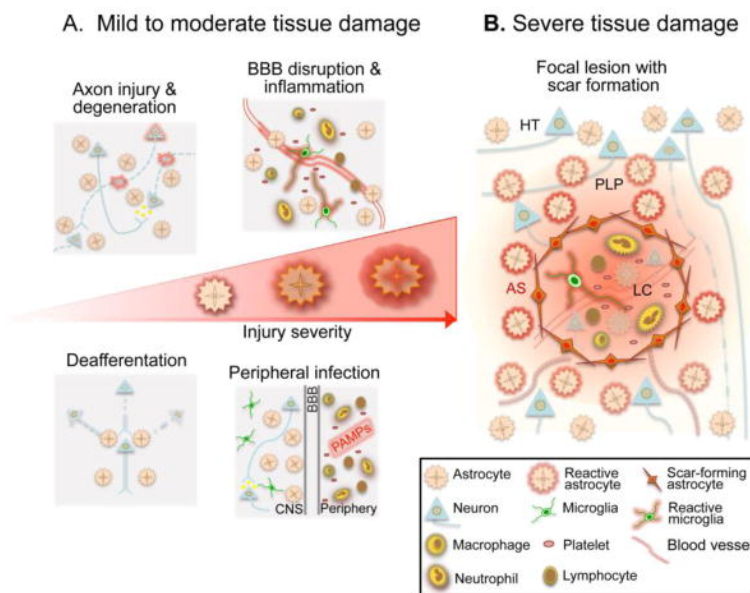


Figure 1.10: Astroglial responses in TBI. This process is a graded response that is reflective of the injury severity. A. Mild or moderate tissue damage from axonal injury, BBB disruption, and inflammation can trigger a variety of astroglial responses. B. Severe cases can result in the formation of astroglial scars that form around the lesion site to prevent the spread of neuroinflammatory signals. Reproduced with permission from (BURDA; BERNSTEIN; SOFRONIEW, 2016)

Neuromodulator dysfunction

Another secondary phase injury is neuromodulator dysfunction, defined as the state in which neuromodulators that govern many neural processes and functions are disrupted (STROKE, 2020). A prominent example of this is glutamate,

the most abundant free amino acid in the brain and the primary agonist for excitatory neurons (ZHOU; DANBOLT, 2014). Critically, the BBB mediates the levels of glutamate between brain cells, blood, extracellular fluid (ECF) and cerebrospinal fluid (CSF) by facilitative and active transport systems. As previously established, TBI often results in the disruption of the BBB, causing an imbalance in glutamate levels between the normally compartmentalized gradients. Several mechanisms responsible for this imbalance include neuronal death, inflammation, and dysregulation of glutamate recycling and transport. Neuronal damage occurs from the sudden, large influx of calcium immediately after the primary insult to the brain, which in turn promotes the release of glutamate and further over-stimulation of excitatory neurons, releasing additional glutamate. The effects of neuroinflammation are again highlighted with respect to glutamate neurotoxicity, as previous studies have shown glutamate dysregulation and metabolism from chronic inflammation are associated with psychiatric disorders like mood swings, depression, anxiety, and stress. (HAROON; FLEISCHER; FELGER; CHEN *et al.*, 2016; HAROON; MILLER; SANACORA, 2017). However, glutamate is not the only neuromodulator affected by TBI, as serotonin and dopamine have also been shown to be dysregulated in the secondary injury phase.

Serotonin, or 5-hydroxytryptamine (5-HT), is perhaps the most well characterized neuromodulator, affecting most, if not all of the nervous system processes and beyond. Serotonin can be found in all regions of the brain, thus the ubiquitous nature of serotonin plays a role in virtually all cognitive, motor, and other behavioral functions (**Figure 1.11**) (BERGER; GRAY; ROTH, 2009). TBI affects all

physiological aspects related to serotonin. For example, damage to the dorsal raphe nucleus (DRN), a midline structure within the dorsal midbrain, has been shown to result in large, abrupt discharge of serotonin, which may be associated with serotonin dysregulation characteristics of both physiological and mood symptoms (SHINODA; YANO; NAKAYAMA, 2021). Furthermore, a cortical contusion model of TBI in rats showed serotonin transporter (SERT), the major transporter in the delivery and re-uptake of serotonin, to be downregulated in neuronal fibers immediately adjacent to the area of impact (ABE; SHIMADA; OKADA; KIBAYASHI, 2016). Prolonged dysfunction of serotonin levels affects has widespread implications on other areas of the brain and neuromodulators like dopamine. There is a high level of crosstalk between serotonergic and dopaminergic neural cells with much overlap in functionality, therefore it is no surprise that TBI also has negative consequences on dopamine regulation as well.

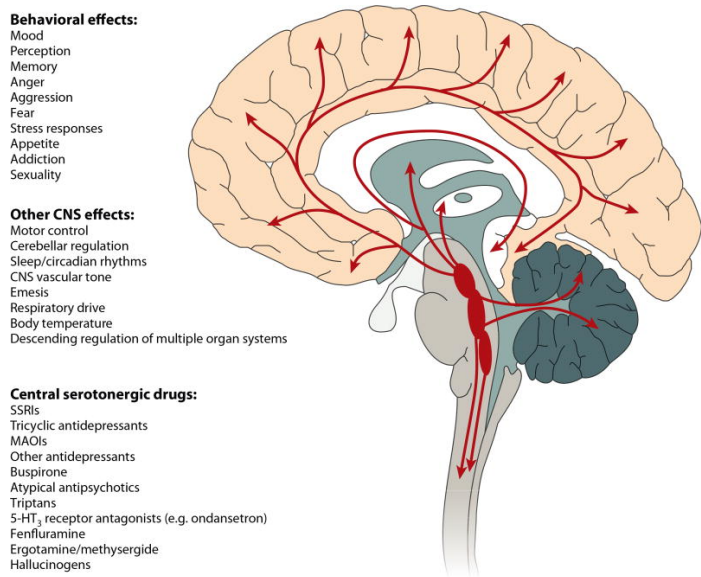


Figure 1.11: Serotonergic brainstem projections into all areas of the brain. The ubiquitous nature of serotonin (5-HT) plays a role in every facet of the central nervous system and beyond. Reproduced with permission from (BERGER; GRAY; ROTH, 2009).

Dopamine, or DA, is most associated with the mesolimbic pathway, more commonly referred to as the reward pathway. This pathway from the ventral tegmental area (VTA) synapses into the nucleus accumbens (NA) and prefrontal cortex, releasing dopamine into these regions in a pleasure- or reward- seeking manner. Dopamine has also been implicated in the modulation of behaviors such as cognition, motor functions, internal motivation, and circadian rhythm (**Figure 1.12**) (CALABRESI; PICCONI; TOZZI; DI FILIPPO, 2007). Similarly, TBI has been shown to affect a plethora of dopaminergic processes. In a fluid percussion injury (FPI) model in rats, there was significant loss of dopaminergic neurons (tyrosine hydroxylase, or TH⁺) at the substantia nigra 4 weeks after injury, concurrently with altered dopamine metabolism and microglia activation of inflammation (VAN BREGT; THOMAS; HINZMAN; CAO *et al.*, 2012). The altered properties of dopamine after TBI are associated with behavioral changes, as aggression and irritability have been reported in humans (HAMMOND; BICKETT; NORTON; PERSHAD, 2014) and motor dysfunction in rats (HUANG; TSUI; KUO; TSAI *et al.*, 2014). TBI-induced imbalances in serotonin may lead to overstimulation of the mesolimbic pathway, thus promoting excessive efforts to seek out pleasure, a behavior that often precedes addiction and substance abuse. (SHINODA; YANO; NAKAYAMA, 2021) (ALCARO; HUBER; PANKSEPP, 2007) (LEWIS; FLORIO; PUNZO; BORRELLI, 2021). The roles of serotonin and dopamine are heavily linked in the brain structures and behaviors of the central nervous system. Taken together, the current field of knowledge undoubtedly suggests TBI impacts both

serotonin and dopamine functionality, contributing to the complex pathophysiology of secondary mechanism of injury.

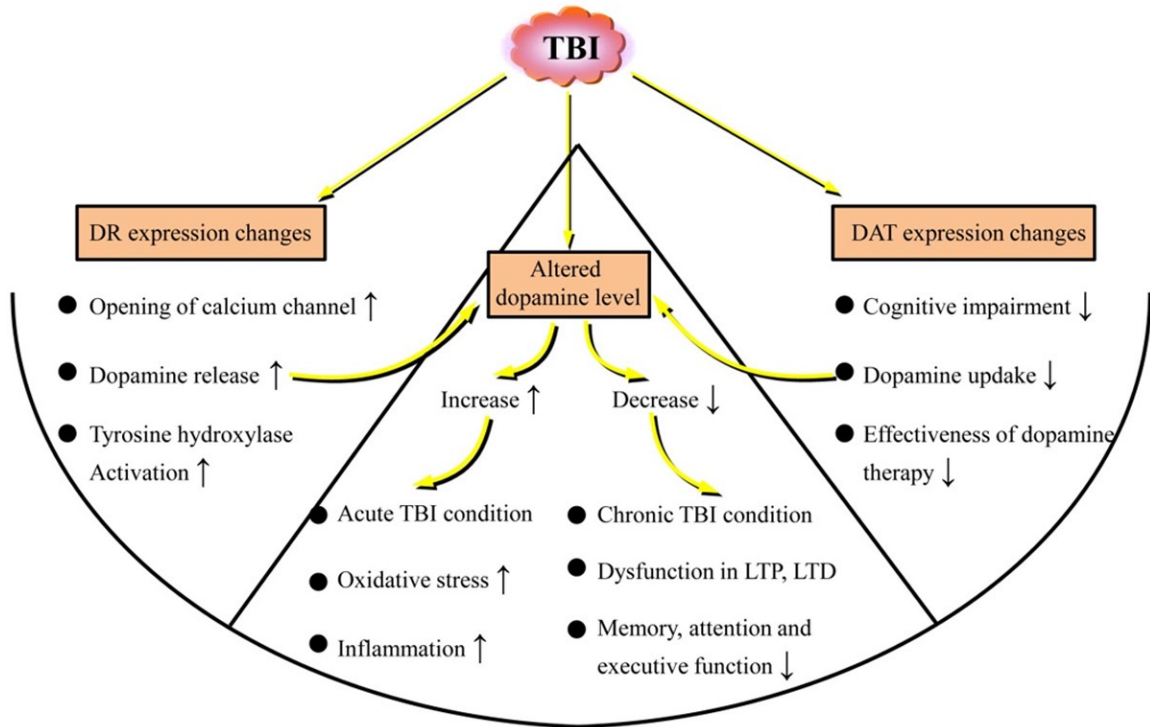


Figure 1.12: Alterations of dopamine after TBI. Various models of TBI have shown wide ranging negative consequences associated with dopamine. The dysregulation of this important neuromodulator can be seen in the manifestation of cognitive, motor and executive decision symptoms in patients. Reproduced with permission from (LAN; LI; LOU; MA *et al.*, 2019).

Cell death

Two main categories of cellular death are apoptosis and necrosis. Under normal conditions, apoptosis, or programmed cell death, functions to remove unnecessary or damaged neurons in a systematic manner with minimal activation of the inflammatory response. On the other hand, necrosis is the unregulated and sudden rupturing of cells, leading to massive swelling and upregulation of inflammatory signals. The overlapping crosstalk between apoptosis and necrosis

has been shown to be regulated by mitochondria through the interactions with the B cell lymphoma-2 (BCL-2) family proteins and the intrinsic pathway, thus it requires stringent control to regulate these two divergent processes.

Excessive apoptosis due to TBI is harmful and plays a role in the previously established secondary injuries mechanism neuroinflammation and neuromodulator dysfunction (**Figure 1.13**). Mitochondria activates various intrinsic pathway signals by interacting with BCL-2 related proteins such as cytochrome C, apoptosis-inducing factor (AIF), endonuclease G, and second mitochondria-derived activator of caspase (Smac), promoting the release of pro-apoptotic proteins into the intracellular space. There are three main groups of BCL-2 family proteins: anti-apoptotic, pro-apoptotic, and BH-3 only proteins. The dynamic interplay between these three groups is highly dependent on the cellular signals involved; for example, cytochrome C binds with procaspase-9 and apoptotic protein-activating factor (APAF-1), forming the apoptosome which subsequently activates caspase-3, promoting apoptosis (LI; NIJHAWAN; BUDI HARDJO; SRINIVASULA *et al.*, 1997) TBI triggers necrosis through the accumulation of calpains, release of damage-associated molecular patterns (DAMPs), and pro-inflammatory cytokines. The latter two types of molecules act in feed-forward signaling to promote necrosis in surrounding cells (KROEMER; GALLUZZI; VANDENABEELE; ABRAMS *et al.*, 2009). A classic stimulator of necrosis is TNF along with its associated death receptors and signaling pathways like receptor-interacting protein kinases (RIPKs). TNF ligand activates subsequent downstream

effector proteins to form a transient complex called complex 1, which acts as a molecular ‘crossroads’ between apoptosis and necrosis.

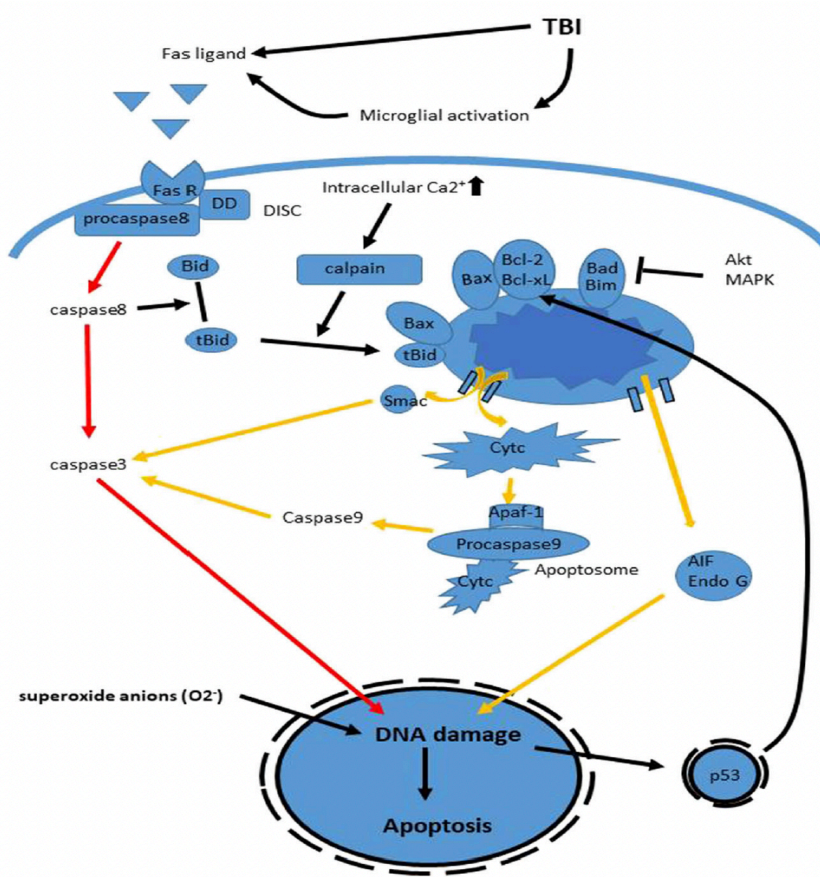


Figure 1.13: Intrinsic and extrinsic pathways of cellular apoptosis in TBI. Immediately following injury, the extrinsic pathway (red arrows) is activated by Fas ligands produced from microglial activation, which ultimately leads to caspase-dependent apoptosis. Intrinsic pathway (yellow arrows) features caspase-independent apoptosis in the form of AIF and Endo G, which translocate from the mitochondrial membrane to the nucleus, mediating DNA damage and subsequent apoptosis. Reproduced with permission from (AKAMATSU; HANAFY, 2020).

Cylindromatosis (CYLD) deubiquitination leads to the formation of complex 2a, which ultimately results in apoptosis. However, complex 1 can also be shunted towards the formation of complex 2b, leading to mitochondrial fragmentation and subsequent necrosis (**Figure 1.14**) (HU; XU; ZHANG; LI *et al.*, 2022)

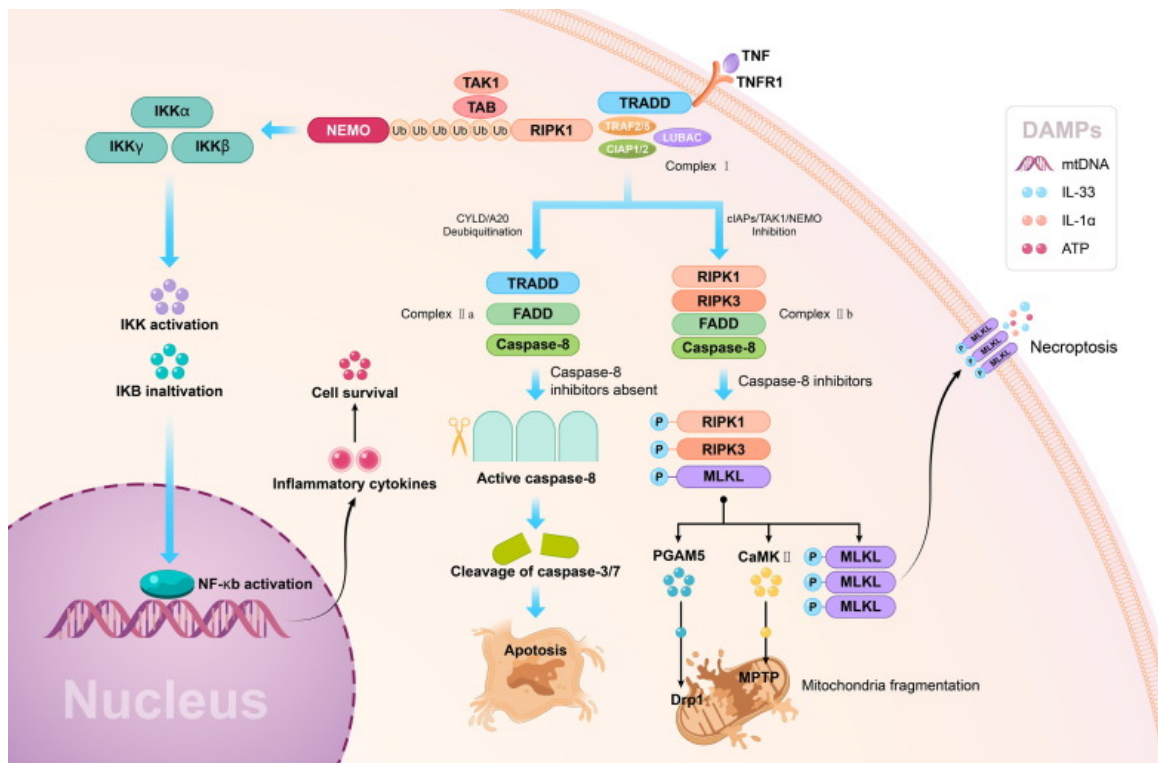


Figure 1.14: Necrotic cell death. This uncontrolled process causes the release of intracellular contents into the extracellular space, resulting in the upregulation of inflammatory signals and swelling. TNF is a classic initiator of this process, forming the transient complex 1. This complex can be shunted towards complex 2a (apoptotic), complex 2b (necrotic), or the activation of NF- κ B (cell survival). Reproduced with permission from (HU; XU; ZHANG; LI *et al.*, 2022).

Mitochondrial dysfunction

Mitochondrial dysfunction is characterized by the general defectiveness of mitochondria. Oxidative stress through reactive oxygen species (ROS), impaired cellular energy production, cellular metabolism, and the above-mentioned contributions to apoptosis are some of the processes associated with mitochondrial dysfunction. After injury, there is a sharp increase in ROS production from damaged neural cells, causing a bias in the highly regulated balance between ROS molecules and endogenous antioxidants such as superoxide dismutase and glutathione. With the imbalance after TBI, ROS overwhelms the antioxidants,

leading to subsequent damage of proteins, lipids, and DNA (**Figure 1.15**) (SALMINEN; PAUL, 2014) (KOSTYUK; POTAPOVICH, 2009) (NATHAN; CUNNINGHAM-BUSSEL, 2013). Additionally, ATP production and calcium buffering are impaired, thus overall bioenergetics of the cell is diminished. The large influx of ROS production causes the mitochondria to release the ROS in a 'burst' manner, which ultimately destroys the mitochondria itself. From this ROS induced apoptosis, a domino effect happens that may also affect nearby mitochondria, ultimately resulting in the destruction of the cell.

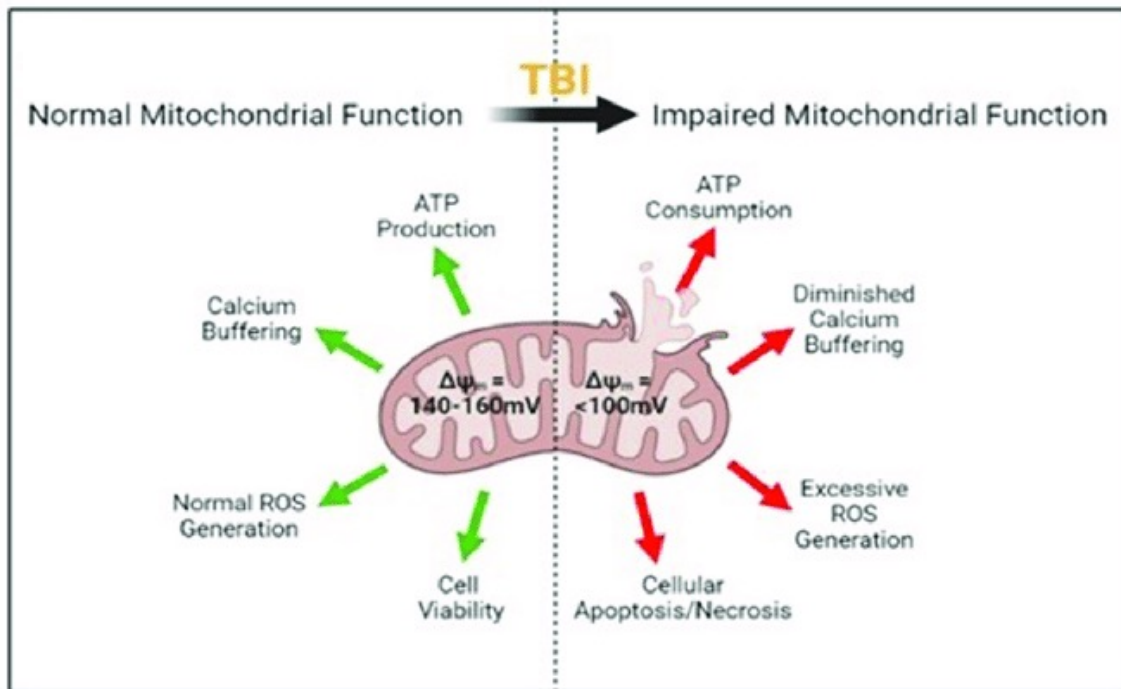


Figure 1.15: Mitochondrial dysfunction. A hallmark secondary mechanism of injury after TBI is mitochondrial dysfunction, resulting in excessive ROS generation. The inability of endogenous antioxidants like superoxide dismutase and glutathione to quench the increased ROS ultimately leads to the mitochondrial dysfunction and triggers cell death processes. Adapted and reproduced with permission from (KALIMON; SULLIVAN, 2021).

1.4 Current diagnosis of TBI

The current standards of diagnoses of TBI includes a neurological exam like the Glasgow Coma Scale (GCS) combined with an imaging modality such as computed tomography (CT) and magnetic resonance imaging (MRI). These assessments aim to evaluate the complex, multifaceted phases of injury as the disease progresses. Clinicians and healthcare professionals face the daunting task of correctly diagnosing the type, severity, and location of the injury, followed by the appropriate patient management treatment options. This deceptively straightforward course of action is anything but simple, as highlighted in previous chapters discussing the complexity of TBI induced neuropathology. From a diagnosis standpoint, earlier detection of a suspected head injury has proved vital to limiting the damage and speedier recovery (PREVENTION, 2019a; b; c; 2020). Neurological surgery intervention and additional procedures may be required depending on the severity of the TBI, as craniotomies and intracranial pressure probes are common for severely wounded patients.

Glasgow Coma Scale

The GCS is a 15-point scale that scores the patient's eye, verbal, and motor responses. Higher scores in the test are correlated with better outcomes and recovery (**Figure 1.16**) (NELL; YATES; KRUGER, 2000) (PREVENTION, 2020). The sum of the patient's score across all three categories is associated with the TBI severity, ranging from ≤ 8 as severe, 9-12 as moderate, and ≥ 13 as mild (PREVENTION, 2020). The extended GCS (GCS-E) is an adaptation to the original scale made specifically for mTBI (NELL; YATES; KRUGER, 2000). GCS-

E is used in combination with the amnesia scale to better parse out the nuances of mTBI. Briefly, the amnesia scale is scored between 0-7 and consistent with the GCS scoring convention, the higher scores indicate better performances (**Table 1.2**).

Behaviour	Response
 Eye Opening Response	4. Spontaneously 3. To speech 2. To pain 1. No response
 Verbal Response	5. Oriented to time, person and place 4. Confused 3. Inappropriate words 2. Incomprehensible sounds 1. No response
 Motor Response	6. Obeys command 5. Moves to localised pain 4. Flex to withdraw from pain 3. Abnormal flexion 2. Abnormal extension 1. No response

Figure 1.16: Glasgow Coma Scale. GCS assesses primarily 3 types of neurological responses- eye movement, verbal responses, and motor movement. A lower GCS score is correlated with a more severe head injury. Inter-rater reliability and subjectivity of responses are primary concerns to the consistency of the GCS. Reproduced with permission from (KNAPP, 2020).

Table 1: Amnesia Scale

Score
7. No amnesia: client can remember impact, can remember falling and striking a solid surface, etc.
6. Amnesia for 30 minutes or less: client regained consciousness while still in vehicle, in street at scene of incident, etc.
5. Amnesia of ½ hour to 3 hours: remembers being loaded into ambulance, in ambulance on way to hospital, arriving at emergency room, admission to ward, etc.
4. Amnesia of 3 to 24 hours: determine duration by content of the first memory, which will be for an event in the ward or other hospital procedure.
3. Amnesia of 1 to 7 days.
2. Amnesia of 8 to 30 days.
1. Amnesia of 31 to 90 days .
0. Amnesia greater than 3 months.
X. Cannot be scored, eg, can speak but responses are inappropriate or unintelligible, cannot speak because unconscious, intubated, facial fractures, etc.

Table 1.2: GCS-E amnesia scale. This scoring system was developed specifically to delineate the minute differences within mild TBI injuries as it is the most common severity of injury. Note that patients who score 12 or under may not qualify for the amnesia scale, but it may be used to inform during recovery process. Reproduced with permission from (NELL; YATES; KRUGER, 2000).

For patients with GCS scores of 12 or less, it is seldom the amnesia score can be applied, but GCS-E may be used to track amnesia through the recovery process. However, there are some limitations to the GCS and GCS-E assessments, starting with inter-rater reliability. This phenomenon is common amongst behavioral testing where scoring certain responses are subjective and may be up to the interpretation of the assessor (GREEN, 2011). In addition to the inter-reliability limitation, other confounding factors such as intubation, intoxication and altered mental states make it difficult to accurately assess the extent of the head injury. Lastly, numerous studies have shown GCS has a poor prognosis of the symptoms resulting from TBI (BALESTRERI; CZOSNYKA; CHATFIELD; STEINER *et al.*, 2004; GREEN, 2011; NELL; YATES; KRUGER, 2000). Although the GCS has its drawbacks, it remains the most widely used standard for initial neurological behavioral assessment of TBI.

Imaging modalities

Following the initial behavioral assessment and upon presentation into the hospital emergency room, the second arm of TBI diagnosis requires patients to undergo CT and/or MRI imaging diagnostics to reveal the underlying gross pathology as a result from head injury (CLINIC, 2021). Imaging tests provide a non-invasive method for clinicians to visualize the gross pathologies and if emergency craniotomy is needed to stabilize the patient (**Figure 1.17A**). Briefly,

CT scans use X-rays to give detailed internal images of the bone, organs, and tissues within a patient. The scanners contain detectors that measure the attenuations of X-rays as photons are beamed through the various layers of tissues and the results are processed using tomographic reconstruction algorithms to produce mainly three orientations of the patient- axial, coronal, and sagittal. The relatively fast and low-cost of CT scans make it a common first choice imaging diagnostic, combined with the compatibility of patients with metallic implants like pacemakers, a contraindication for MRIs. However, CT scans have their own limitations, as they require large, dedicated space for the equipment, and they require specialized personnel to operate the machine (FISHMAN; JEFFREY, 1995). Furthermore, the cost of the equipment is another limiting factor for hospitals or rural areas that may not have the resources to acquire a CT scanner. This limitation is further highlighted by frontline battlefield conditions for bTBI. Upon stabilization of the patient, clinicians may order MRIs as an additional follow up imaging diagnostic.

In addition to CT imaging, MRIs are also utilized in the diagnosis of TBI patients. MRI takes advantage of magnetic fields and gradients to generate detailed images of the organs in the body, providing a better contrast of soft tissues (i.e. brain) in comparison to CT (**Figure 1.17B**). Briefly, most clinical and research MRI scans use hydrogen atoms to generate the polarization spin within all the tissue layers of the body, and this spin induces a radio signal that can be picked up by detectors in the machine. Functional MRI (fMRI) is an adaptation that measures brain activity by tracking cerebral blood flow. Brain activity and blood

flow are coupled, thus higher activity in specific areas of the brain will result in increased blood flow to that region (HUETTEL; SONG; MCCARTHY, 2009). fMRI is particularly useful in tracking which regions of the brain may be affected post TBI, informing clinicians on the location, functionality, and pathophysiology of the injury. As with CT scans, MRIs have their own limitations, including the cost-effectiveness of such a diagnostic imaging test, the potential for overdiagnosis, speed of test, and as previously mentioned, the incompatibility with any metallic implanted device (SMITH-BINDMAN; MIGLIORETTI; JOHNSON; LEE *et al.*, 2012). Even with excellent healthcare insurance, MRIs can cost almost double (\$400- \$3,000) the amount for CT scans and studies have shown there may be a factor of diminishing returns with additional imaging tests after the initial CT scan (SMITH-BINDMAN; MIGLIORETTI; JOHNSON; LEE *et al.*, 2012). Additionally, an important MRI contraindication is implanted metallic devices, as the strong magnetic fields from the machine will cause any metal object in its proximity to malfunction or worse, create a dangerous projectile missile. While useful in detecting gross pathologies, skull structure, and cerebral blood flow activity, imaging modalities fail to capture the more nuanced pathologies associated with TBI, thus novel forms of detection and assessment are needed.

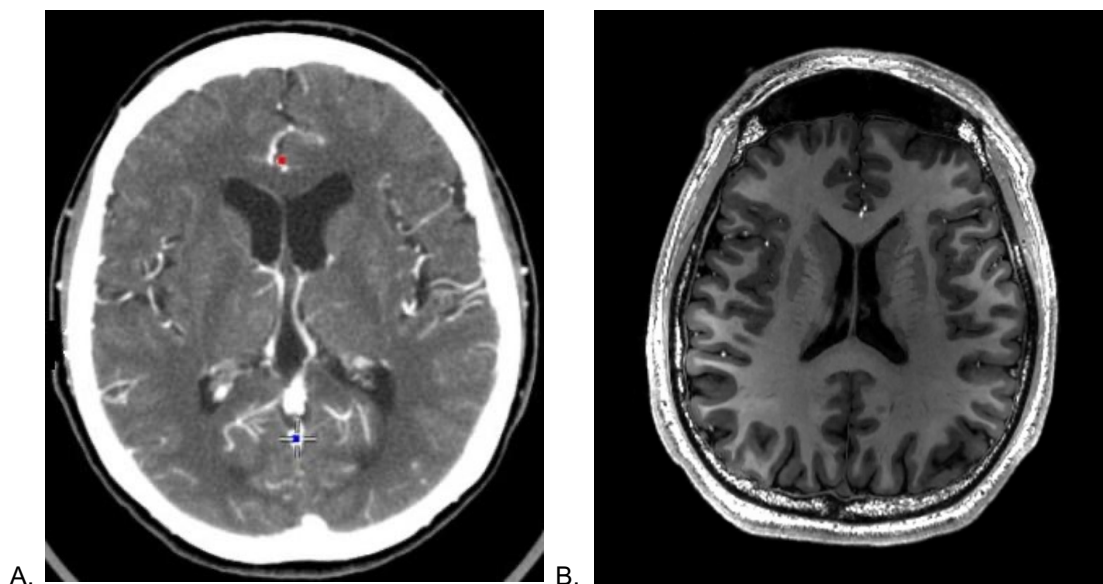


Figure 1.17: CT and MRI scans of the brain. A. Coronal cross section CT slice of the brain. The skull, brain, and cavities within the tissues are delineated by X-rays that detect the attenuation of photons when beamed through the patient. B. Coronal cross section of MRI slice of the brain. Finer details like the gyrification (folds) of the brain are more evident as MRIs use magnetic fields to create detailed images of soft tissue. Reproduced with permission from (SINAI, 2023) and (WIKIPEDIA, 2023).

Current treatments for TBI

To this day, there are no known drugs or compounds that are specifically prescribed to treat TBI. Over the last decade, there have been many therapeutics that have failed Phase II or III clinical trials due to the lack of consistent improvement for outcomes of patients (XIONG; MAHMOOD; CHOPP, 2009). Some notable examples of classes of compounds include erythropoietin (EPO), carbamylated form of EPO (CEPO), statins, bone marrow stromal cells (MSC), progesterone, dexamethasone, and rivastigmine (XIONG; MAHMOOD; CHOPP, 2009). Compounds like EPO to MSC and progesterone aimed to promote neuroprotection, neurogenesis, angiogenesis, and axonal regeneration. (XIONG;

MAHMOOD; CHOPP, 2009). Clinicians and healthcare professionals may also combine prescription medication along with rehabilitative physical and cognitive therapies to improve patient recovery and quality of life (QoL) (DEVELOPMENT, 2020). In most mTBI cases, patients recover most, if not all, of their previous cognitive and motor functions with little to no permanent disabilities. However, cognitive behavioral therapy aims to reduce the psychological damage from the incident in which patients may struggle to cope with. The social and economic burdens for treatment of head injury patients are often long lasting, requiring support from all levels of society. Overall, there is a need for improvement of current diagnostic capabilities and novel treatments are to better serve the TBI patient population.

Chapter 2. Extracellular vesicles

Extracellular vesicles (EVs) is the collective name of nanosized membrane vesicles that are released by most, if not all types of cells, into the extracellular environment (HESSVIK; LLORENTE, 2018; RAPOSO; STOORVOGEL, 2013; YÁÑEZ-MÓ; SILJANDER; ANDREU; ZAVEC *et al.*, 2015). The three main categories of EVs are exosomes, microvesicles, and apoptotic bodies; with each type of EVs displaying both unique and overlapping characteristics that present exciting challenges for this growing field. EVs have also been labeled by other names such as ectosomes, but here we will adhere to the latest guidelines proposed by the International Society of Extracellular Vesicles (ISEV) regarding the nomenclature, isolation, separation, characterization and functional studies of EVs (THÉRY; WITWER; AIKAWA; ALCARAZ *et al.*, 2018).

Originally believed to be “platelet dust” by Wolf over 50 years ago, the field has evolved and grown to appreciate the complexity in cellular, molecular and biophysical properties of these nanosized membrane vesicles (WOLF, 1967). EVs are non-replicable, round molecules ranging in size from the smallest (~50 nm) to the largest (>1 μm) with a lipid bilayer that houses the cargo contents from the origin cell of secretion. EVs have been shown to participate in a wide range of cellular processes across a plethora of scientific fields ranging from neurodegeneration to cancer to immunology and even TBI (BUZAS, 2023; CHANG; CERIONE; ANTONYAK, 2021; DONG; DONG; ZHANG, 2023; RAGHAV; ASHRAF; JEONG, 2022; RAGHAV; SINGH; JEONG; GIRI *et al.*, 2022; RAPOSO; STOORVOGEL, 2013).

The latest ISEV guidelines were introduced mainly in response to the initial attempts of EVs classification led to incongruities and confusion amongst the field. Namely, the nomenclature has been a highly debated topic due to the lack of consensus on specific markers of each type of EVs, thus assigning EVs to a particular class was challenging. For example, the previous definition of exosomes were vesicles of 40-150 nm in size that are released from multivesicular endosomes (MVE) fusion with the plasma membrane (HARDING; HEUSER; STAHL, 1984; PAN; TENG; WU; ADAM *et al.*, 1985; TRAMS; LAUTER; SALEM; HEINE, 1981). On the other hand, microvesicles are created by the direct folding and outward blebbing of the cellular plasma membrane, ranging from 100- 1,000 nm in size. Finally, apoptotic bodies are formed in the late stages of apoptosis and are the largest of the three classes with sizes ranging from 1- 5 μm (STÅHL; JOHANSSON; MOSSBERG; KAHN *et al.*, 2019). The original nomenclature relied on pathways of secretion and sizes to define EVs, but studies have repeatedly shown significant overlap between the categories of EVs, rendering the previous attempts to classify the particles challenging (RAPOSO; STOORVOGEL, 2013; THÉRY; WITWER; AIKAWA; ALCARAZ *et al.*, 2018). Therefore, the new guidelines aim to describe EVs by their physical characteristics, such as size (small, medium, large EVs) with ranges defined (< 150 nm, 150-250 nm, and 250 < nm, respectively), biochemical composition (CD63⁺, CD9⁺, CD81⁺), and descriptions of their cellular origin (neuronal, microglial, lymphocytic) (THÉRY; WITWER; AIKAWA; ALCARAZ *et al.*, 2018). For example, a particular type of EVs may be described as small, 50 nm in diameter, CD63⁺ of neuronal origin.

Therefore, the term “extracellular vesicles” in this document will be used as a blanket term to encompass exosomes, microvesicles, and apoptotic bodies unless otherwise specifically noted.

The ubiquitous nature of EVs, combined with their ability to protect their cargo contents from degradation, are some key factors that make them highly attractive targets for potential therapeutic applications. Indeed, EVs have recently been touted and explored as a method of drug delivery, biomarker discovery, diagnostics, and others (MURPHY; DE JONG; BROUWER; WOOD *et al.*, 2019; RAGHAV; JEONG, 2021).

2.1 Biogenesis of EVs

The biogenesis involved in the secretion of the three different classes of EVs are distinct, yet some elements may overlap as previous studies have suggested. This has led to heated debates of characterization and classification of these heterogenous vesicles, but recent advances and ISEV’s position statement has gained consensus in the field. The most well characterized class remains exosomes, while more studies have now turned towards microvesicles and apoptotic bodies.

Exosomes

Exosomes start off in the endosomal system, initially as intraluminal vesicles (ILVs) inside multivesicular bodies (MVBs) (KOWAL; TKACH; THÉRY, 2014). These molecules have bipartite fates: degradation through fusion with lysosomes or merging with plasma membrane for the release of exosomes into the

extracellular space (**Figure 2.1**). The formation of MVBs has been shown to be mediated by the presence of perfringolysin and cholesterol, where lipid rich MVBs are trafficked to the plasma membrane for release, but the cholesterol poor MVBs without the toxin are destined for lysosomal degradation (MÖBIUS; OHNO-IWASHITA; VAN DONSELAAR; OORSCHOT *et al.*, 2002). Furthermore, the discovery of the endosomal sorting complex responsible for transport (ESCRT)-0, 1, 2, and 3 complexes partly unveiled the mechanistic machinery behind the biogenesis of MVBs. ESCRT-0, 1, and 2 complexes recognize and sequester ubiquitinated proteins at the early endosome formation stage, while ESCRT-3 is responsible for membrane budding and release of exosomes (HURLEY; HANSON, 2010; RAIBORG; STENMARK, 2009). However, further investigation revealed that cells have ESCRT-independent pathways, as seen in the conversion from sphingomyelin into ceramide by oligodendroglial cell lines, which is consistent with the observation of enrichment of ceramides in exosomes (TRAJKOVIC; HSU; CHIANTIA; RAJENDRAN *et al.*, 2008; WUBBOLTS; LECKIE; VEENHUIZEN; SCHWARZMANN *et al.*, 2003). The process of exosomes release appears to be partly regulated by the coordination of the cytoskeleton, motor proteins, and fusion proteins. Examples like Rab GTPases like Rab 11 and Rab27 have been shown to be crucial in exosome secretion in reticulocyte and HeLa cell lines, respectively. (OSTROWSKI; CARMO; KRUMEICH; FANGET *et al.*, 2010; SAVINA; VIDAL; COLOMBO, 2002).

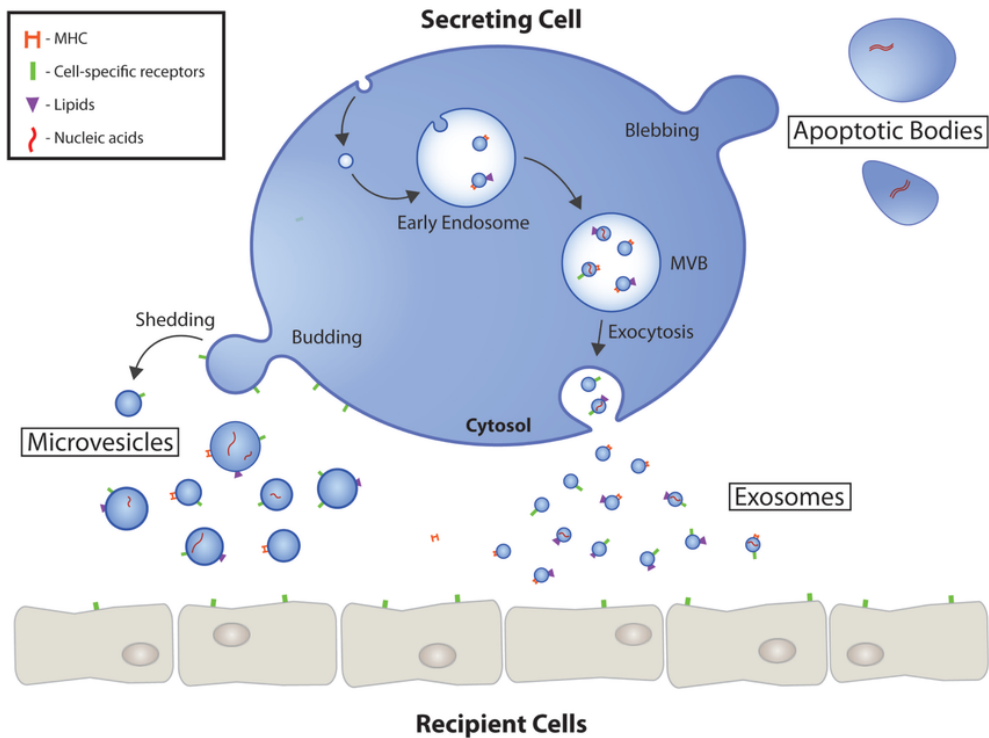


Figure 2.1: Schematic of EVs release into the extracellular space. Microvesicles are formed by the budding directly off of the plasma membrane while exosomes are created inside multivesicular bodies/endosomes (MVBs/MVEs). These bodies typically have two fates: trafficked to lysosomal degradation or to the plasma membrane for exosomes release. Microvesicles are mediated by phospholipid distribution and cytoskeletal proteins. Apoptotic bodies are formed during programmed cell death which are partly regulated by actin-myosin membrane blebbing. Reproduced with permission from (GUSTAFSON; VEITCH; FISH, 2017).

Microvesicles

The largest of the extracellular vesicles are apoptotic bodies and unlike exosomes or microvesicles, these large vesicles are only generated by plasma membrane blebbing of apoptotic cells (GUSTAFSON; VEITCH; FISH, 2017). However, it remains unclear the exact mechanism of apoptotic bodies formation, but membrane blebbing is partly mediated by actin-myosin interactions (COLEMAN; SAHAI; YEO; BOSCH *et al.*, 2001). As programmed cell death occurs and the disintegration of the cellular content, apoptotic bodies have been shown

to encapsulate organelles (TAYLOR; CULLEN; MARTIN, 2008). During normal development, most apoptotic bodies are degraded by macrophages. This clearance is mediated by receptor specific interactions between recognition receptors on phagocytes and the surface of the apoptotic cell's membrane. The most well-characterized examples involve the translocation of phosphatidylserine to the outer leaflet of the plasma membrane, where they bind to Annexin V, eventually leading to the degradation of these vesicles. Other examples include thrombospondin and C3b, both of which are recognized by phagocytes after their respective oxidation modification (ERWIG; HENSON, 2008). It is worth noting that apoptotic bodies are not ideal sources of biomarkers as they are actively phagocytosed and degraded by macrophages and lysosomes. These studies suggest that while some characteristics of apoptotic bodies are known, much remains to be discovered for this relatively understudied class of EVs.

As highlighted above, the three separate classes of EVs have similar, yet overlapping pathways to biogenesis. From ESCRT-mediated to ESCRT-independent pathways, the diverse amount of cellular and molecular processes of EVs highlights the complexity of biogenesis. Likewise, the biomolecule contents packaged inside are also diverse and may influence subsequent cellular function and processes.

2.2 Contents of EVs

A unique and key characteristic of EVs structure is their lipid bilayer plasma membrane, protect their cargo from degradation by DNAses, RNAses, and proteases present in body fluids. This critical feature allows the intercellular

communication via EVs between both nearby and distant cells. EVs have been shown to carry a wide variety of cargo ranging from proteins to DNA, RNA, lipids, metabolites, and others (RAPOSO; STOORVOGEL, 2013; VEZIROGLU; MIAS, 2020). Proteins like Rab GTPases, Annexins, flotillin and Alix are highly enriched in EVs populations due to the endosomal origins, along with protein microdomains that cluster together on the plasma membrane. These grouped proteins are often from the tetraspanin superfamily and have been proposed as specific markers for EVs subtype populations; however, a consensus has yet to be reached due to overlaps in marker specificity. The most common members from this superfamily of transmembrane proteins are CD63, CD81, and CD9 (VEZIROGLU; MIAS, 2020). EVs also contain lipid rafts, which are microdomains that are enriched in multiple lipoproteins and saturated fats including cholesterol, glycosylphosphatidylinositol, and sphingomyelin. Previous studies have shown the enrichment of these lipid rafts in EVs and may partially explain the bias towards exosome secretion instead of microvesicle budding at the early MVE stage (RAPOSO; STOORVOGEL, 2013). Lastly, the versatility of EVs packaging can be seen as previous studies have shown various types of nucleic acids in both DNA and RNA forms are enriched in EVs.

DNA

Before 2014, only single stranded DNA (ssDNA), mitochondrial DNA (mtDNA) and repetitive transposons were described in EVs (BALAJ; LESSARD; DAI; CHO *et al.*, 2011; GUESCINI; GENEDANI; STOCCHI; AGNATI, 2010). The discovery of double stranded DNA (dsDNA) in EVs released by cancer cells was

an important discovery as this suggested dsDNA can be a diagnostic marker of cancer cell properties. (GHANAM; CHETTY; BARTHEL; REINHARDT *et al.*, 2022). Both small fragments (~100 bp) to large (~10 kb) nuclear DNA (nuDNA) and mtDNA have been found in EVs (KAHLERT; MELO; PROTOPOPOV; TANG *et al.*, 2014; THAKUR; ZHANG; BECKER; MATEI *et al.*, 2014). It has long been postulated that EVs package cytoplasmic damaged or unwanted DNA fragments; this has been demonstrated by the loading of harmful cytoplasmic DNA for excretion or lysosomal degradation to protect cellular homeostasis (TAKAHASHI; OKADA; NAGAO; KAWAMATA *et al.*, 2017). Inhibiting EVs secretion results in the accumulation of the damaged or unwanted DNA fragments, triggering the cytoplasmic inflammatory pathway cGAS/STING and inducing apoptosis through the NLRP3 pathway (**Figure 2.2**) (ZHENG; LIU; XIA; CHEN *et al.*, 2023). Release of EVs containing mtDNA have been shown to be potential markers for cellular response to insult or injury in both neurological and non-neurological models REFS NEEDED. We have showed that low level oxidative stress enhance relase of EVs containing mtDNA from retina pigmented epithelial cells that are capable of activating microglia (REF). More in-depth details on RPE's EVs DNA content are discussed in the results section (**Chapter 5**).

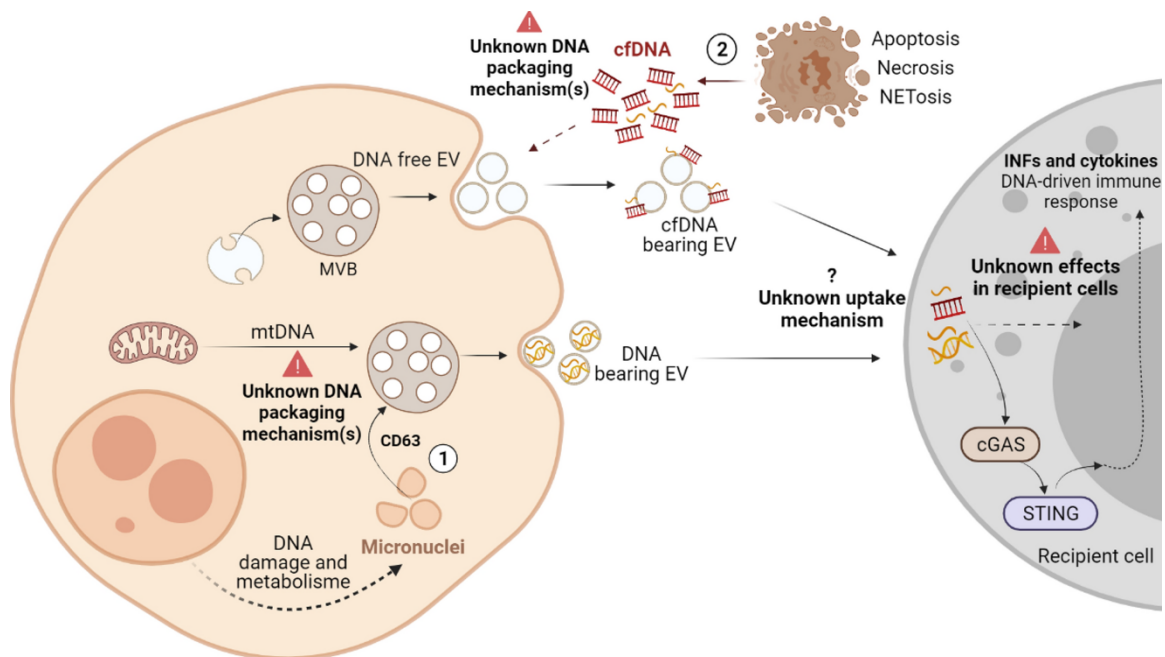


Figure 2.2: DNA origins and unknown packaging mechanisms. The current body of knowledge on the exact mechanisms of DNA packaging within EVs remains nascent, with some proposed mechanisms like micronucleated cells, mitochondria, cell free DNA (cfDNA), and MVE mediated by tetraspanins (i.e. CD63). Uptake by recipient cell of damaged DNA may induce cGAS/STING pathway as a host inflammatory defense against cellular damage. Reproduced with permission from (GHANAM; CHETTY; BARTHEL; REINHARDT *et al.*, 2022).

RNA

DNA is not the only form of nucleic acid that has been found within EVs; similarly, different forms of RNA are also present in EVs ranging from messenger RNA (mRNA) to micro-RNA (miRNA). For example, breakthrough papers on mRNAs delivered via EVs are associated with cellular changes like increased protein translation (RATAJCZAK; MIEKUS; KUCIA; ZHANG *et al.*, 2006; VALADI; EKSTRÖM; BOSSIOS; SJÖSTRAND *et al.*, 2007). However, these findings fail to directly show whether these cellular changes are indeed RNA-dependent or driven by an alternative mechanism resulting from EVs cargo delivery. Studies utilizing

RNA-seq and computational algorithmic analysis have attempted to answer these critical questions by characterizing the RNA content. For example, an unbiased deep sequencing approach demonstrated ncRNA, structural RNA, and transfer RNA (tRNA) are present, but again fail to establish causality of changes due to RNA (BELLINGHAM; GUO; COLEMAN; HILL, 2012; NOLTE-'T HOEN; BUERMANS; WAASDORP; STOORVOGEL *et al.*, 2012). On the other hand, miRNAs, which are ~20 bp long and can modulate gene expression by mRNA silencing and translational activation, are the most well characterized type of RNA in EVs. There is strong evidence that miRNA composition in a given liquid biopsy is reflective of the health status of patients, including pregnancy, cancer, neurological disorders, diet and exercise (KONSTANTINIDOU; MOUGIOS; SIDOSSIS, 2016; ROME, 2015; WEBER; BAXTER; ZHANG; HUANG *et al.*, 2010). Indeed, miRNAs packaged within EVs in human liquid biopsies have been proposed as potential diagnostic tools for high-risk clinical applications like cancer, where frequent sampling can provide crucial information into patient status. Similar to miRNA in relative abundance and potential impact, tRNA are known regulators of translation by binding to ribosomal subunits and tRNA synthetases (MLECZKO; CELICHOWSKI; BAŁKOWSKA-ŻYWICKA, 2018). Their importance has been demonstrated by the apparent mediation of T-cell activation and cytokine release, along with skeletal muscle homeostasis. The wide variety of RNAs and selective enrichment of certain types suggests there are mechanisms that regulate which RNAs are packaged into the EVs. For example, some proposed mechanisms of this selectivity stem may be from specific sequence motifs that may act as targets

for EV packaging (BATAGOV; KUZNETSOV; KUROCHKIN, 2011) and that the ESCRT-2 is an RNA binding complex (IRION; ST JOHNSTON, 2007).

Proteins

Proteins are also carried within EVs and may offer valuable insight into the physiological state of the cell. Similar to the other cargo types, a wide range of proteins can be found within EVs depending on their sizes. The most popular and comprehensive method of analyzing protein content in these particles is mass spectrometry, which allows the researcher to examine specific protein content differences (targeted proteomics) or a hypothesis-free driven process (global proteomics). The latter approach provides an ideal way to potentially discover novel biomarkers for different diseases including TBI. Indeed, several previous studies have highlighted the usefulness of proteomics in addressing the role of EVs in the TBI disease process (DONG; DONG; ZHANG, 2023; FLYNN; LEETE; SHAHIM; PATTINSON *et al.*, 2021; GUEDES; DEVOTO; LEETE; SASS *et al.*, 2020). For example, a previous study by Manek *et al.* used global mass spec to elucidate the comprehensive protein profiles of EVs from TBI patients' CSF. The authors found that EVs from TBI patients had both more statistically significant proteins and abundance. The classes of proteins and their respective biological pathways include complement factors involved in the inflammatory response, apolipoproteins and the transport of lipids and BBB repair, and mitochondrial heat shock proteins involved in mitochondrial function (MANEK; MOGHIEB; YANG; KUMAR *et al.*, 2018). A critical challenge of measuring blood-based protein biomarkers may include low levels in the periphery, as in the case of tau

(BOGOSLOVSKY; GILL; JEROMIN; DAVIS *et al.*, 2016). Proteolytic degradation, permeability of the BBB, interstitial clearance are also other factors that can influence the levels of protein biomarkers in blood after injury. EVs are able to cross the BBB and bypass some of the aforementioned challenges, thus offering additional insight into the disease progression that blood-based biomarkers may lack. More in depth review of proteins in EVs with relation to TBI is discussed later in this chapter and in the results (**Chapter 5**).

Lipids and metabolites

Lipids and small molecule metabolites composition remain relatively understudied compared to the RNA and protein profiles. Many lipid species have been identified in EVs, including cholesterol, phosphatidylcholine, and sphingomyelin related compounds. As previously mentioned, lipids play a role in the biogenesis of the three classes of EVs, along with the distribution of lipid rafts and the subsequent bias of exosome secretion pathway. EVs lipid composition may be different than their origin cell of secretion, a possible clue into the potential mechanism of cell membrane homeostasis and the modulation of recipient cell membrane endocytosis or fusion (LYDIC; TOWNSEND; ADDA; COLLINS *et al.*, 2015; SKOTLAND; HESSVIK; SANDVIG; LLORENTE, 2019; SKOTLAND; SANDVIG; LLORENTE, 2017; SUBRA; LAULAGNIER; PERRET; RECORD, 2007). Furthermore, lipid composition may differentiate healthy vs. diseased states, as both *in-vitro* and *in-vivo* experiments have revealed normal or healthy controls have a distinct profile compared to tumorigenic or diseased patients (BRZOZOWSKI; JANKOWSKI; BOND; MCCAGUE *et al.*, 2018; TAO; ZHOU;

YUAN; ZHANG *et al.*, 2019). Pharmacological studies of phospholipid interactions have shown these molecules can have an affinity for G-protein coupled receptors and modulate their activities, thus the importance of the composition and relative abundance of lipids must be considered in the context of cellular changes in response to EV-mediated intercellular communication. Lastly, small molecule metabolites like amino acids, polysaccharides, and fatty acids have been identified using metabolomic analysis of EVs. Pathways like tRNA biosynthesis, nitrogen metabolism, and amino acid metabolism are all enriched in cancer derived EVs (EYLEM; YILMAZ; DERKUS; NEMUTLU *et al.*, 2020; VANDER HEIDEN; CANTLEY; THOMPSON, 2009; ZHAO; YANG; BADDOUR; ACHREJA *et al.*, 2016). Notably, these tumorigenic EVs can drive the Warburg effect, thus exacerbating the pathological diseased state. The growing body of evidence that EVs can carry metabolites that serve as nutrients or building blocks to influence cellular metabolism highlights the need for further investigation.

These aforementioned studies highlight the potential of EV cargos, in contributing to the knowledge base of TBI and other diseases (**Figure 2.3**). Furthermore, each type of cargo can be analyzed using different methods that may produce previously uncharacterized molecules, thus potentially providing exciting leads for future studies. Overall, the contents within EVs provide a window into the physiological state of cells in a non-invasive manner.

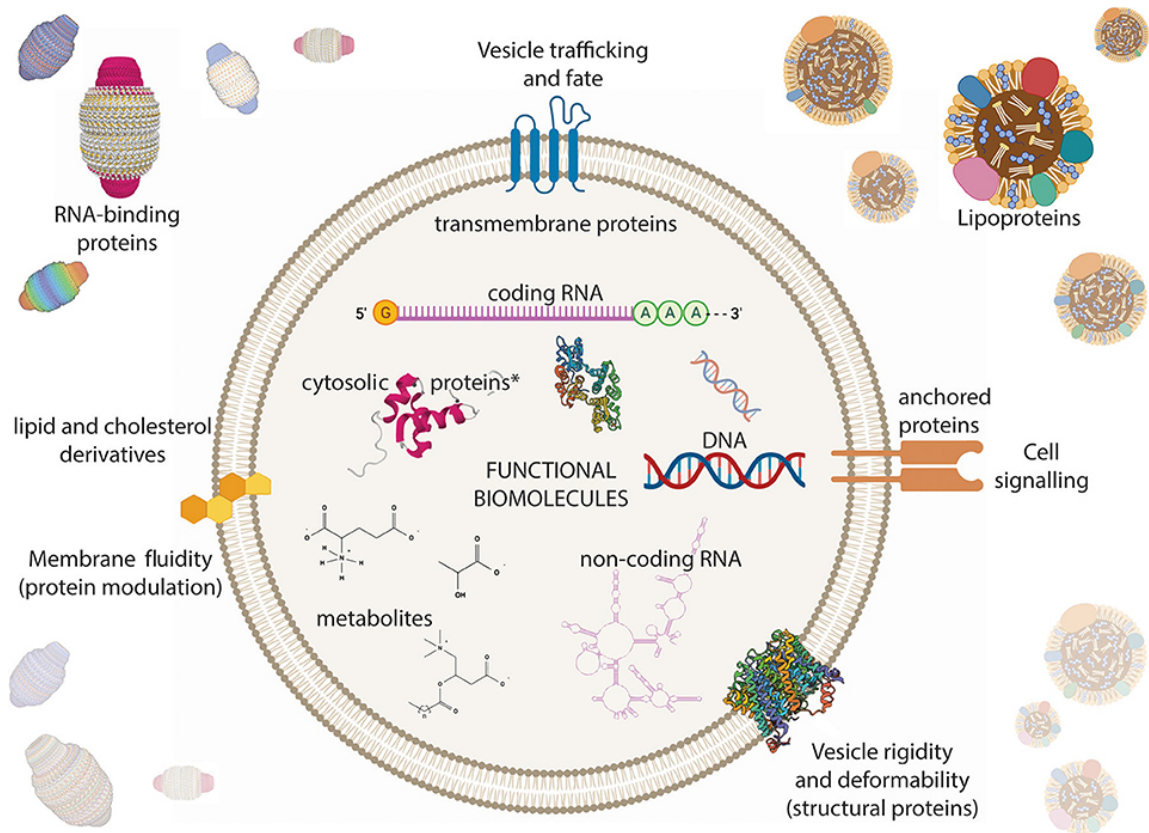


Figure 2.3: Summary of cargo and composition in EVs. Many different types of biomolecules can be found in the lumen or incorporated into the lipid bilayer of EVs, including nucleic acids in various forms (DNA, ncRNA, mRNA), proteins, small molecule metabolites (lipids, sugars, tRNA). Distinct populations and relative abundance of each type of cargo can often be distinguished between healthy vs. diseased samples, further emphasizing the fact EVs provide a snapshot into the cellular origin state. Transmembrane proteins (i.e. tetraspanins) and anchored proteins play roles in cellular trafficking, modulation of recipient cell intake and downstream cellular signaling. Reproduced with permission from (VEZIROGLU; MIAS, 2020).

2.3 EVs isolation techniques

Isolation techniques have been standardized by the Minimal Information for the Studies of EVs (MISEV) guidelines to ensure consistency in the field (THÉRY; WITWER; AIKAWA; ALCARAZ *et al.*, 2018). The first step of any EVs work is to identify the research needs and which appropriate isolation technique fits the approach. The techniques fall into four main categories: centrifugation,

precipitation, chromatography, and immunoaffinity. MISEV encourages authors to differentiate between EVs “separation” and “concentration” when discussing various approaches, but ultimately every technique has some form of both. Separation refers to selectively isolating one subtype of EVs from the pool of many, like using anti-CD63 capture beads, while concentration increases the EVs amount within the biofluid, but not necessarily discriminating one type from another. To this date, there is no single method that combines both high selectivity and high yield in one step. Moreover the type of biofluid, sample volume, cost, time, purity and yield are all important factors to consider when choosing the right experimental approach, as all approaches have pros and cons (THÉRY; WITWER; AIKAWA; ALCARAZ *et al.*, 2018). Furthermore, cell culture media is by far the most common biofluid; the guidelines warn that researchers using less well characterized sample fluids should take extra caution in the experimental approaches. Standardization of techniques is a key part in progressing the EVs field forward and should be noted in every research paper.

Centrifugation

Differential ultracentrifugation (DUC) is the primary and most popular method of EVs separation. The products of differential ultracentrifugation are dependent on the centrifugal force and time, thus EVs are enriched based on their size and density. This technique can be used with gradient columns like sucrose, cesium chloride, or more recently, iodixanol for researchers to isolate EVs with specific densities. Most DUC procedures contain incremental stepwise increases in spin speed and time, with the idea that each step isolates a specific EV fraction

(i.e., large, medium, small). For example, a typical DUC protocol may have a variation of the 3-step method: a first spin of 2,000 x g to remove cellular debris, organelles, and other waste products, followed by a second spin of 12,000 x g to isolate large/medium EVs, and finally a spin of 150,000 x g to harvest small EVs (**Figure 2.4**). The relative feasibility, adaptability, and cost-effectiveness make this technique the most accessible for most researchers. However, DUC does have several limitations. Firstly, DUC spins may take several hours to overnight from start to finish, which can prove cumbersome if many samples are required for DUC. Furthermore, there are no standardized protocols for this technique due to the differences in experiment setup (i.e., biofluid of interest), thus comparison across studies may be difficult to achieve. Lastly, DUC alone is not sufficient for high quality EVs separation studies due to overlapping physical characteristics of EVs (JEPPESEN; FENIX; FRANKLIN; HIGGINBOTHAM *et al.*, 2019), thus a combinatorial approach may be required if a highly specific fraction of EVs is required. Nonetheless, DUC is a mainstay technique in the field with most researchers adapting some form of DUC in their separation process.

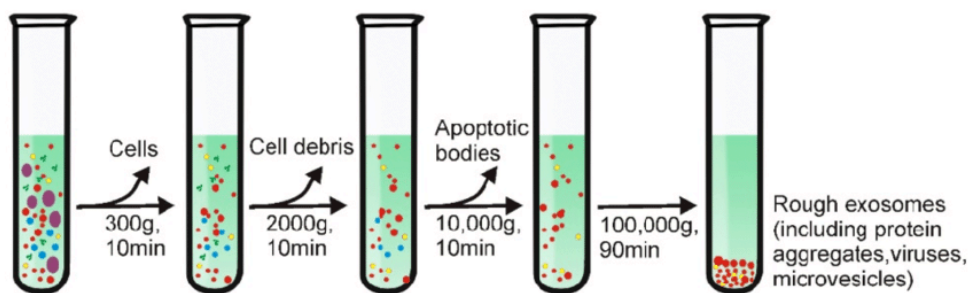


Figure 2.4: Example of a DUC protocol. Sample fluid is processed in a step-wise manner with increasing speeds and/or times to isolate EVs fraction of interest. Initial steps are taken to remove dead cells, debris or large organelles from sample fluid before ultracentrifugation for EVs. Reproduced with permission from (YANG; ZHANG; ZHANG; ZHANG *et al.*, 2020).

Precipitation

EVs separation by precipitation is an alternative technique that may prove advantageous over DUC. This technique's principle uses polymers (i.e. polyethylene glycol, PEG) to decrease the volume of solvent available, thus 'crowding' out the EVs of interest by increasing the native particle concentrations in the sample solution. Furthermore, manufacturer supplied kits are available for ease of use and the yields have been reported to be higher than DUC, thus making this an attractive option if sample volume is limited. Precipitation also avoids the potential shearing or damage from high centrifugal forces by only requiring conventional tabletop centrifuges with lower speeds and shorter spin times compared to DUC. However, just like DUC, precipitation does come with its own set of drawbacks that should be considered. Introducing a polymer into the sample solution promotes non-EVs protein aggregation that is co-precipitated with EVs and the polymer itself contaminates the sample, potentially hindering downstream experiments. For example, high concentrations or molecular weight of PEG can affect protein activities, promote cytotoxicity, and autophagy (PHAM LE KHANH; NEMES; RUSZNYÁK; UJHELYI *et al.*, 2022). Thus, researcher must remove the polymer agent from isolated fractions before proceeding. These EVs can be cleaned using column-based chromatography to remove the chemical and non-EVs aggregates. Precipitation is an attractive option to maximize yield from a small sample volume if purity of EVs fraction is not the highest priority.

Chromatography

A number of filtration methodologies exist to manipulate fluid samples on a very small scale (μL to pL). Filtration is the simplest method where the sample fluid is passed through a single or series of filters with nanosized pores. Depending on the size of the pores, certain sized EVs will be collected on the filter while the rest will pass through. Researchers often combine filtration with other techniques like DUC or precipitation to further enrich for specific sized EVs. Filtration is straightforward and simple in design, but suffers from potential filter clogging or EVs damage due to applied pressure. Non-EVs aggregates may also be filtered with the EVs of interest; thus, it is common to combine size exclusion filters with low protein binding polycarbonate membranes to reduce the contamination. Size exclusion chromatography (SEC) operates on a similar principle as filtration as the sample is passed through a column packed with porous resin beads of particular sizes. EVs that are able to fit in these pores are slowed due to their longer path to elution, while larger EVs can pass through faster (**Figure 2.5**). SEC's limitations are similar to filtration's namely due to the emphasis placed on size, thus any particles (i.e., lipoproteins, non-EV aggregates) may also be enriched with the target fraction (KARIMI; CVJETKOVIC; JANG; CRESCITELLI *et al.*, 2018). Researchers may overcome these potential problems by using different sized beads to further purify their fractions. On the other hand, affinity chromatography exchanges the porous beads of SEC for beads with specific affinity for certain particles. For example, these beads can be customized to attract only negatively charged molecules or have antibodies that target specific epitopes. The flow

through contains all unbound molecules, while the target fraction remains tightly bound to the beads. To elute the target molecules, a solution with comparable or stronger affinity to the beads is passed through the column, displacing the previously bound particles. Affinity based chromatography has added advantages over SEC, mainly in that the beads are highly customizable in regards to their composition and functionality (ACQUAH; DANQUAH; YON; SIDHU *et al.*, 2015). It should be noted that chromatography techniques often require large amount of sample volumes to pass through the columns, which may be a challenge if sample quantities are limited. However, despite its limitations, these can be combined with DUC or precipitation to further enrich and purify for the target EV population.

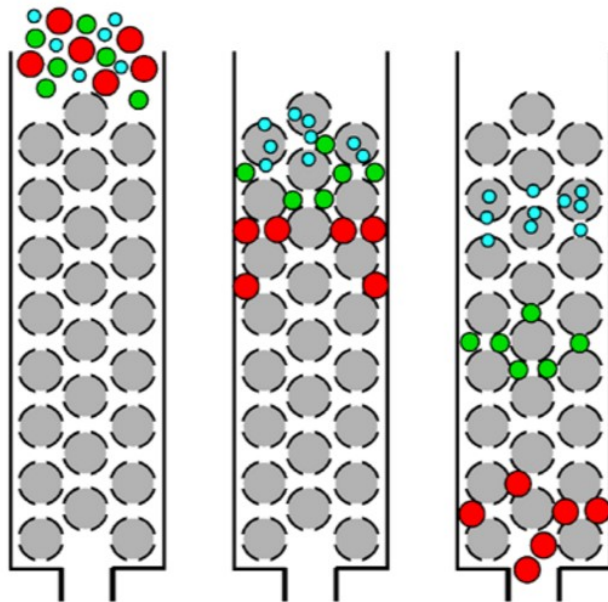


Figure 2.5: Basic principles of size exclusion chromatography. Beads (grey circles) inside a column contain pores of certain sizes which act to slow down EVs (blue circles) that enter them. This prolongs their path to elution; the retention time is increased inside the column. In contrast, biomolecules such as large lipoproteins (red circles) and small proteins (green circles) that do not fit inside the pores are able to take a more direct path to elution, shortening the amount of time they are present in the column. As a result, separate fractions according to retention times are enriched with different biomolecules. Reproduced with permission from (BARTH; BOYES; JACKSON, 1994).

Immunoaffinity

Immunoaffinity isolation is based on immunocapture principles where antibodies conjugated to beads are mixed with the sample. These beads bind to the target epitope on the surface of the EVs (i.e. CD63, CD81, CD9, Annexin, clathrin, etc.) and can be purified out of the sample. Once the beads are separated from the rest of the solution, they must be detached from the bound EVs. The crux of immunocapture-based techniques is the functionality of the conjugated antibody- the end result is highly dependent on how well the antibody recognizes and binds to the intended epitope; thus, the quality of the antibody is paramount. Furthermore, researchers must know beforehand the surface epitope(s), of the desired EVs. This key aspect may prove challenging in exploratory studies where comprehensive profiling of different subtypes of EVs requires an unbiased approach. Additionally, researchers may opt for customized antibodies to be conjugated instead, which will undoubtedly add to the cost of the assay. While biochemical capture by pull down can be highly specific and used to generate an ultrapure fraction, one must consider the aforementioned factors above and the aims of the project before utilizing immunocapture beads.

Isolation Method	Isolation Principle	Advantages/Limitations
Differential centrifugation	EV separation based on particle density, size and shape	<ul style="list-style-type: none"> - Commonly used; standardized; vesicle enrichment as pellet; EV subtypes isolation by density gradient centrifugation - Vesicle aggregation; protein and soluble factors contamination; low recovery; laborious
Polymer-based precipitation	EV precipitation using polymers altering solubility	<ul style="list-style-type: none"> - Easy and inexpensive; high yield; effective with small amount of starting material; preservation of bioactivity - Co-precipitation of protein contaminants and polymeric materials; not suitable for large scale studies; long incubation times
Size-exclusion chromatography (SEC)	EV isolation by gel filtration chromatography based on size	<ul style="list-style-type: none"> - Inexpensive; reproducible; high yield and purity; preservation of integrity and activity. - Specific equipment; not suitable for large scale studies; long run times.
Immunoaffinity capture-based techniques	EV immuno-purification using magnetic beads conjugated with antibodies direct toward specific EV surface markers	<ul style="list-style-type: none"> - Sensitivity; specificity; high purity; EV subtypes isolation. - Expensive; antibody cross-reactivity; low yield

Table 2.1: Summary of EVs isolation techniques. The most common types of EVs isolation techniques are listed with their respective pros and cons. Researchers should adapt, combine, and customize their isolation approach(es) to suit their experimental needs. Reproduced with permission from (CHIRIACÒ; BIANCO; NIGRO; PRIMICERI *et al.*, 2018).

2.4 EVs characterization techniques

A key step after separation and concentration of the desired EVs population is the characterization of the targets. Generally, there are two categories of types of characterization techniques: physical and biochemical. As proposed in the MISEV guidelines, researchers should aim to describe the subtype population with as many descriptive characteristics as possible (THÉRY; WITWER; AIKAWA; ALCARAZ *et al.*, 2018). Physical characterization techniques including light scattering based techniques such as nanoparticle tracking analysis (NTA) and optics-based methods such as transmission electron microscopy (TEM) aim to describe the sizes and concentration of EVs in the sample. Biochemical methods

such as mass spectrometry (MS), nucleic acid sequencing (i.e RNA-Seq), lipidomics or metabolomics have been developed to accommodate high throughput multiplexing of many samples of populations. Both physical and biochemical characterization approaches combine to accurately describe the EVs of interest and should be incorporated in downstream experiments post isolation.

Nanoparticle tracking analysis

NTA is one of the most common techniques to profile EVs. It relies on light scattering to reveal the properties associated with the sample population. A laser is beamed through the sample and based off the light refraction and Brownian motion of each particle, the size and concentration of each are recorded and analyzed by the software (**Figure 2.6**) (DRAGOVIC; GARDINER; BROOKS; TANNETTA *et al.*, 2011). Newer NTA technologies are capable of measuring particle charge under an applied electrical field, which can give insight into the possible membrane bound proteins that are associated with the particles. Notably, studies have suggested NTA may overestimate EVs sizes compared to TEM imaging, thus researchers should be cautious when interpreting their NTA results (BACHURSKI; SCHULDNER; NGUYEN; MALZ *et al.*, 2019). Furthermore, there are concerns that NTA has a detection limit of around 60-70 nm, thus it should not be the absolute reference for sizing.

Single particle interferometric reflectance imaging (SP-IRIS) is a newer optics-based approach that combines the light refraction principles of NTA with immunocapture antibodies. The sample fluid is applied to an antibody microarray chip before a beam of light is applied to the chip.

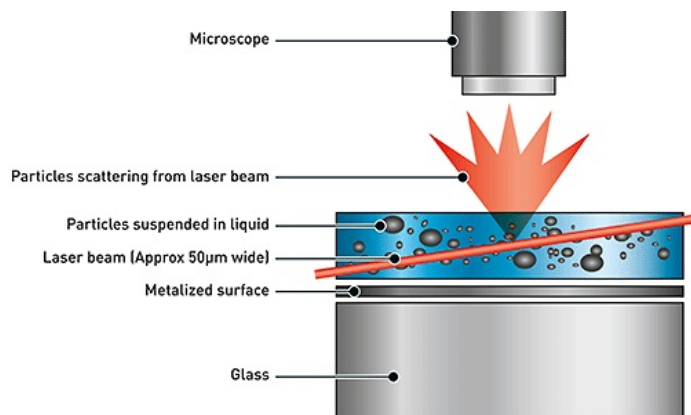


Figure 2.6: Schematic of nanoparticle tracking analysis (NTA). A laser is beamed into the sample fluid, causing light to refract off the particles. The light refraction properties and Brownian motion are detected through the microscope and analyzed. The size and concentration of each particle is calculated from the recorded videos. Reproduced with permission from (AZONANO.COM, 2015).

Refraction from the particles is collected and the properties of each particle within the chip is reported based on their respective locations. Even though SP-IRIS may be more accurate in measurements, NTA's distinct advantages over SP-IRIS are its label-free quantification and cost-effectiveness. As the number of options for physical characterization methods continues to expand, researchers are developing and innovating new techniques to better describe EVs size, morphology, and number.

Transmission electron microscopy

TEM is a microscopy technique in which a beam of electrons is passed through a sample to form an image. The sample is mounted on an ultrathin section of a copper mesh grid and can be stained with various dyes to provide contrast. The image is produced through the interaction of the electrons with the sample, which subsequently gets magnified and focused through a camera lens for a

detailed picture of the sample. Coupled with a high powered camera and software for analysis, samples can be quantified for their morphological properties like size and shape. TEM can be used to image EVs in liquid samples by negative staining with uranyl acetate to produce clear images of the particles. Depending on the capabilities of the microscope, images can be magnified many times over to provide clear pictures of the EVs. Although TEM is a good method of identifying EVs, it suffers from some limitations such as slow scanning speed and sample processing times, thus taking a long time to image for a large number of samples.

Mass spectrometry

Mass spectrometry is staple in many disciplines, and it is no surprise MS has been widely adopted as a viable biochemical characterization technique of EVs. MS studies have led to the many discoveries spanning various biological systems (GONZALES; PISITKUN; HOFFERT; TCHAPYJNIKOV *et al.*, 2009; MELO; LUECKE; KAHLERT; FERNANDEZ *et al.*, 2015; WHITHAM; PARKER; FRIEDRICHSEN; HINGST *et al.*, 2018). MS improves biomolecule discovery and identification which are crucial in elucidating potential biomarkers for therapeutic purposes. This technique has been proven to have a wider range of sensitivity than traditional antibody-based techniques, thus MS is able to detect proteins that may not be abundantly expressed but are potentially significant in the experimental context. (BRUNNER; THIELERT; VASILOPOULOU; AMMAR *et al.*, 2022; MEHTA; AHKAMI; WALLEY; XU *et al.*, 2022). It is worth noting that MS is commonly used for protein discovery and screening, whereas targeted immunoblotting (i.e. Western blot) can be used to specifically test for the presence of a particular protein

in the sample. MS studies can provide great insight into EVs components and are commonly combined with omics approaches to wholly describe EVs contents.

Nucleic acid sequencing

Next generation sequencing (NGS) technologies have become very advanced to provide a powerful tool applied in many different fields. An important feature of advanced sequencing technologies is not only the ability to detect lowly expressed sequences by increasing the depth of reads, but also the capability to generate large data sets in omics type approaches. One such omics type approach is RNA-Seq. As previously described, RNA contents are the most well-characterized cargo of EVs. RNA-Seq is now highly advanced with many adaptations, offering sensitivity to a wide range of transcripts such as non-coding RNA, mRNA, miRNA, and others (MCCOMBIE; MCPHERSON; MARDIS, 2019). Similar to MS, sample pre-processing steps like rRNA depletion or mRNA enrichment can help uncover low expression transcripts that may otherwise be undetected due to the amount of rRNA present in most samples. The depth of reads in RNA-Seq has also been improved, meaning the amount of times the samples are read is increased, thus increasing the likelihood of finding rare or novel transcripts (WEI; BATAGOV; SCHINELLI; WANG *et al.*, 2017). On the other hand, DNA based sequencing efforts have been understudied relative to its single stranded counterpart. Both nuDNA and mtDNA have been discovered in EVs, but the mechanisms surrounding the packing or roles of these types of DNA are still unknown. Further questions are raised in regards to how the DNA structure, intracellular origin, and localization affect downstream recipient cell processes.

mtDNA has been associated with inducing inflammatory pathways, presumably through an apoptosis-mediated mechanism. Akin to MS and proteins, NGS may be used to sequence and screen large amplicons, but targeted quantitative PCR (qPCR) approaches are used to test for particular DNA sequences. Overall, cell-free DNA in EVs has the potential to reveal new biological insights and serve as diagnostic biomarkers for diseases; DNA sequencing studies are well positioned to facilitate in these areas.

Metabolomics and lipidomics

Metabolomics and lipidomics are defined as the comprehensive analysis of metabolites or lipids in a biological specimen, respectively. Both have emerged to be powerful tools for researchers to understand the profile and distribution of these biomolecules and how they correlate with a healthy or disease state. To purify these biomolecules out of a EVs sample, isopropanol or methanol is used to separate the compounds from the rest of the fractions. Each fraction containing metabolites or lipids can be further purified using different chromatography techniques like reverse phase, hydrophilic interaction, carbon 18, etc. Finally, the purified samples can be analyzed by mass spectrometry to reveal potential novel compounds (CLISH, 2015). Similar to other omics approaches, these techniques are useful to determine specific EVs cargos.

2.5 Therapeutic and diagnostic applications of EVs

EVs key characteristics of stability in biofluids and ability to protect their cargo from degradation provide an exciting opportunity for potential translational

therapeutic applications in clinical settings. Indeed, advances in the field have attempted to exploit the advantages of EVs in translational settings as a means for targeted compound delivery and biomarkers of diseases. The promising potential of EVs can be seen across various fields of use ranging from diagnostic imaging, cardiovascular diseases, neurological diseases, cancer, and pulmonary disorders (KODAM; ULLAH, 2021). In addition to the variety of cargo, biodistribution patterns, distances of distribution, and ubiquitous nature of EVs, these biomolecules are able to cross the BBB, a crucial characteristic when specifically addressing neurological diseases like TBI. However, the lack of consensus of diagnostic biomarkers for TBI remains a challenge in the field. Many questions still remain to be addressed between the dynamics of EVs and how to leverage the advantages of EVs against the respective pathophysiology of diseases. Despite its limitations, EVs still offer unique potential to fill the gaps in TBI diagnostics and other therapeutic applications.

EVs as a vehicle for drug delivery

A concerted effort to engineer EVs as a drug delivery mechanism has resulted in some exciting results. In oncology, these biomolecules have been manipulated to deliver chemotherapeutic compounds (YANG; XU; GU; SHI *et al.*, 2022), antibody-based immunotherapy (NAJAFI; MAJIDPOOR; MORTEZAEI, 2023), or more recently, a combinatorial approach (CHEN; TAN; YANG; JIN, 2022). The traditional monotherapy treatment using one type of therapeutic often does not elicit the intended outcomes due to drug resistance, heterogeneity of cancer, and efficacy of the compound. These mitigating factors are part of the larger

challenge in the translational applicability using EVs as a drug delivery vehicle. Additional challenges come from the lack of clear understanding of the pharmacokinetic (PK) and pharmacodynamic (PD) profile of EVs. While EVs have been shown to package many types of biomolecules, much remains to be discovered in how therapeutic drugs interact with the intended cells/tissues when delivered by EVs (PK) and how the human body responds to this type of treatment (PD) (MURPHY; DE JONG; BROUWER; WOOD *et al.*, 2019). On top of the pharmacological concerns, controlling the biodistribution of the exogenous vesicles after administration has yet to be fully established. Lastly, the targeting, uptake and intracellular trafficking of EV-delivered compounds are unknown. Target specificity coincides with appropriate biodistribution; if EVs cannot reach the intended tissue or cells, target specificity is a moot point. Realistically, a high degree of bioengineering to customize and control every facet of EVs will be needed if these particles are to be used in real-world drug delivery applications.

EVs in diagnostics

Biomarkers can be categorized into fluid based, digital based, or behavioral based. Fluid based biomarkers are taken from liquid biopsies such as blood plasma, cerebrospinal fluid, urine, and saliva. Digital based ones can be in the form of electroencephalogram (EEG), CT or MRI imaging. Behavioral markers come in the form of questionnaires (i.e., GCS) to quickly gauge the extent of patient injury. The most effective and accurate diagnoses often combine as many different forms of biomarkers as possible. For example, a specific protein isolated from blood plasma correlates with MRI imaging and GCS score to inform clinicians of a

patient's TBI severity and the appropriate course of treatment. In the context of oncology, there is a growing body of evidence that EVs play a role in tumor progression, promotion of angiogenesis, and contribute to the heterogeneity of the tumor microenvironment, emphasizing the diagnostic potential of EVs.

Nucleic acids in EVs are also indicative of the disease state; both RNA and DNA sequences have been found in EVs. More specifically, miRNA, mRNA, and ncRNA profiles have been established in multiple cancer types including ovarian cancer, where miRNAs could reliably distinguish between benign or malignant tumors (LANE; KORBIE; HILL; TRAU, 2018). DNA fragments isolated in EVs from melanoma, pancreatic, breast, lung and leukemia cancer cell lines represent the entire genomic DNA and reflect the pathological status of the respective cancer cells (THAKUR; ZHANG; BECKER; MATEI *et al.*, 2014). In summary, EVs harvested from the complex heterogeneric tumor mass provide valuable insight into the pathophysiological network and may be exploited for their diagnostic potential. These biomolecules contain a wealth of information that can often be leveraged to find potential novel druggable targets for therapeutic treatments.

An understudied area is the role of EVs in the visual system. The visual process requires photoreceptors that receive light stimulus from the external environment, which transmits the light signal into the retinal ganglion cells (RGCs). The RGCs inside the retina of the eye converts the light signal into an electrical stimulus which travels through the optic nerve and into the brain for visual processing. Similar to neurodegenerative diseases in the brain, the eyes are also be affected by aging. Glaucoma and age-related macular degeneration (AMD) are

examples of disorders in the elderly visual system, resulting in reduced vision or blindness. Although there are no available treatments for these ocular diseases, recent reports have highlighted the emerging potential beneficial effects of EVs in glaucoma and AMD. EVs cargos, namely miRNAs and proteins, have been shown to correlate with certain aspects of AMD. Previous studies identified cathepsin D, cytokeratin 8, actin, myosin-9 and heat shock protein 70 within RPE-secreted EVs to be associated with AMD's aqueous humor (KANG; BANG; CHOI; YOON *et al.*, 2014; MANUKONDA; ATTEM; YENUGANTI; KALIKI *et al.*, 2022). An upregulation in miR-410 and miR-19 results in reduced VEGF expression, subsequently contributing to abnormal choroidal neovascularization (CNV) (CHEN; WANG; HU; CUI *et al.*, 2014). Similarly in glaucoma, dysregulation of EVs-derived miR-486-5p, miR-204, and miR-184 negatively affects aqueous humor inflow and outflow (DISMUKE; CHALLA; NAVARRO; STAMER *et al.*, 2015). Upon increased intraocular pressure, EVs are released from immature microglial cells that promote the secretion of proinflammatory cytokines, enhance phagocytosis, and generate ROS to mediate the status of RGCs (AIRES; RIBEIRO-RODRIGUES; BOIA; CATARINO *et al.*, 2020).

The diagnostic potential of EVs are evident in their usage in TBI, oncology and ocular diseases. Various EVs-derived proteins and nucleic acids have implications on their respective pathologies, thus making EVs an attractive option for sources of biomarkers.

2.6 EVs in TBI pathology

The ubiquitous nature of EVs undoubtedly precludes their involvement in TBI pathology. The roles of these particles in supporting neurological recovery or exacerbating the injury symptoms remain a challenge due to the complexity of EVs and their subtypes. For example, previous studies have demonstrated that different types of EVs can have different or completely opposite effects in TBI (ZHANG; BULLER; CHOPP, 2019; ZHAO; ZHOU; TIAN; LI *et al.*, 2017), and that these same subtype of EVs are case-dependent as they exert a different effect on other neurological diseases (GHARBI; ZHANG; YANG, 2020). The duality of the help/harm nature of EVs in TBI raises challenges in classifying specific types of EVs are either beneficial or harmful. Thus, EVs can be broadly divided into pathological EVs (PEVs) and biological EVs (BEVs) in order to more clearly link subtypes with their respective effects in TBI. It is worth noting the dynamic nature of these EVs as some particles may be classified as PEV under certain conditions, but BEV in others, such as different stages of TBI progression.

Pathological EVs

PEVs have been shown to mediate the secondary phase of injury after the initial insult. For example, brain-derived EVs along with phosphatidylserine enriched EVs are released into the circulation to promote a procoagulant state, with the phosphatidylserine and tissue factor membrane proteins playing a key role in driving this process in the acute phase post injury (TIAN; SALSBERY; WANG; YUAN *et al.*, 2015). Additionally, cardiolipin EVs from mitochondria have also been demonstrated to promote coagulation (ZHAO; WANG; TIAN; HILTON *et al.*, 2016).

Other dysregulated processes like inflammation, BBB disruption, edema, and overall systemic complications have also been reported in the context of PEVs (HAZELTON; YATES; DALE; ROODSELAAR *et al.*, 2018; WANG; XIE; WU; ZHOU *et al.*, 2022; WU; LIU; ZHOU; HILTON *et al.*, 2018). Notably, PEVs have been shown to regulate glial cell propagation of the inflammatory response via pro-inflammatory mediators and specific miRNAs (KOROTKOV; PUHAKKA; GUPTA; VUOKILA *et al.*, 2020; KUMAR; STOICA; LOANE; YANG; ABULWERDI; KHAN; THOM *et al.*, 2017; YIN; HAN; HU; ZHANG *et al.*, 2020). This exacerbates the inflammatory symptoms and contributes to BBB disruption and cerebral edema. Previous works highlighted PEVs enhancement of BBB permeability to promote edema during the acute phase of TBI (DONG; LIU; SHEN; HOUCK *et al.*, 2021; WU; LIU; ZHOU; HILTON *et al.*, 2018). Of particular interest is von Willebrand factor (VWF), which activates platelets and interacts with endothelial cells in the BBB through CD62 and integrins to promote coagulation and inflammation (HUANG; ROTH; HEUSER; SADLER, 2009; PADILLA; MOAKE; BERNARDO; BALL *et al.*, 2004). Attenuating VWF-mediated activity by targeted degradation or blocking the active binding site reduced the PEV induced symptoms post injury. As mentioned previously, PEVs play a role in other neurological diseases such as AD, PD, HD and ALS. For example, PEVs carry AD hallmark proteins such as A β and tau, which subsequently promote AD-like pathology and symptoms (RAJENDRAN; HONSHO; ZAHN; KELLER *et al.*, 2006; SAMAN; KIM; RAYA; VISNICK *et al.*, 2012). The same is true for α -synuclein released by EVs contributes to the dissemination and amplification of PD associated pathologies, huntington protein

for HD, and PEVs may contribute to the release of intracellular TAR DNA-binding protein 43 aggregates to mediate the occurrence of ALS (EMMANOUILIDOU; MELACHROINO; ROUMELIOTIS; GARBIS *et al.*, 2010; NONAKA; MASUDA-SUZUKAKE; ARAI; HASEGAWA *et al.*, 2013; SCHNEIDER; SIMONS, 2013). Overall, the aforementioned roles of PEVs highlights their part in exacerbating and/or mediating the pathologies associated with TBI and other neurological diseases in part via their cargos.

Biological EVs

BEVs act in a contradictory manner to PEVs by promoting protective or healing effects. These beneficial effects can stem from either different subtypes of EVs or by specific cargos themselves. For example, neuroinflammation is a key part of the recovery process, but a prolonged, uncontrolled response leads to poorer outcomes. Due to the paradoxical neuroinflammatory responses, it remains a challenge to mediate and 'fine tune' this key process to maximize the recovery potential. Notably, efforts to control microglia response to injury by promoting the transition from pro-inflammatory M1 state to pro-regenerative M2 state have yielded insight into BEVs (LI; SUN; WANG; CAO *et al.*, 2022). BEVs derived from astrocytes containing miR-873a-5p have been shown to modulate the communication between astrocytes and microglia by inhibiting the NF- κ B signaling pathway to reduce neuroinflammation caused by TBI in a mouse model (LONG; YAO; JIANG; YANG *et al.*, 2020). Furthermore, microglia's BEVs carrying miR-124-3p may promote anti-inflammatory responses by inhibiting the mTOR signaling pathway and promoting neurite outgrowth (HUANG; GE; YU; HAN *et al.*,

2018). BEVs can also aid in the tissue repair and subsequent neurological recovery after TBI. It has been shown in a target dependent manner that EVs derived from mesenchymal stem cells (MSCs) significantly increase the number of neurons in the dentate gyrus in rats after injury (ZHANG; CHOPP; MENG; KATAKOWSKI *et al.*, 2015). The cross talk between astrocyte- and microglia-derived EVs can modulate neuronal connections and promote neurite outgrowth and survival, which are key mechanisms closely related to neuroprotective/neurotrophic factors such as apolipoproteins and synapsins (GHARBI; ZHANG; YANG, 2020; HUANG; GE; YU; HAN *et al.*, 2018; WANG; CESCO; LOERS; SCHWEIZER *et al.*, 2011). BEVs facilitate neurological recovery such as motor, sensory, cognitive, and learning functions through a variety of routes. Functional improvements in cognitive and learning abilities may be attributed in part to improving hippocampal function after brain injury through the actions of MSC-derived EVs carrying a variety of miRs. However, the exact mechanisms of how these functional RNAs promote recovery are currently unknown. Similar to PEVs' ability to influence outcomes in other neurological diseases, BEVs have been reported to improve symptoms in models of stroke, autism, and peripheral nerve injury (PERETS; HERTZ; LONDON; OFFEN, 2018; XIN; LI; CUI; YANG *et al.*, 2013). The versatility in both BEVs and PEVs to modulate outcomes after TBI speaks to the dynamic nature of these particles. It is worth emphasizing again that the classification of these types of EVs is highly dependent on the specific targets, cell types, cargos, and timing; BEVs can be

PEVs in certain conditions and vice versa. This complexity is one of the challenges researchers face in translating the therapeutic potential of EVs into practice.

2.7 EVs biomarkers in TBI

“Free floating” biomarkers in liquid biopsies

The variability of injury severity and heterogeneity of the underlying pathophysiologies of TBI progression are fundamental challenges that researchers must address in the search for the most accurate diagnostic, prognostic, and predictive biomarkers of TBI. Nonetheless, several prominent “free floating” fluid-based protein candidates have been proposed: ubiquitin C-terminal hydrolase L1 (UCH-L1), glial fibrillary acidic protein (GFAP), neurofilament light (NFL), and S100 calcium binding protein (S100 β) among others. While these markers are well characterized in the brain, TBI systematically impacts a wide range of physiological processes including the endocrine, immune, respiratory and cardiovascular systems (GADDAM; BUELL; ROBERTSON, 2015). For example, pulmonary and hepatic complications by peripheral EVs propagating proinflammatory cytokines endocytosed by pulmonary cells trigger inflammation damage in the lungs in mice post-injury (KERR; DE RIVERO VACCARI; ABBASSI; KAUR *et al.*, 2018). This type of modulation was repeated in the brain-liver axis as EVs exacerbated the inflammatory response immediately post TBI (COUCH; AKBAR; ROODSELAAR; EVANS *et al.*, 2017).

Despite the merits of the UCH-L1, GFAP, NFL and S100 β , each proposed candidate suffers from drawbacks such as lack of consistency, sensitivity,

specificity, and predictive prognosis (GAN; STEIN; SWANSON; GUAN *et al.*, 2019). For example, GFAP and UCH-L1 have been proposed as the gold-standards for TBI detection, but studies have shown GFAP may not be sensitive enough to delineate the severity of injury (LEI; GAO; FENG; JIN *et al.*, 2015; OKONKWO; YUE; PUCCIO; PANCZYKOWSKI *et al.*, 2013). Furthermore, GFAP and UCH-L1 are inadequate in predicting recovery six months after injury (DIAZ-ARRASTIA; WANG; PAPA; SORANI *et al.*, 2014). Additionally, these protein markers show transient elevations in the periphery due to BBB disruption, and are not directly indicative of specific TBI sequelae. Lastly, UCH-L1 is not specific to the CNS and is expressed in the peripheral nervous system, endocrine system, and smooth muscle cells, thus presenting additional challenges to its use. Nonetheless, Abbott's blood-based iSTAT-TBI Plasma device and Brain Trauma Indicator (BTI), first of a kind device to detect TBI in liquid biopsies, measure GFAP and UCH-L1 levels up to 12 hours post injury (NISHIMURA; CORDEIRO; AHMED; YOKOBORI *et al.*, 2022). The major limitation with these devices is that it is used to inform clinicians on the patient's need for a CT scan in a Yes/No manner. Other candidates like NFL and S100 β have been linked to specific phases in the disease process (**Figure 2.7**), but again they have demonstrated limited diagnostic and prognostic potential (DADAS; WASHINGTON; DIAZ-ARRASTIA; JANIGRO, 2018). These proteins exhibit low concentrations in the blood and CSF, and are rapidly degraded in the liver and kidneys, all of which dramatically decreases their bioavailability (ZETTERBERG; SMITH; BLENNOW, 2013).

The current “free floating” protein biomarkers highlight the difficulties in the field. It is worth noting that the complex mechanisms and recovery processes of each TBI sequelae makes it unlikely that a single protein biomarker will be useful in all cases (**Figure 2.7**). Additional challenges such as signal degradation/bioavailability and sample accessibility require new venues to overcome these concerns. Therefore, the handful of blood and CSF based markers with their respective drawbacks has opened the doors for researchers to look elsewhere in the search for assessment and predicting outcomes after TBI.

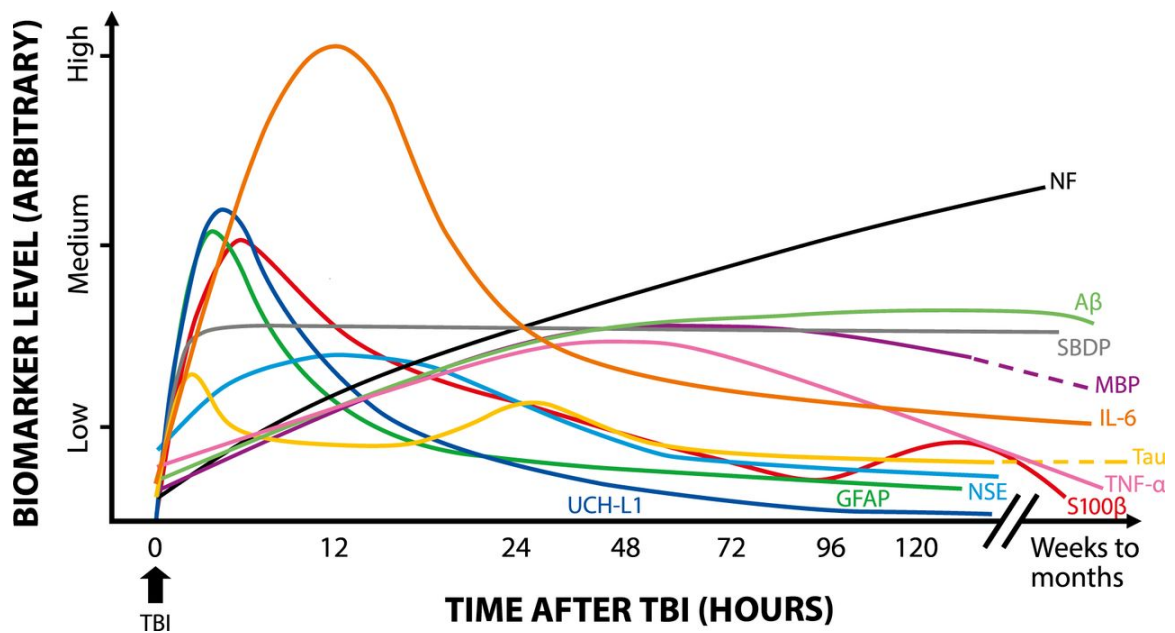


Figure 2.7: Fluid-based TBI biomarkers. The fluctuation of proposed biomarkers in serum or plasma across different time points and phases. Major challenges of TBI biomarkers include sensitivity, specificity, and predictive prognosis. No single protein has displayed all the characteristics of the ideal biomarker. Furthermore, many of these are not able to discern the severity of TBI, especially in mTBI where nuanced differences are not readily detectable by traditional serum or plasma tests. Reproduced with permission from (ADRIAN; MÅRTEN; SALLA; LASSE, 2016).

EVs-based biomarkers in liquid biopsies

The search for an alternative to “free floating” biomarkers opens the door for EVs to fill this need. In addition to their previously mentioned key characteristics, EVs are able to cross the intact BBB (DONG; DONG; ZHANG, 2023), allowing for less invasive peripheral blood draws rather than spinal taps which are often painful and potentially dangerous. Indeed, recent advances in EVs TBI biomarkers have produced a number of interesting leads for the early detection and diagnosis of TBI. For example, previous reports highlighted the presence of well-established “free floating” based biomarkers in EVs from different TBI injuries such as sports-related, bTBI, and repetitive TBI. (GOETZL; ELAHI; MUSTAPIC; KAPOGIANNIS *et al.*, 2019; KAWATA; MITSUHASHI; ALDRET, 2018; KENNEY; QU; LAI; DEVOTO *et al.*, 2018; MONDELLO; GUEDES; LAI; CZEITER *et al.*, 2020). Furthermore, cell-specific subpopulations of EVs have provided additional potential targets, highlighting the practicality of the roles of EVs in TBI pathology. However, a challenge remains in discerning specific EVs subpopulations across studies due to variability in nomenclature, thus highlighting the importance for all members in the field to adopt the ISEV guidelines for consistency.

Neuron-derived EVs

Currently, most efforts to develop EVs-based biomarkers have followed the traditionally studied proteins such as UCH-L1, tau and amyloid β as diagnostic and predictors of outcomes after TBI (GILL; MUSTAPIC; DIAZ-ARRASTIA; LANGE *et al.*, 2018). One outcome that has garnered significant interest is chronic traumatic encephalopathy (CTE), a debilitating neurodegenerative disease. Previous reports

showed a transient increase of UCH-L1 in neuron-derived EVs in the acute phase after mTBI, but elevated levels of pathogenic forms of tau and amyloid β were present in EVs in the acute and chronic phase of veterans with a history of 3 or more TBI (KENNEY; QU; LAI; DEVOTO *et al.*, 2018). Indeed, neuron-derived tau proteins in EVs have been correlated with TBI psychiatric and behavioral symptoms in veterans and increased risk of developing CTE in professional football players (GILL; MUSTAPIC; DIAZ-ARRASTIA; LANGE *et al.*, 2018; KENNEY; QU; LAI; DEVOTO *et al.*, 2018; THARMARATNAM; ISKANDAR; TABOBONDUNG; TOBBIA *et al.*, 2018). A recent study highlighted the differences between “free floating” proteins in blood plasma compared to GluR2⁺ brain-derived EVs. The authors reported GFAP and IL-6 were both significantly different in plasma and GluR2⁺ brain-derived EVs compared to healthy controls, but NFL, tau, UCH-L1, IL-10 and TNF α were only significantly elevated in plasma compared to controls (BEARD; YANG; HABER; FLAMHOLZ *et al.*, 2021). Furthermore, the authors show that plasma and GluR2⁺ brain-derived EVs possess distinct protein compositions that are each altered by TBI, reinforcing the theory of systemic-wide changes in the body post-injury. In a longitudinal study, EVs-derived GFAP, but not NFL, were elevated in moderate to severe TBI patients within one year after injury (FLYNN; LEETE; SHAHIM; PATTINSON *et al.*, 2021). Increased GFAP and NFL levels were associated with lower 1 year GCS scores, suggesting these markers are related to injury severity and poor recovery outcomes.

Microglia- and astrocyte-derived EVs

In addition to neuron-derived EVs, other cell types such as microglia and astrocytes have also become potential sources for biomarkers. For example, miR-124 in microglia-derived EVs has been shown to play a role in post-injury recovery by promoting neurite outgrowth, inhibiting neuronal apoptosis, attenuating pro-inflammatory cytokines, while promoting the release of anti-inflammatory mediators (HUANG; GE; YU; HAN *et al.*, 2018; LI; HUANG; YIN; ZHU *et al.*, 2019; YANG; YE; KONG; SU *et al.*, 2019). The opposite is true for astrocyte-derived EVs as they have been reported to promote the peripheral inflammatory response, driving the recruitment of peripheral leukocytes into the brain post-injury (DICKENS; TOVAR-Y-ROMO; YOO; TROUT *et al.*, 2017). Furthermore, pro-inflammatory proteins such as ASC, NLRP1, and caspase were found in astrocyte-derived EVs isolated from patient CSF (DE RIVERO VACCARI; BRAND; ADAMCZAK; LEE *et al.*, 2016). A more recent study reported higher complement protein levels in astrocyte-derived EVs compared to their neuronal counterparts, and these differences persisted up to 4 years after TBI (GOETZL; YAFFE; PELTZ; LEDREUX *et al.*, 2020)

In addition to specific EVs-associated cargo, transcriptomics and proteomics of EVs expand the scope from conventional markers of TBI to a more comprehensive and dynamic assessment of biomarkers. For example, mass spectrometry from EVs derived from TBI patients' CSF displayed differential levels of cytoskeletal proteins MAP2, TUBB and GFAP, along with mitochondrial factors such as HSPD1 and INA. Additionally, synaptic vesicle proteins like SNAP25 and

PCLO with nuclear factors HDAC6, TTN and SYNE2 were all significantly different in TBI patients compared to controls (MANEK; MOGHIEB; YANG; KUMAR *et al.*, 2018). miRNA sequencing of GluR2⁺ EVs in a preclinical mouse model of mild and moderate TBI showed a differential expression of miRNAs involved in 56 unique pathways ranging from long-term potentiation, neuromodulator signaling and intracellular signaling pathways (KO; HEMPHILL; YANG; BEARD *et al.*, 2020). Other studies highlighted miRNA-21-5p induces M1-like microglia to release cytokines that inhibit neurite outgrowth and promote neuronal apoptosis (GAO; XIONG; LI; HAN *et al.*, 2020), while miRNA142 was found in the lesion of cerebral cortex of rats two weeks post injury and may contribute to the activated astrocytes in the region (KOROTKOV; PUHAKKA; GUPTA; VUOKILA *et al.*, 2020)

EVs biomarkers are presented with some challenges that need to be addressed. Firstly, the correlation between specific subpopulations of EVs (i.e. CD63⁺) and specific pathologies (i.e. reactive gliosis) is not currently available. Secondly, proteomics studies with longitudinal time points across the different phases of TBI have been understudied, especially in severe TBI cases. Furthermore, an -omics type approach would provide more comprehensive analysis of EVs cargo and the dynamic release of specific EVs subpopulations in response to injury. Elucidating phase-specific markers would help track, correlate, and predict TBI disease progression. These results, combined with the currently available testing methods, would ultimately help progress the EVs and TBI fields forward towards better clinical diagnosis, biomarker development, and targeted therapies.

Chapter 3. Gap in Knowledge and Project Design

Parts of this chapter is published and reproduced with permission from Tang, T.Z., et al., “Serum Amyloid A and Mitochondrial DNA in Extracellular Vesicles are Novel Markers for Detecting Traumatic Brain Injury in a Mouse Model.”, *iScience*, 2024.

The current proposed protein-based biomarkers like GFAP and UCH-L1 are well established, as seen in their usage in the iSTAT-TBI and Brain Trauma Indicator devices currently available in the market for TBI detection. However, additional biomarkers may aid in more accurate specificity, sensitivity, and predictive prognostic capabilities for overall better outcomes.

The value of EVs as a source for biomarkers in neurotrauma has only been recently appreciated. EVs key characteristics such as their ability to cross the BBB, stability in various biofluids, and protect their cargo from degradation are critical to their diagnostic potential. Furthermore, EVs versatility allows them to package a variety of different cargos ranging from proteins, nucleic acids, metabolites, and other biomolecules reflecting cellular processes of their origin. Of these cargos, omics based RNA studies have been the most extensive, as the potential various roles of miRNA in TBI have been proposed (CHAPUT; THÉRY, 2011; RAPOSO; STOORVOGEL, 2013; RATAJCZAK; MIEKUS; KUCIA; ZHANG *et al.*, 2006; VALADI; EKSTRÖM; BOSSIOS; SJÖSTRAND *et al.*, 2007). However, DNA-based studies remain relatively understudied, particularly mtDNA, in TBI. This type of DNA has been implicated in many processes including cellular apoptosis, mitochondrial dysfunction, and inflammatory response, all of which are related to

TBI pathophysiology progression (GUESCINI; GENEDANI; STOCCHI; AGNATI, 2010; KILBAUGH; LVOVA; KARLSSON; ZHANG *et al.*, 2015; WALKO; BOLA; HONG; AU *et al.*, 2014).

Our project aims to fill this gap in knowledge by investigating EVs-based biomarkers to better assess and monitor TBI disease progression in a longitudinal fashion. This study will have two aims which will describe the biophysical properties of EVs post-injury, and highlight the importance of mtDNA and novel proteins as potential biomarkers in EVs. Our results will progress the field further by highlighting the value of EVs and may ultimately be translated into the development of a mobile, handheld device for the diagnosis of TBI.

Aim 1: Characterization of the biophysical properties of EV's after TBI.

In this study, we used 10–12-week-old male C57BL/6J mice with a total of 10 animals/experimental group. Aim 1 is divided into two sub-aims. In sub-aim 1.1, we characterized the severity of our preclinical weight drop TBI model on mice using Neurological Severity Score (NSS) and CT imaging of mouse skulls. Additionally, we quantified physiological parameters such as brain parenchymal volume, skull fracture diameter, and fracture distance from midline to evaluate for gross anatomical changes post-injury. By characterizing our TBI model, we can begin to understand the subsequent pathophysiology of the disease. In sub-aim 1.2, we determined EVs dynamics post-injury by profiling the number and sizes of the EVs along with their cell-specific origin of release. We isolated EVs from blood plasma of animals at six different time points post injury, ranging from acute (3-24 hours), sub-acute (3-10 days), and chronic (30 days) phases. Using

Nanoparticle Tracking Analysis (NTA), evaluated for changes in number and sizes of EVs at each time point. Significant differences from the NTA data may suggest possible enrichment of EVs subpopulations, hence we assessed for these changes using targeted immunoblotting for cell-specific markers. Finally, we used Transmission Electron Microscopy (TEM) to confirm our NTA data for changes in biophysical properties. The results of this aim can be found in **Figures 5.1 to 5.7**.

Aim 2: Characterization of EVs DNA and protein content for the identification of novel biomarkers for TBI

Aim 2 is also divided into two parts. In sub-aim 2.1, we characterized the contents of the EVs. Using qPCR, we quantified the amount of mtDNA and nuDNA in EVs post-injury along with their location of release. In sub-aim 2.2, we used targeted immunoblotting of brain-derived markers to determine their presence and changes within EVs after TBI. We also employed global mass spectrometry proteomics of our EVs and subsequently analyzed the data using biostatistical and computational methods to discover potential novel biomarkers for TBI. The experimental design summary of the main project can be seen in **Figure 3.1**.

In parallel, but separate from our main project, we investigate the dynamics and DNA content of EVs in response to an injury *in-vitro*. We used rapid stretch injury (RSI) model to mimic the shearing forces of a blunt force TBI on rat hippocampal neural stem cells (rHNSC), and examined the EVs biophysical properties using NTA. Furthermore, we evaluated the sequence specificity and sizes of mtDNA in EVs released from human retinal pigment epithelial cells (ARPE-

19) under glucose oxidase (GOx) treatment. Our intent was to demonstrate the universal release of mtDNA within EVs as an acute cellular response to injury.

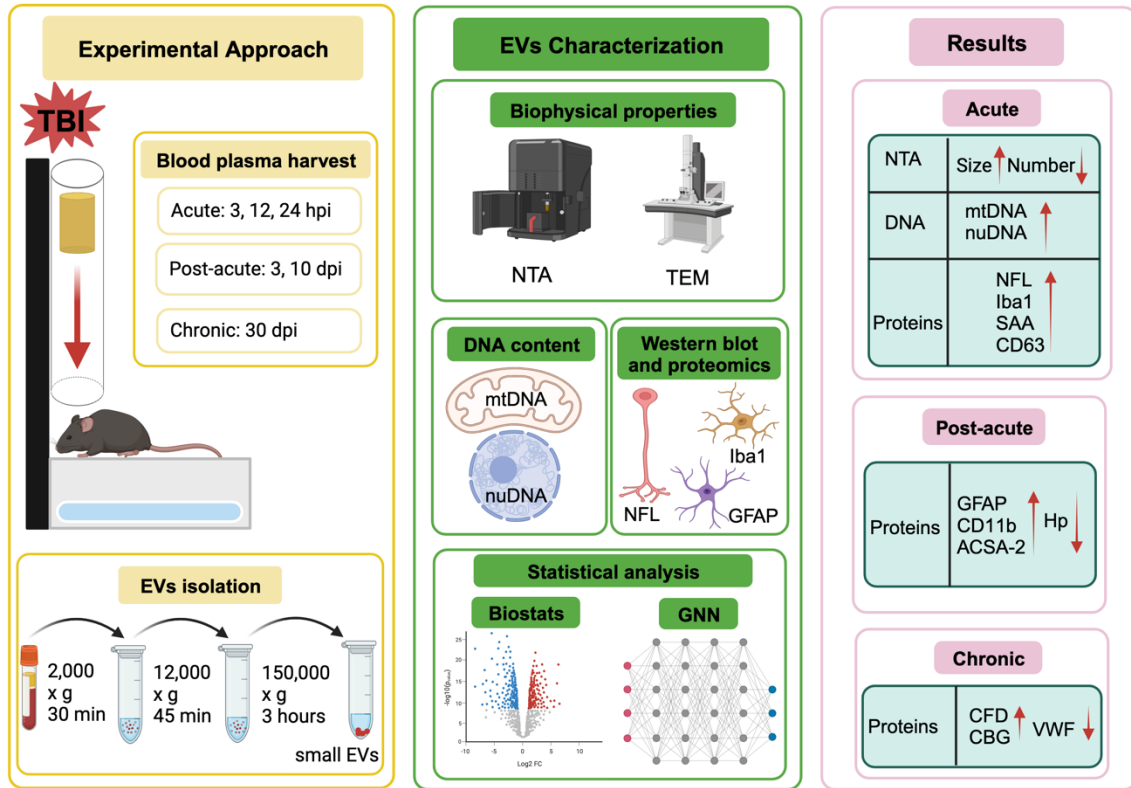


Figure 3.1: Graphical abstract of the main project. Young male C57BL/6 mice aged 10-12 weeks were subjected to a preclinical weight drop TBI model. Blood plasma harvest and EV isolation were performed at 6 different time points post injury, ranging from acute to chronic phases. The isolated EVs were characterized, and contents were profiled using various downstream biochemical experiments. Computational analysis of proteomics data from isolated EVs revealed potential novel biomarkers. Figure produced using BioRender.

Chapter 4. Methods and Materials

4.1 Preclinical weight drop mouse model of TBI

All animal procedures were conducted in accordance with the guidelines of the Institutional Animal Care and Use Committee at the University of Texas Medical Branch and adhered to the US National Institutes of Health guidelines (IACUC protocol number #1911088). C57BL/6J mice (The Jackson Laboratory, #000664), aged 10-12 weeks, were housed in a controlled environment with a 12-hour light/12-hour dark cycle at a temperature of 21-23°C, and had free access to water and a standard chow diet. To induce TBI, a non-penetrating, closed-skull, weight-drop model was employed on unrestricted mice, adapted from previously published methods (CHEN; CONSTANTINI; TREMBOVLER; WEINSTOCK *et al.*, 1996; MARMAROU; FODA; VAN DEN BRINK; CAMPBELL *et al.*, 1994). Mice underwent general health assessments and handling for 10 minutes the day prior to the injury to minimize stress related to handling. On the day of the procedure, mice were anesthetized with 3-5% isoflurane until the righting reflex was lost, and they were immediately placed in a prone position on top of a tin foil with slits, with the cranium directly underneath a plunger with a brass disc at the end. A 150 g weight was dropped from a height of 1.5 meters onto the plunger; the impact from the plunger to the top of the skull caused the mice to break through the aluminum foil barrier and undergo a 180-degree flip while falling 10 cm onto a foam cushion. After injury, mice were placed on a warm pad for monitoring until they regained consciousness and regained righting reflex. Sham animals underwent the identical procedure except for injury.

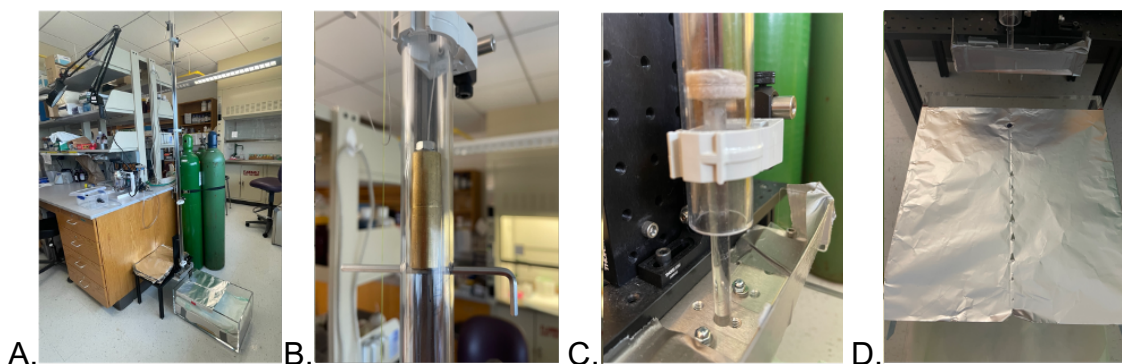


Figure 4.1: Preclinical weight drop mouse model of TBI. A. An overview of the TBI rig used to induce the injury. B. A 150-gram brass weight is dropped from a height of 1.5 meters, striking the plunger at the base of the rig. C. The plunger impacts the top of the cranium of the anesthetized mouse laying prone directly underneath the plunger. D. The force of the injury causes the mouse to break through the slitted tin foil sheet and flip over, mimicking the acceleration/deceleration of the brain within the skull similar to a motor vehicle accident.

4.2 Neurological Severity Score

For the assessment of TBI severity, we utilized a modified Neurological Severity Score (NSS) testing method, adapted from previously established protocols (FLIERL; STAHEL; BEAUCHAMP; MORGAN *et al.*, 2009; TSENER; BENI-ADANI; ASSAF; ALEXANDROVICH *et al.*, 2008). Mice were handled for 5 minutes and acclimated to the NSS testing setup for 10 minutes. Baseline scores were recorded 24 hours before inducing the TBI injury, followed by subsequent testing at different time points after the injury. The NSS test consisted of evaluating cognitive and motor neurological functions, including exit circle behavior, seeking behavior, monoparesis/hemiparesis (partial paralysis of one limb or one side of the body), paw grip/grip strength, straight walk, startle reflex, beam balancing on beams of 3 cm, 2 cm, and 1 cm width, and round stick balancing. The NSS scores were used to classify the severity of TBI. A score ranging from 1 to 3 indicated mild TBI, 4 to 7 indicated moderate TBI, and scores above 8 indicated severe TBI.

4.3 CT imaging and quantification of total brain parenchymal volume

Mice were anesthetized with 3-5% isoflurane for 5 minutes in gas chamber and then placed into the Inveon Preclinical CT scanner (Siemens) with continuous flow of isoflurane. CT scans were performed with a field of view (FOV) of 5 x 8 cm and 520 projections. The reconstructed image resolutions were 512 x 512 x 768 with an isotropic resolution of 0.1 mm, utilizing the Feldkamp reconstruction algorithm, beam hardening correction, and Hounsfield units calibration. To analyze brain parenchymal volume, the Inveon's Research Workplace software was used. Singular images from axial, coronal, and sagittal slices were selected, ensuring consistent anatomical landmarks were used to obtain the largest brain volume per slice. For axial slices, the mandible bone was used as the landmark; for coronal slices, the tip of the nasal bone with the widest skull diameter was used; and in sagittal slices, the appearance and location of the C2 spinal vertebrae served as the landmark. Using the ROI (Region of Interest) function, brain parenchymal volume was calculated by highlighting the space within the skull for each slice. This analysis allowed for precise assessment of brain parenchymal volume and ensured consistent measurements across different image slices.

4.4 Blood plasma harvest

Mice were anesthetized with 3-5% isoflurane until the righting and pain reflex (tail pinch) was lost. Each animal was placed in a supine position with their head in a nose cone and a continuous flow of isoflurane administered throughout the procedure. An incision was made in the skin from the bottom of the rib cage to expose the chest cavity, ensuring that the intrathoracic pressure remained intact.

The heart was located and a 1 mL syringe with a 25G x 5/8 in. needle (BD, #309626) was carefully inserted at a 45-degree angle to puncture the apex of the left ventricle. Blood plasma was then slowly extracted, and the animals were humanely euthanized by cervical dislocation followed by decapitation.

4.5 Isolation of EVs from mouse plasma

The total pool of circulating small EVs in plasma was isolated by a previously established method (THÉRY; AMIGORENA; RAPOSO; CLAYTON, 2006). Blood plasma was collected and mixed with an equal volume of sterile dPBS in Vacutainer K2 EDTA collection tubes (BD, #367841). The tube was inverted seven times to ensure proper mixing. All subsequent centrifugation steps were performed at 4°C. Samples were centrifuged for 30 minutes at 2,000 x g to remove circulating cells and large cellular debris. The supernatant was carefully transferred into a fresh 1.5 mL centrifuge tube and centrifuged for 45 minutes at 12,000 x g to remove any remaining cellular debris, organelles, or large EVs/apoptotic bodies. At this stage, each sample is deemed as 'precleared' plasma and stored in -80°C for subsequent downstream experiments. To isolate the EVs, the desired volume of precleared plasma was transferred to fresh UC tubes and was subjected to ultracentrifugation for 3 hours at 150,000 x g using the FiberLite F50L-24 x 1.5 Fixed-Angle Rotor (ThermoFisher). After the UC step, the supernatant and pellet fractions were used for analysis.

4.6 Characterization of biophysical properties of EVs with NTA

Nanoparticle Tracking Analysis (NTA) was used to determine the biophysical properties (number and size) of EVs. The NanoSight NS300 (Malvern Analytical) instrument was set up with the following settings: camera level 7 and screen gain 10. EVs were isolated from 100 μ L of precleared plasma through ultracentrifugation and then resuspended in 1 mL of sterile dPBS. A 1:100 dilution was prepared by adding 10 μ L of the resuspended pellet to 990 μ L of sterile dPBS. Using a 1 mL syringe (Henke Sass Wolf #4010-200V0), the diluted sample was slowly pushed through the fluid lines, and videos of the samples were recorded for 60 seconds each for subsequent image analysis. To ensure accuracy, three technical replicates were generated for each sample by advancing 100 μ L of the sample between each recording.

4.7 Transmission electron microscopy imaging of EVs

Isolated EVs were visualized and characterized using transmission electron microscopy (TEM). The EVs pellet was resuspended in 100 μ L of dPBS, and 10 μ L of the sample was further diluted with 90 μ L of dPBS. 10 μ L of the diluted EVs was placed onto a parafilm strip and then incubated with a graphene oxide on a holey carbon copper mesh grid (Electron Microscopy Sciences, #GOHC300Cu10) for 5 minutes. Excess sample was removed using filter paper, and the grid was subsequently incubated with 1 drop of uranyl acetate (Electron Microscopy Sciences, SKU #22400) for 5 minutes. Excess uranyl acetate was removed using filter paper. Images of the EVs were captured using a Philips CM-100 transmission

electron microscope at 60 kV, equipped with an Orius SC2001 digital camera (Gatan).

4.8 Analysis of DNA content within EVs

Each sample volume was standardized to 100 million particles, as determined by NTA. EVs were isolated using ultracentrifugation, and the total DNA was extracted from the isolated EVs using the Qiagen DNasy Blood and Tissue Kit (#69504), following the manufacturer's protocol. To assess the amount of mtDNA and nuDNA, quantitative real-time PCR (qPCR) was performed with Maxima SYBR Green/ROX qPCR Master Mix (Thermo Scientific #K0221) and specific mouse primers. mtDNA specific primers targeted the COXIII gene and nuDNA specific primers against ACTB. The primers used were as follows:

mtDNA COXIII Forward: 5'-CCC AGC TAC TAC CAT CAT TCA AGT-3'

mtDNA COXIII Reverse: 5'-GAT GGT TTG GGA GAT TGG TTG ATG T-3'

nuDNA ACTB Forward: 5'-TTT GCT CCT GGG CCT CCA AGT T-3'

nuDNA ACTB Reverse: 5'-AGC CCG TGA CTG CCA CAA ATC A-3'

The qPCR reactions were carried out using the CFX96 Touch™ Real-Time PCR Detection System (Bio-Rad) with the following thermal cycle: 95°C for 10 minutes, followed by 40 cycles at 95°C for 15 seconds and 60°C for 1 minute. Each qPCR reaction was performed in technical duplicates. To compare the amount of DNA within EVs with that in the "free-floating" form present in the supernatant, each sample was normalized to 100 million particles, as determined by NTA. EVs were then isolated as described above. The supernatant was separated from the EVs pellet after UC; the pellet was resuspended in 100 µl of dPBS. A total of 100 µl of

the supernatant was used for total DNA extraction and qPCR, following the same protocol as described above.

4.9 Targeted immunoblotting analysis of EVs

Each EVs sample was standardized to 100 million particles as determined by NTA and isolated by DUC. The EVs pellet were then resuspended in 10 μ L of Laemmli sample buffer with 2-mercaptoethanol, heated at 95°C for 2 minutes, briefly cooled, and loaded into a NuPAGE 4-12% Bis-Tris gel (Invitrogen, #NP0322). The separated proteins were transferred to 0.2 μ m nitrocellulose membranes (Cytiva Amersham Protran, #10600011). The membranes were washed in TBS-T (Tris-buffered saline containing 0.5% Tween), blocked in 5% milk TBS-T for 1 hour at room temperature, and then incubated with primary antibodies at a 1:1,000 dilution in 5% milk TBS-T overnight at 4°C. The following primary antibodies were used: Mouse anti-Iba1, #ab283319; Rabbit anti-NFL, #ab9035; Mouse anti-GFAP, #ab279290; Rabbit anti-UCH-L1, #ab108986; Rabbit anti-CD11b, ab133357; Rabbit anti-S100b, ab41548; Rabbit anti-Tau, ab254256; Rabbit anti-ACSA-2, ab133664 (all from Abcam); Rabbit anti-CD63, #PA5-92370 (Thermo Fisher); Rabbit anti-NSE, #8171 (Cell Signaling). Subsequently, the membranes were incubated with secondary antibodies (goat anti-Rabbit HRP-linked, #7074, or horse anti-Mouse HRP-linked, Cell Signaling Technologies, #7076; both from Cell Signaling) conjugated with HRP at a 1:1,000 dilution in 5% milk TBS-T for 1 hour at room temperature. Finally, the membranes were probed with ECL reagent (Cytiva Amersham, #RPN3243) or ECL Femto reagent (SuperSignal West Femto Maximum Sensitivity Substrate; Thermo Fisher,

#34095). Images were captured on G-Box (Syngene), and the signal intensity was quantified using GeneTools software (Syngene). For quantification, the signal for sham samples from each blot were averaged and arbitrarily set as 1. All experimental group values were normalized to the average value of the sham samples to determine the relative abundance of the target protein.

4.10 Global mass spectrometry of isolated EVs

The proteomics analysis of EVs isolated from mouse plasma was performed as described previously (MAROTO; ZHAO; JAMALUDDIN; POPOV *et al.*, 2017; ZHAO; JAMALUDDIN; ZHANG; SUN *et al.*, 2017; ZHAO; TIAN; SUN; ZHANG *et al.*, 2019). EVs were dissolved in 20 μ L of 9M urea, were reduced with 10 mM DTT for 30 min, followed by alkylation with 30 mM iodoacetamide for 60 min in the dark. The sample was diluted 10:1 with 50 mM ammonium bicarbonate and digested with 1.0 μ g trypsin for 16 h at 37 °C. The digestion was stopped with 10% trifluoroacetic acid. The peptides were desalted on a reversed-phase SepPak C18 cartridge (Waters, #WAT036945) and eluted with 80% acetonitrile. The eluate was dried in a SpeedVac, and the peptides were acidified with 2% acetonitrile-0.1% trifluoroacetic acid. A nanoflow ultra-high-performance chromatography Easy nLC instrument (Thermo Fisher Scientific) was coupled to a Q Exactive mass spectrometer (Thermo Scientific) with a nanoelectrospray ion source (Thermo Scientific). Peptides were loaded onto a C18 reversed-phase column (25 cm long, 75 μ m inner diameter), and separated with a linear gradient of 5–35% buffer B (100% acetonitrile in 0.1% formic acid) at a flow rate of 300 nL/min over 120 min. Mass spectrometry (MS) data were acquired using a data-dependent Top15

method dynamically choosing the most abundant precursor ions from the survey scan (400–1400 m/z) using HCD fragmentation. Survey scans were acquired at a resolution of 70,000 at m/z 400. The isolation window was set to 3 Da and fragmented with normalized collision energies of 28. The maximum ion injection times for the survey scan and MS/MS scans were 20 ms and 60 ms, respectively, and the ion target values were set to 2E6 and 1e5, respectively. Selected sequenced ions were dynamically excluded for 10 seconds. Data were acquired using Xcalibur software. Mass spectra were analyzed using MaxQuant software version 1.5.2.8 using the default setting (COX; MANN, 2008). Enzyme specificity was set to trypsin, defined as C-terminal to arginine and lysine excluding proline, and a maximum of two missed cleavages was allowed. Carbamidomethylcysteine was set as a fixed modification and methionine oxidation as a variable modification. The spectra were searched with the Andromeda search engine against the mouse SWISS-PROT sequence database (containing 17,000 mouse protein entries) combined with 248 common contaminants and concatenated with the reversed versions of all sequences. Protein identification required at least one unique or razor peptide per protein group. Quantification in MaxQuant was performed using the built-in XIC-based label-free quantification (LFQ) algorithm (COX; MANN, 2008). The required false positive rate for identification was set to 1% at the peptide level and 1% at the protein level, and the minimum required peptide length was set to 6 amino acids. Contaminants, reverse identification, and proteins only identified by modified peptides were excluded from further data analysis. The 'match between runs' feature of MaxQuant was used to transfer identifications to

other LC-MS/MS runs based on their masses and retention time (maximum deviation 0.7 min), and this was also used in quantification experiments. The MaxQuant results were further analyzed using the Perseus platform (TYANOVA; TEMU; SINITYCYN; CARLSON *et al.*, 2016). The LFQ MS intensities were log₂-transformed. After filtering (at least two valid LFQ values in at least one group), the remaining missing LFQ values were imputed from a normal distribution of log₂ LFQ intensity of proteins in each sample by shrinking the distribution of 0.3 of standard deviation and shifting it down by 1.8 of standard deviation. The imputation was performed only once.

4.11 Biostatistical analysis of proteomics

R version 4.2.2 was used to perform the proteomics data analysis. Initially, one-way ANOVA was used to analyze the results. Then, the False Discovery Rate method was performed to correct for multiple comparisons testing (KORTHAUER; KIMES; DUVALLET; REYES *et al.*, 2019). For paired comparisons between the Sham control group and TBI groups, Dunnett post-hoc test was used; for comparisons between only TBI groups (excluding the control group), Tukey post-hoc test was used. Statistical significance was determined with a p-value of < 0.05. Additionally, heat maps were generated by calculating the Pearson correlation coefficient among experiments. The figure legends indicate the sample sizes and statistical tests used for each experiment. Fold change (FC) values were transformed and expressed in logarithmic form from LFQ intensities of each protein resulting from unbiased global proteomics. Simply, $\text{LOG}(\text{FC}) = \text{LOG}(\text{Avg. LFQ})$

intensity protein X in TBI group/Avg. LFQ intensity protein X in Sham Control group).

4.12 Computational analysis of proteomics

Each round of proteomics data was manually refined by eliminating duplicate entries of the same proteins. This total list of proteins was uploaded into the STRING database to create a Protein-Protein Interaction (PPI) network by mapping proteomics results to existing entries within the STRING database. Each protein represents a node and the interactions between individual protein molecules constitute the links/edges of the PPI network. LFQ intensity values captured over different time points are pre-processed and attributed as node features. This helps to incorporate the temporal structure among LFQ intensity values of proteins within the machine learning GNN framework. All STRING runs were performed with default setting parameters and a confidence level of 0.9. Identification of potential biomarkers was formulated as a node classification problem, where the node labels represent the ranks between 1 (highest) to 6 (lowest) probability of the corresponding protein being a potential biomarker. A small fraction (< 5%) of nodes are labeled based on prior domain knowledge and inputs from existing databases. Once the graph is constructed, GNN-based learning techniques are implemented to predict the labels (i.e., probability of individual proteins being potential biomarkers) for all the nodes in the network. GraphSAGE was used as an inductive node embedding approach that concurrently learns both the topological structure and distribution of features for a

node in its local neighborhood. The operation executed at i^{th} node embedding layer is given by the following equation:

$$h_u^{(i)} = f^{(i)}(h_u^{(i-1)}, h_{N(u)}^{(i-1)}) = g[\theta_C^{(i)} h_u^{(i-1)} + \theta_A^{(i)} \tilde{A}(h_{N(u)}^{(i-1)})]$$

Here, $h_u^{(i)}$ represents the node embedding of node u at i^{th} layer; \tilde{A} denotes the aggregation operation; θ_C and θ_A are the parameters of the combination and aggregation operation of GNN, respectively; $N(u)$ describes the neighborhood of node u ; and $g[\cdot]$ denotes the activation function.

4.13 Culturing and propagation of rat hippocampal neural stem cells

rHNSC cells were purchased from Millipore Sigma (#SCR022) and maintained in EmbryoMax DMEM/F12-HEPES (Millipore Sigma #DF-042-B) that was supplemented with Glutamax (Gibco #35050061), B27 without RA (Gibco #12587-010), Antibiotic/antimycotic (Gibco #15240062), recombinant human FGF Basic (20 ng/mL, Millipore Sigma GF003AF). The media was changed every 2-3 days. To differentiate rHNS cells, DMEM/F12 was supplemented with Glutamax (Gibco #35050061), B27 without RA (Gibco #12587-010), Antibiotic/antimycotic (Gibco #15240062), retinoic acid (100 μM , Sigma Aldrich #R2625), Forskolin (5 mM, Sigma Aldrich #F6886) and mature neurons were generated after 5 days (MICCI; KRISHNAN; BISHOP; ZHANG *et al.*, 2019).

4.14 In-vitro rapid stretch injury model

Approximately 100,000 rHNSC cells were plated onto 24-well high throughput Bioflex culture plates (Flexcell International Corporation) pre-coated with collagen type I, 0.01% poly-D-Lysine (PDL, Sigma-Aldrich) and 1 $\mu\text{g/mL}$

mouse laminin (Invitrogen) to reach 80% confluency. To induce RSI, each plate was set on the FX-500T™ Tension System (Flexcell International Corporation) and cells were stretched at a frequency of 20 cycles with a minimum vacuum pressure of 80 kPa over 45 seconds (0.67 Hz) at room temperature. After RSI, cells were returned into the 37°C cell culture incubators.

4.15 Culturing and propagation of human retinal pigment epithelial cells

Human ARPE-19 cells were obtained from ATCC and maintained in a humidified incubator at 37°C with 5% CO₂. Human retinal pigment epithelial cells, ARPE-19 (CRL-2302), were propagated in DMEM: F12 medium (ATCC 30–2006) supplemented with 10% heat-inactivated Fetal Bovine Serum (FBS, GIBCO #10082147) and 100 U/ml of Penicillin-Streptomycin (GIBCO #15140148). ARPE-19 cells were differentiated in DMEM: F12 medium supplemented with 1% heat-inactivated FBS and 100 U/ml of Penicillin-Streptomycin for 3 months with medium changed twice per week.

4.16 Glucose oxidase (GOx) induced oxidative stress on cells

ARPE-19 cells were treated with various concentrations of GOx (SIGMA #G2133–50KU) to generate constant, low-level oxidative stress. GOx was resuspended in phosphate buffered saline (PBS) to prepare 100X stock that was diluted into to the culture medium.

4.17 Analysis of mtDNA in GOx-induced EVs released by ARPE-19 cells

Total DNA was isolated from EVs sedimented from 300,000 differentiated ARPE-19 cells. PCR primers were designed using the NCBI Primer-BLAST tool

with reference mtDNA (accession number NC_012920.1). For each PCR reaction (25 µl), 2 µl of sample DNA and 0.5 µl of each primer (10 mM) were used together with other components according to manufacturer's recommendations for Standard *Taq* and Long Amp *Taq* DNA Polymerases (both from New England BioLabs, #M0273S, M0323S). Using a Thermocycler C1000 Touch (BioRad), the PCR programs include initial denaturing step at 95 °C for 3 min followed by 32 cycles of 95 °C for 30 s, 55 °C for 30 s, and 68 °C for 1 min, and final extension at 68 °C for 5 min. We used 1 min extension step for amplicons 200 bp-1 kb and 6 min for amplicons 3–6 kb. The PCR products were separated using 1% agarose gel and visualized using G:Box with GeneSnap software. We used following primers:

Site I FW1 5'-TCAACCTCACCCACCTCTTGC-3'

RV1.1 5'-GGCC CTGTTCAACTAAGCAC-3'

RV1.2 5'-TTGCGCCAGGTTTCAATTTCT-3'

RV1.3 5'-GTGGGTGTTGAGCTTGAACG-3'

RV1.4 5'-CAGGGAGGTTAGAAGTAGGGTC-3'

RV1.5 5'-CCGGATAGGCCGAGAAAGTG-3'

Site II: FW2 5'-ACG TTGTAGCCCACTTCCAC-3'

RV2.1 5'-GGGGTAGTCCGAGTAACGTC-3'

RV2.2 5'-CGCTGCATGTGCCATTAAGATA-3'

RV2.3 5'-TCAACGTCAAGGAGTCGCAG-3'

RV2.4 5'-ACAAAATGCCAGTATCAGGCG-3'

RV2.5 5'-GG TGAGGCTTGGATTAGCGT-3'

Site III: FW3 5'-ACGCTAATCCAAGCCTCACC-3'

RV3.1 5'-GTGGTGATAGCGC CTAAGCA-3'

RV3.2 5'-AATGCTAGGCTGCCAATGGT-3'

RV3.3 5'-TTGTGCGGTGTGTGATGCTA-3'

RV3.4 5'-GAG GATGGTGGTCAAGGGAC-3'

Chapter 5. Results

5.1 Characterization of weight drop model reveals moderate to severe TBI

Neurological severity score

NSS evaluation of TBI was performed at different time points, representing the acute (3 hpi, 24 hpi), sub-acute (3 days post injury (dpi), 10 dpi) and chronic (30 dpi) phases post-injury. At the acute 3 hpi, 6/8 animals scored in the severe TBI (NSS>8) range, and 2/8 were in moderate TBI (NSS 4-7) (Figure 5.1B). Simple motor and cognitive function tests like open circle exit, straight walk, paw grip, and beam crossing tests demonstrated the quickest improvement post-injury. More difficult tests such as beam balancing and round sick balancing took the longest time for improvement. However, most animals returned to baseline pre-injury levels by the chronic 30 day time point. The NSS testing suggests our preclinical TBI weight drop model induces a moderate/severe injury.

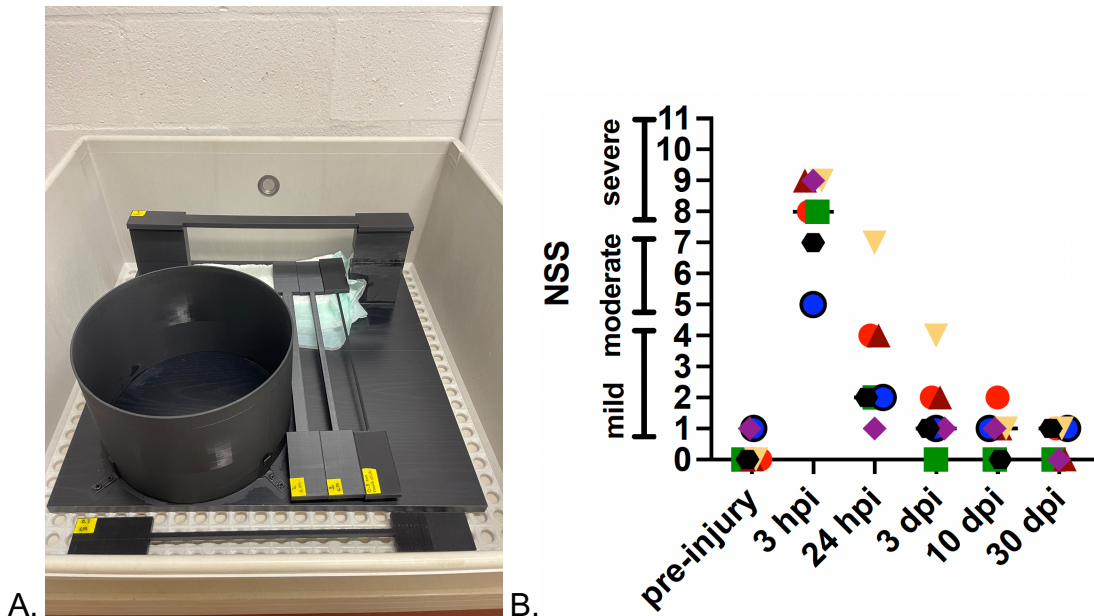


Figure 5.1: NSS assessment of preclinical TBI weight-drop model. A. NSS includes neurological motor and cognitive tests including beam crossing of different width,

beam/rod balancing, straight walk test, paw grip paralysis, and other exams that gauges the functionality of the animal at various time points post injury. B. Repeated measures test of mice undergone TBI shows a moderate/severe injury response at 3 hpi before gradually recovering to baseline levels around 10 to 30 dpi. Individual animals are color coded, experiments based on animals of N=7.

CT imaging

We performed CT imaging to further characterize the extent of the injury model. Gross pathology showed the presence of blood beneath the skull, which suggests a possible subdural hematoma and a compromised BBB. CT imaging revealed fractures (both simple and comminuted) present in 4/6 animals as axial and sagittal slices showed clear breaks in the animal skulls (**Figure 5.2A**). Quantification of fracture diameters displayed substantial damage in the acute phases before a gradual return to pre-injury levels 30 dpi (**Figure 5.3A**). The location of the fractures was consistent as measured by fracture distance from midline (axial) and from C1 vertebrae (sagittal) (**Figure 5.3B**). A possible hematoma was noticed in one animal that was clearly present by 24 hpi extending through 10 dpi before completely healing by the chronic phase. TBI had no effect on the overall skull diameter (**Figure 5.3C**), but there may appear to be an increase in brain parenchymal volume at 30 dpi (**Figure 5.3D**). This set of data shows the consistent location of our injury with little to no change in overall skull dimensions.

Together, this preclinical weight drop model successfully induces a moderate to severe TBI as assessed by NSS, from which animals recover similarly to previous reports (FLIERL; STAHEL; BEAUCHAMP; MORGAN *et al.*, 2009; KHALIN; JAMARI; RAZAK; HASAIN *et al.*, 2016).

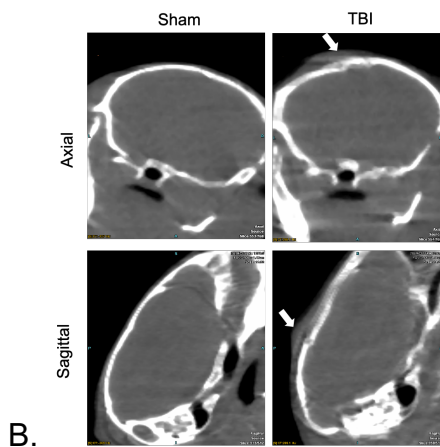
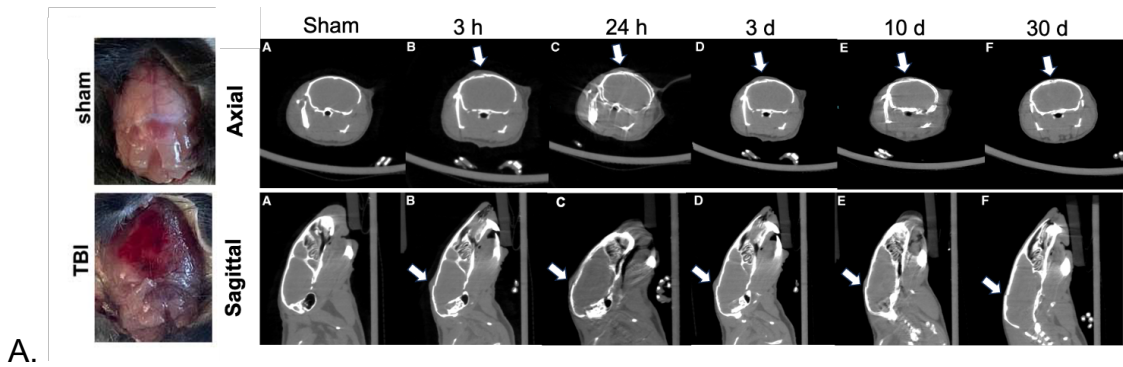


Figure 5.2: CT images of animals at various time points post injury. A. Axial and sagittal slices reveal gross anatomy changes that were subsequently quantified. Experiments based on animals of N=8. B. Zoomed in view with white arrows indicating fractures and possible hematoma. Experiments based on animals of N=2.

Likewise, gross pathology showed bleeding underneath the skull and CT images revealed fractures in several animals. Thus our data confirmed that a combination of neurological examination (NSS) and imaging testing (CT), which is the current clinical practice, provides limited information regarding the underlying neuropathology induced by TBI, highlighting the need for different approaches and the development of more advanced and comprehensive diagnostic methods to better understand and monitor TBI-induced neurological alterations.

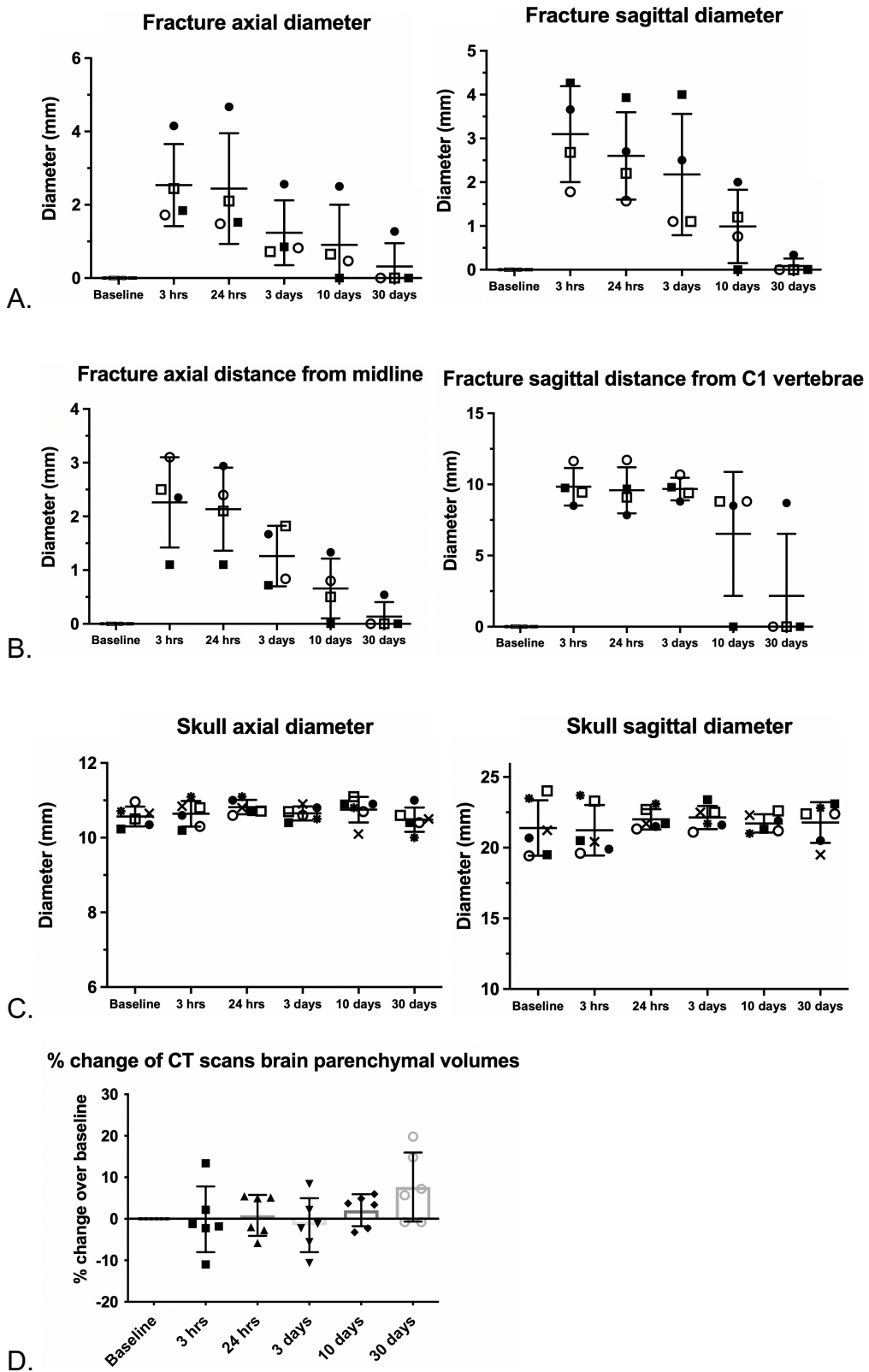


Figure 5.3: Characterization of TBI by CT imaging measurements. A, B. The sizes and location of fractures quantified showed consistency in animals with clear breaks in their skulls. Simple and comminuted fractures were present in the animals, with both types of

breaks displaying a similar pattern of recovery as the skull heals and regains integrity. Individual animals are coded by unique patterns, N=4. C. TBI and subsequent gross pathologies did not have an effect on overall skull diameters and morphology. D. However, a slight increase in brain parenchymal volume was observed at the chronic phase. Experiments based on animals of N=6.

5.2 TBI induced changes in biophysical Properties of Circulating EVs and EVs subpopulations

Temporal Dynamics of Circulating in Plasma EVs in post injury

Although EVs in TBI have been studied, the changes in the biophysical properties (number and size) of EVs in bodily fluids following TBI remain poorly characterized (GUEDES; DEVOTO; LEETE; SASS *et al.*, 2020). NTA revealed a marked 10-fold decrease in EVs number at 12 hpi ($8.8 \times 10^8/\text{ml}$) and a 6-fold decrease at 24 hpi (1.8×10^9) compared to sham controls (both $\sim 8 \times 10^9/\text{ml}$) (**Figure 5.4A**). Interestingly, EVs number at 3 and 10 dpi were comparable to sham controls, but once more a significant decrease in EVs number was observed at 30 dpi (4.0×10^9). In addition, EVs size concurrently showed significant increases at 12 and 24 hpi compared to sham controls (**Figure 5.4B,C**). To ensure these results are true and not artificially induced by ultracentrifugation, we performed NTA on the precleared plasma samples. Indeed, our precleared NTA data follows the same trend we observed in the isolated EVs samples (**Figure 5.5**).

Transmission electron microscopy confirms presence of EVs

TEM imaging of isolated EV fractions confirms the presence of the biomolecule particles, thus verifying our methodology of isolation by DUC. Sizes of EVs were quantified by the TEM software. The analysis showed a variety of

particles ranging from small ~70 nm in diameter to large ones ~300-400 nm in diameter. This heterogeneity can be seen in samples from sham control (**Figure 5.7A**), 3 hours post-injury (**Figure 5.7B**), 12 hours post-injury (**Figure 5.7C**), 24 hours post-injury (**Figure 5.7D**), 3 days post-injury (**Figure 5.7E**) 10 days post-injury (**Figure 5.7F**) and 30 days post-injury (**Figure 5.7G**). Close up views of EVs confirmed the circular and oblong shaped morphologies of EVs. The heterogeneity of sizes observed across all time points is a testament that DUC isolation method that does not bias itself towards a specific size of EVs.

Temporal dynamics of different EVs subclasses in TBI

The interesting relationship between number and sizes of EVs at the acute phase and chronic phases is noteworthy, suggesting there may be an enrichment of EVs subpopulation at these time points. Thus, we examined the expression of CD63, a common exosome marker (VAN NIEL; D'ANGELO; RAPOSO, 2018), and observed a 10-fold increase of CD63⁺ signal at the acute TBI phase (**Figure 5.6B**). Furthermore, we tested the levels of CD11b, a macrophage/microglia marker, and ACSA-2, an astrocyte marker (BATIUK; MARTIROSYAN; WAHIS; DE VIN *et al.*, 2020; PRINZ; PRILLER; SISODIA; RANSOHOFF, 2011). Both CD11b⁺ and ACSA-2⁺ displayed a gradual increase, peaking at 3 and 10 dpi, respectively (**Figure 5.6C,D**). This is consistent with previous findings that an upregulation of glial cell reactivity, with microglia and astrocytes playing key roles in the post-injury process.

Together, these data suggests TBI induces dynamic changes in the biophysical properties of EVs post injury, and subsequent enrichment of EV subpopulations across different TBI phases.

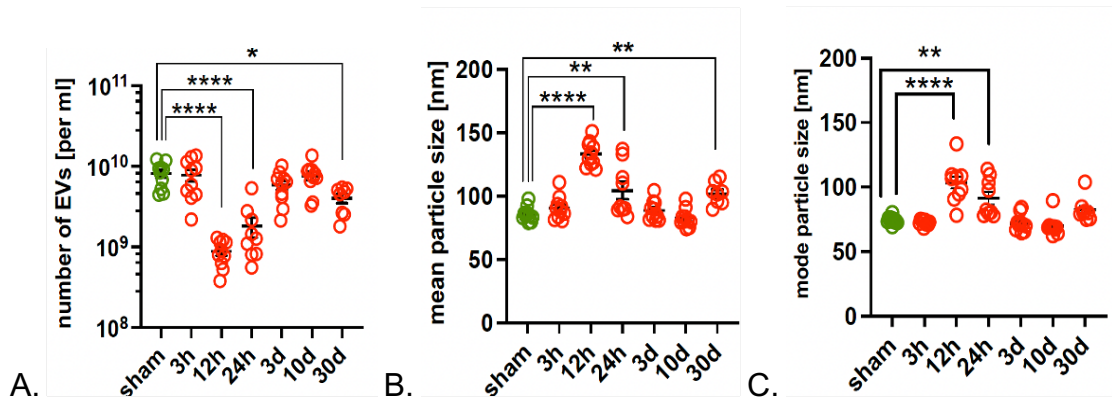


Figure 5.4: NTA of circulating EVs in blood plasma post injury. A. The number of EVs markedly decreases in the acute phase (12 and 24 hpi) and the chronic phase (30 dpi). B, C. This drop in the number of particles coincides with a significant increase in the mean and mode sizes of the particles at the same time points. This may suggest an enrichment of a specific subtype of EVs at these acute time points post injury. * = $p < 0.05$, ** = $p < 0.01$, **** = $p < 0.0001$, based on one-way ANOVA with Dunnett correction for multiple comparisons to sham. Experiments based on animals of $N = 8/\text{group}$.

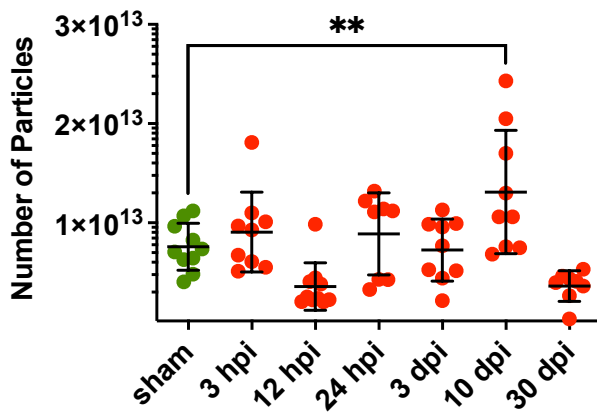


Figure 5.5: NTA of particles in precleared plasma. The number of particles throughout the different time points follows the same trend as circulating EVs, although only 10 dpi is statistically significant. It is worth noting the significantly higher amounts of particles in the samples (y-axis) compared to isolated EVs fractions due to the presence of organelles, large EVs or apoptotic bodies. ** = $p < 0.01$, based on one-way ANOVA with Dunnett correction for multiple comparisons to sham. Experiments based on animals of $N = 8/\text{group}$.

	sham	3hpi	12hpi	24hpi	3dpi	10dpi	30dpi
number [$\times 10^9/\text{ml}$]	8.1 \pm 2.8	7.8 \pm 4.0	0.88 \pm 0.3	1.8 \pm 1.5	5.8 \pm 2.4	7.6 \pm 2.9	4.0 \pm 1.4
mean size [nm]	85.8 \pm 5.6	90.6 \pm 9.1	133.3 \pm 9.8	104.4 \pm 20.2	88.7 \pm 7.8	82.7 \pm 7.1	102.1 \pm 8.6
mode size [nm]	74.4 \pm 2.8	72.6 \pm 2.0	103.6 \pm 14.6	91.5 \pm 14.6	72.1 \pm 6.5	69.9 \pm 7.3	82.5 \pm 9.1

Table 5.1: Summary of biophysical properties of EVs as measured by NTA. The number, mean size, and mode size of all samples from each time point is listed. Experiments based on samples of N= 8/group.

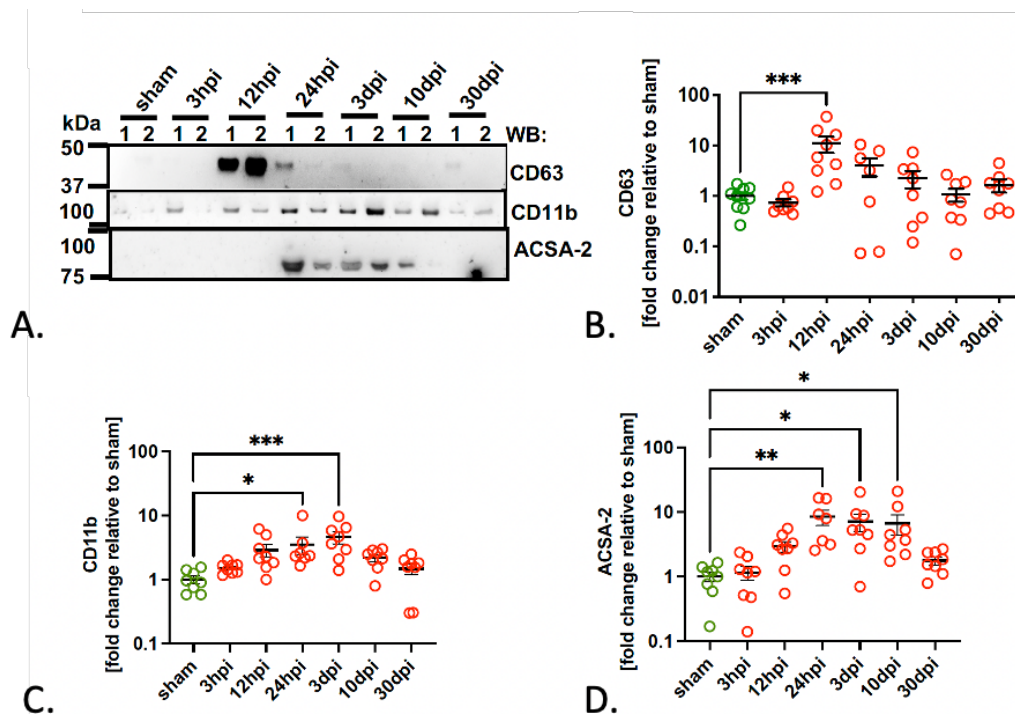
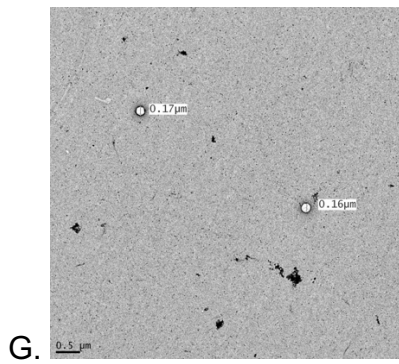
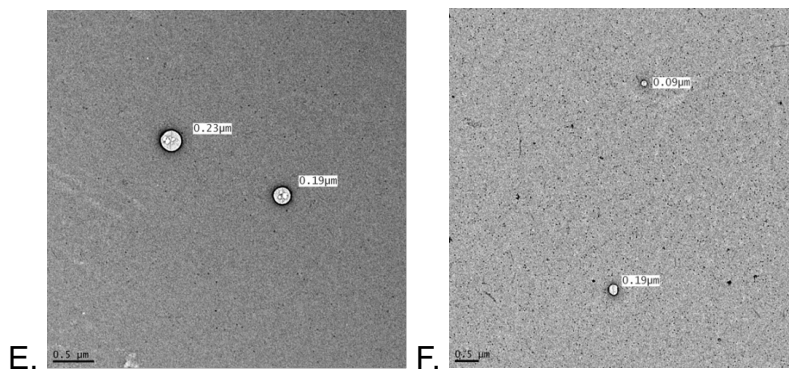
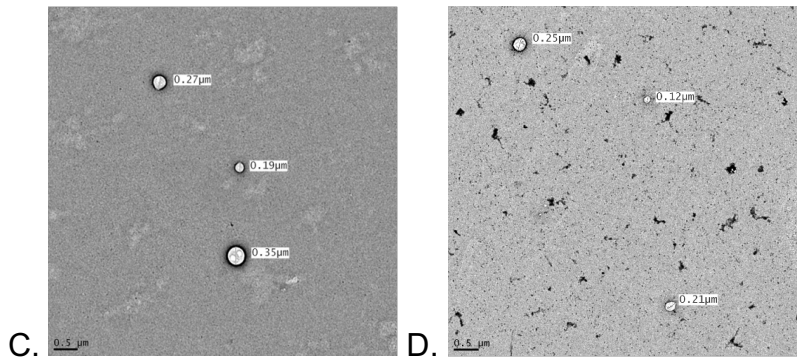
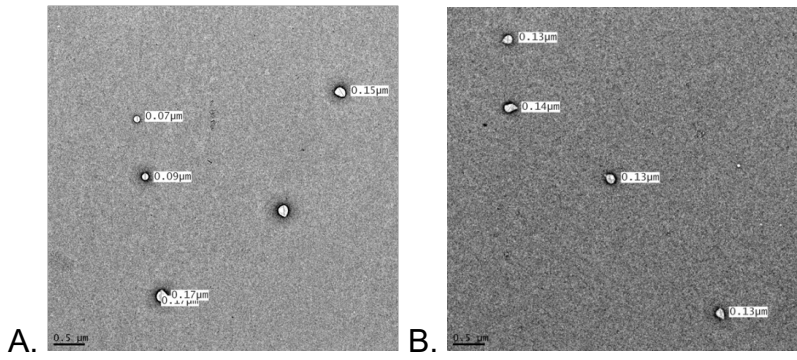


Figure 5.6: TBI induces changes in EVs subpopulations. A. Example Western blot analysis of EVs isolated from 2 animals in each experimental group. Quantification of the changes in the (B) CD63⁺ EVs (exosomes), (C) CD11b⁺ EVs (microvesicles derived from microglia/macrophages) and (D) ACSA2⁺ EVs (microvesicles derived from astrocytes). * p < 0.05, ** p < 0.01, *** p < 0.001, based on one-way ANOVA with Dunnett correction for multiple comparisons to sham. Experiments based on animals of N= 8/group.



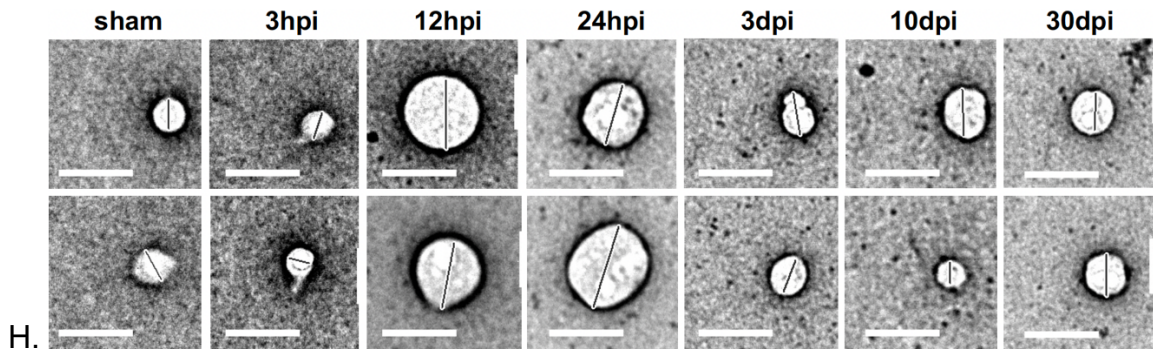


Figure 5.7: Representative TEM images of EVs isolated by UC. A. Sham control B. 3 hours C. 12 hours D. 24 hours E. 3 days F. 10 days and G. 30 days. Note the range of small (~70 nm) to large (~300 nm) diameter sizes of the particles. Particles are mostly round, with some oblong shaped. H. Two representative close up views of EVs shown. Marker is 250 nm. Measurements made using the TEM software.

5.3 Elevated DNA content within EVs in the acute phase post injury

Previous studies in rat (OHAYON; BOYKO; SAAD; DOUVDEVANI *et al.*, 2012) and porcine (KILBAUGH; LVOVA; KARLSSON; ZHANG *et al.*, 2015) models of TBI demonstrated increased amounts of DNA in circulation, but specific measurements in EVs were lacking. We recently reported elevated DNA levels, particularly mitochondrial DNA (mtDNA), within EVs in human subjects during the acute phase post-TBI and proposed quantifying DNA in EVs as an independent indicator of TBI severity in liquid biopsies (MARCATTI; SAADA; OKEREKE; WADE *et al.*, 2021). However, how DNA levels within EVs change over time post-injury is currently unknown.

Since we measured significant changes in EV number post-TBI, we used 100 million EVs to normalize for the number of particles in our samples for the quantification of DNA content. Using qPCR with mtDNA and nuDNA specific primers, we measured marked increase of both mtDNA and nuDNA content at 12 hpi with subsequent decrease at later time points (**Figure 5.8**). Next, we tested

whether circulating DNA in plasma was exclusively present in EVs or also in “free floating form”. Indeed, we measured more than 90% of the circulating mtDNA is present within EVs compared to their “free-floating form” (**Figure 5.9**). Given the significantly lower amount of nuDNA (3 orders of magnitude less than mtDNA), detecting differences in nuDNA content between EVs and the “free-floating form” was challenging due to qPCR detection limits. Further analysis into the data revealed additional insights into the dynamic changes of DNA content within EVs post injury. A fold change analysis shows a trend of preferential release of mtDNA over nuDNA compared to sham control (**Figure 5.10**).

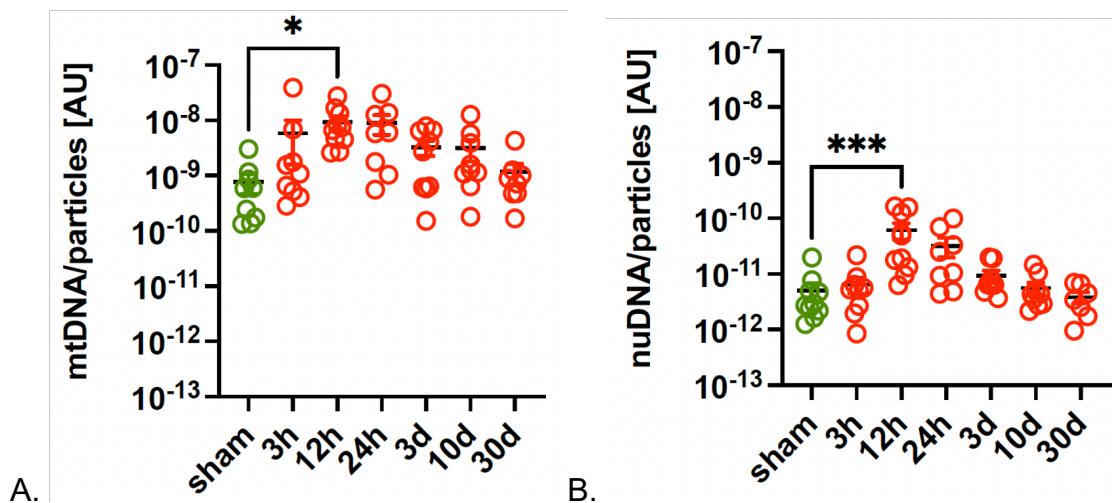


Figure 5.8: DNA levels are elevated in the acute phase post injury. A. mtDNA and B. nuDNA content within EVs are significantly higher at 12 hpi compared to sham control levels. Notably, overall mtDNA content is 3 orders of magnitude higher than their nuDNA counterparts. * = $p < 0.05$, *** = $p < 0.001$, based on one-way ANOVA with Dunnett correction for multiple comparisons to sham. Experiments based on animals of $N=8$ /group.

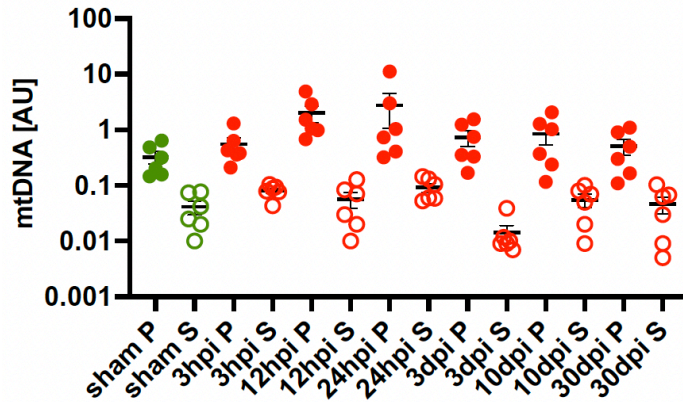


Figure 5.9: mtDNA is predominantly found in EVs. The majority of mtDNA is found encapsulated within EVs as opposed to “free floating” in the supernatant. Over 90% of all mtDNA is in the pellet with the EVs. nuDNA content quantification was difficult due to the technical detection limits of qPCR. Experiments based on animals of N=6/group.

Together, this set of data demonstrates that TBI triggers the release of EVs with enhanced DNA content, particularly of mtDNA origin, during the acute phase. These results support the potential of examining DNA content in EVs as an independent indicator for TBI detection.

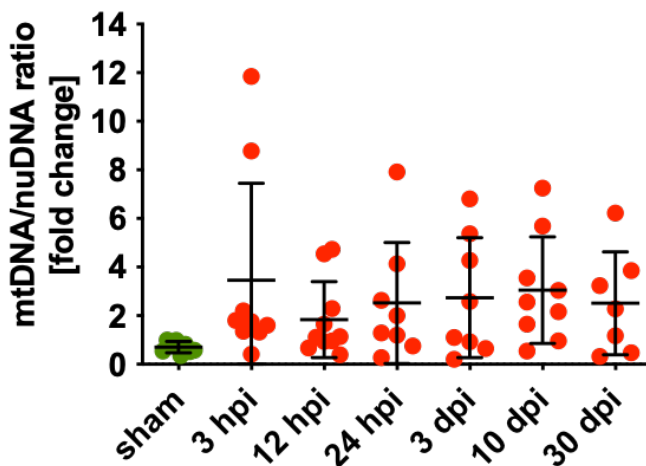


Figure 5.10: Preferential release of mtDNA over nuDNA. Although no time points are statistically significant, there is a clear trend of upregulated release of mtDNA over nuDNA across all phases post-injury. Experiments based on animals of N= 8/group.

5.4 Targeted immunoblotting for temporal alterations of neuronal, microglial, and astrocytic markers in circulating EVs post injury

We investigated currently the best characterized TBI-related protein markers: GFAP, NFL, S100 β , NSE (neuron specific enolase), UCH-L1, and Tau (CZEITER; AMREIN; GRAVESTIJN; LECKY *et al.*, 2020; GAN; STEIN; SWANSON; GUAN *et al.*, 2019; MARTINEZ; STABENFELDT, 2019; MONDELLO; SORINOLA; CZEITER; VAMOS *et al.*, 2018; THELIN; ZEILER; ERCOLE; MONDELLO *et al.*, 2017). However, so far only NFL, GFAP, and tau were previously examined in EVs (FLYNN; LEETE; SHAHIM; PATTINSON *et al.*, 2021; GUEDES; DEVOTO; LEETE; SASS *et al.*, 2020; KAWATA; MITSUHASHI; ALDRET, 2018; MONDELLO; GUEDES; LAI; CZEITER *et al.*, 2020; MONDELLO; SORINOLA; CZEITER; VAMOS *et al.*, 2018; WINSTON; ROMERO; ELLISMAN; NAUSS *et al.*, 2019). Due to temporal variations in the number of EVs post injury, we again normalized the changes in levels of these proteins to 100 million EVs isolated at each time point post-TBI. Surprisingly, we did not detect S100 β , NSE, UCH-L1, and Tau proteins in the isolated EVs at any time point, although antibody specificity were confirmed using cortex homogenates (**Figure 5.11**). This suggests that these proteins are either not localized within EVs or are present in amounts below the detection limit of Western blotting. However, we observed an increased presence of NFL (neuronal marker) and Iba1 (microglia marker) mainly at 12 hpi (**Figure 5.12B,C**), while GFAP (astrocyte marker) gradually increased and peaked at 3 dpi (**Figure 5.12D**).

Together, our analysis revealed cell-type-specific responses to TBI that can be measured in circulating EVs, with neuronal and microglial reactivity during the acute phase and astroglial reactivity during the acute and sub-acute phases of TBI. Furthermore, these temporal patterns of brain-derived marker expression suggests TBI pathophysiology dynamically affects neural cell types differently as the disease progresses.

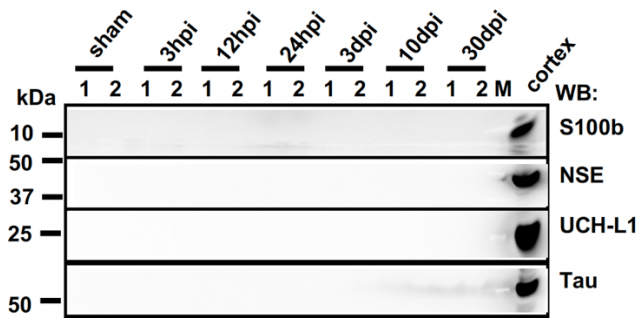


Figure 5.11: TBI induced circulating EVs do not contain S100 β , NSE, UCH-L1 and Tau proteins. Example of Western blot analysis of EVs isolated from two individual mice using antibodies as indicated. Mouse cortex (40 μ g) was used to control for antibody specificity. Experiments based on animals of N= 2/group.

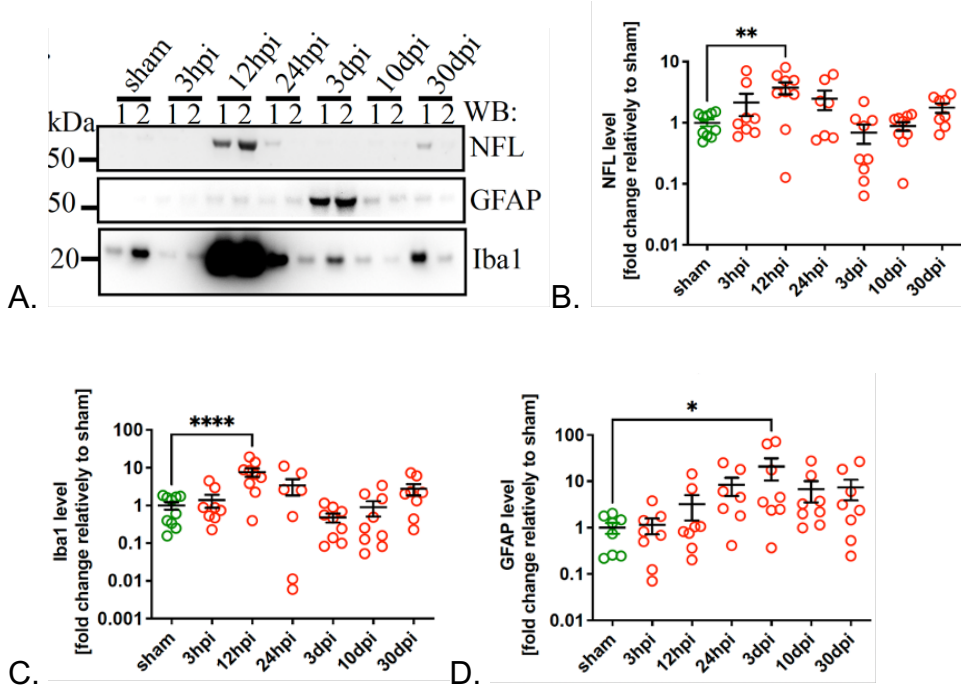


Figure 5.12: Dynamics of brain-derived markers in EVs post injury. A. Representative Western blots of neuronal (NFL), microglial (Iba1), and astrocytic (GFAP) markers expression across all time points post injury. B, C. NFL and Iba1 peak in the 12 hpi acute phase. D. However, GFAP displays a slightly delayed response at 3 dpi. Protein intensities reported as relative to sham control. * = $p < 0.05$, ** = $p < 0.01$, **** = $p < 0.0001$, based on one-way ANOVA with Dunnett correction for multiple comparisons to sham. Experiments based on animals of N= 8/group.

5.5 EVs Proteomics and Biostatistical Analysis identify several novel promising TBI biomarkers

Previous studies mostly focused on individual brain-related targets in liquid biopsies post injury using antibodies based approaches. However, recognizing the systemic effects of TBI, we conducted global unbiased mass spectrometry proteomics analysis of 100 million EVs of each sample at all time points post injury. We identified approximately 250 distinct proteins with 229 that were previously reported in one or both of the comprehensive EVs-protein specific databases Vesiclopedia and ExoCarta (**Figure 5.13A**). Notably, we discovered 13 unique proteins specific to our proteomics data that have previously not been reported in the databases (**Figure 5.13B**). These proteins include several major urinary proteins and subunits of complement C. These findings are not surprising, as TBI affects renal function (DE VLIEGER; MEYFROIDT, 2023; PESONEN; BEN-HAMOUDA; SCHNEIDER, 2021), while the activation of the complement system is well reported post injury (ALAWIEH; LANGLEY; WEBER; ADKINS *et al.*, 2018; HAMMAD; WESTACOTT; ZABEN, 2018).

Figure 5.14: Pearson correlation coefficient heat map. Every protein and their respective LFQ intensities were compared to all other samples for correlation in presence and expression intensities. Darker coloring represents higher correlation. The overall good correlation between all samples suggests a high consistency in technical and experimental procedures. It is worth noting the 12 hpi and 30 dpi groups have the least amount of correlation compared to sham control, suggesting there may be enrichment of potential biomarkers due to significant differences in protein composition in those experimental groups.

Next, we conducted a one-way analysis of variance (ANOVA) and Dunnett's post-hoc test ($p < 0.05$) for all proteins' LFQ values that are significantly up or downregulated compared to sham control. To minimize the chances of a false positive, we employed the false discovery rate (FDR) correction (KORTHAUER; KIMES; DUVALLET; REYES *et al.*, 2019) with fold change cutoffs of $\text{LOG}(\text{FC}) > 2$ or $\text{LOG}(\text{FC}) < -2$ as potential biomarkers, reflecting significant up- or downregulation, respectively. A number of identified proteins met our threshold criteria at different time points post-TBI: 8 proteins at 3 hpi (**Figure 5.15A**), 29 at 12 hpi (**Figure 5.15B**), 8 at 24 hpi (**Figure 5.15C**), 14 at 3 dpi (**Figure 5.15D**), 20 at 10 dpi (**Figure 5.15E**), and 37 at 30 dpi (**Figure 5.15F**). Among these, 23 proteins were upregulated and belonged to two major groups: antitrypsin/serine protease inhibitors and apolipoproteins. These proteins were identified at multiple time points, limiting their value as specific markers for distinct phases post-TBI. However, we also found specific proteins that could serve as potential novel biomarkers for acute and chronic phases post-TBI. Notably, serum amyloid A (SAA) protein were specifically upregulated for the acute phase (12 hpi) (**Figure 5.15B**), while complement factor D (CFD) and corticosteroid-binding globulin (CBG) were specific for the chronic phase (30 dpi) (**Figure 5.15F**). Interestingly, the elevated levels of these proteins were already shown in the plasma of human

TBI subjects but whether they localized with EVs was not tested (ALAWIEH; LANGLEY; WEBER; ADKINS *et al.*, 2018; HAMMAD; WESTACOTT; ZABEN, 2018; WICKER; BENTON; GEORGE; FURLOW *et al.*, 2019). Furthermore, we identified 4 proteins that were downregulated by at least 2-fold with $p < 0.05$. Among these, there was a marked reduction of haptoglobin (Hp) at 3 dpi (**Figure 5.15A**) and von Willebrand factor (VWF) at 30 dpi (**Figure 5.15F**), both known markers of vascular injury in TBI (GRAW; YU; REZOAGLI; WARREN *et al.*, 2017; LIP; BLANN, 1997). Lastly, we have compiled a list of proteins that were significantly changed by TBI, but did not meet the 2-fold increase (**Table 5.2A**) or 2-fold decrease (**Table 5.2B**).

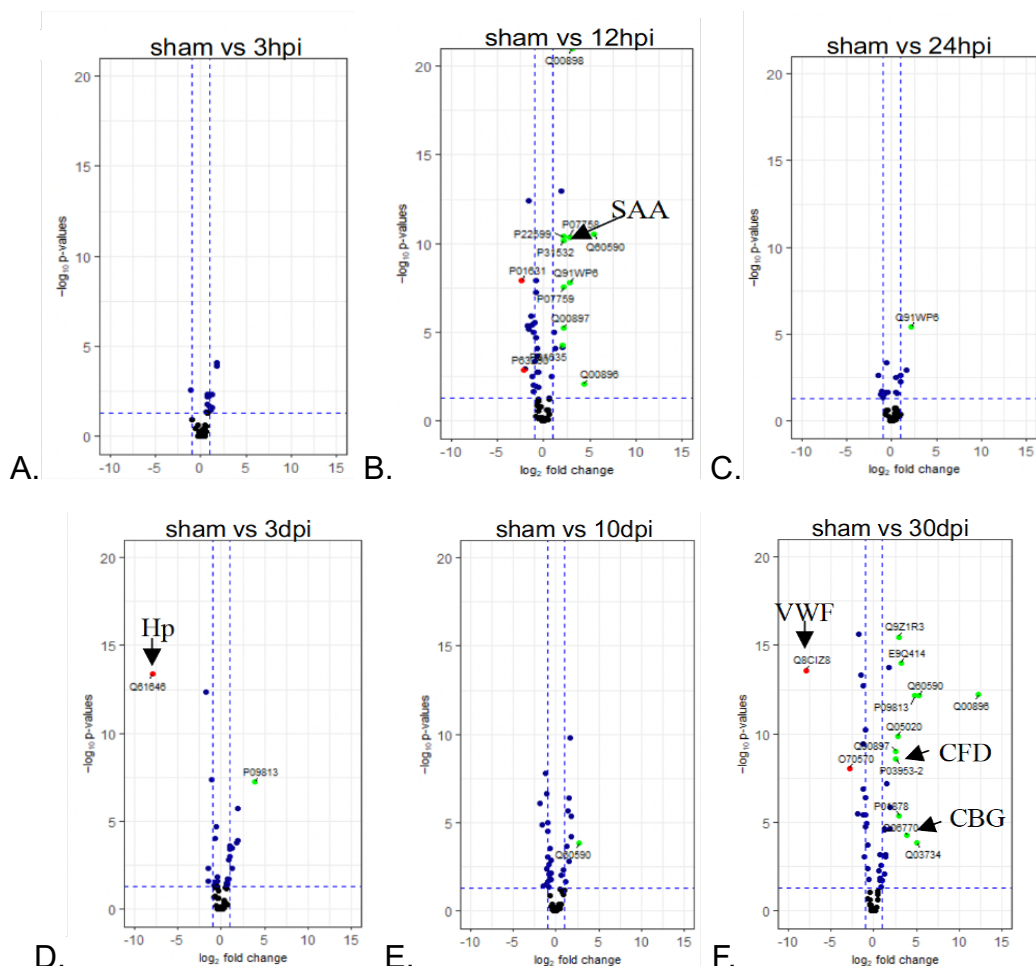


Figure 5.15: Potential targets from biostatistical analysis of proteomics. Volcano plots of each time point compared to sham control reveals proteins that are significantly up- or downregulated and have a fold change of >2 or <-2. False discovery rate (FDR) correction was used to minimize the chances of a false positive. A, B, C. Majority of significant potential targets belonged to 12 hpi in the acute phase time points. D, E, F. Similarly, 30 dpi in the chronic phase provided the greatest number of potential biomarkers. As predicted by the Pearson correlation heat map, these 2 time points had the least amount of correlation to sham control, thus resulting in many statistically significant proteins. Notable proteins warranting further investigations are highlighted in green (upregulated) and red (downregulated). Experiments based on animals of N= 10/group.

protein ID	protein name	fold change	p value
sham vs 3hpi			
P07758	Alpha-1-antitrypsin 1-1	1.023504	0.00546614
P33622	Apolipoprotein C-III	1.082324	0.03420398
P52430	serum paraoxonase/arylesterase 1	1.282574	0.00485485
P70274	Selenoprotein P	1.311104	0.02396177
P01942	Hemoglobin subunit alpha	1.755942	0.00012752
Q00897	Alpha-1-antitrypsin 1-4	1.793412	7.94E-05
sham vs 12hpi			
Q06890	Clusterin	1.106806	1.08E-05
P06728	Apolipoprotein A-IV	1.252962	7.85E-05
Q00623	Apolipoprotein A-I	1.922746	1.11E-13
P33622	Apolipoprotein C-III	1.97753	7.35E-05
sham vs 24hpi			
P07759	Serine protease inhibitor A3K	1.0022735	0.00568024
P01942	Hemoglobin subunit alpha	1.581428	0.00112563
sham vs 3dpi			
P14106	Complement C1q subunit B	1.036334	0.00035869
Q00897	Alpha-1-antitrypsin 1-4	1.281304	0.00451282
P07758	Alpha-1-antitrypsin 1-1	1.302188	0.00035728
P01942	Hemoglobin subunit alpha	1.74365	0.00016776
P33622	Apolipoprotein C-III	1.86793	0.00012038
Q05020	Apolipoprotein C-II	1.88958	1.96E-06
sham vs 10dpi			
P01942	Hemoglobin subunit alpha	1.079006	0.02259358
P07759	Serine protease inhibitor A3K	1.267862	0.00022671
P22599	Alpha-1-antitrypsin 1-2	1.340944	2.19E-06
Q07968	Coagulation factor XIII B chain	1.483868	4.32E-07
P33622	Apolipoprotein C-III	1.553044	0.00148613
Q00898	Alpha-1-antitrypsin 1-5	1.686654	1.59E-10
P07758	Alpha-1-antitrypsin 1-1	1.720412	4.28E-06
Q00897	Alpha-1-antitrypsin 1-4	1.792788	6.50E-05
sham vs 30dpi			
Q8CG16	Complement C1r-A	1.2188895	2.34E-05
P07759	Serine protease inhibitor A3K	1.2724635	2.85E-05
Q8CG14	Complement C1s-A	1.439023	0.00085242
P34928	Apolipoprotein C-I	1.501331	6.69E-08
Q00623	Apolipoprotein A-I	1.839652	1.78E-14
P33622	Apolipoprotein C-III	1.847221	2.24E-05
P98064	Mannan-binding lectin serine protease 1	1.9180455	1.34E-06

A.

protein ID	protein name	fold change	p value
sham vs 3hpi			
P46412	Glutathione peroxidase 3	-1.0926	0.00272223
sham vs 12hpi			
P70389	Insulin-like growth factor-binding protein complex acid labile subunit	-1.797704	4.15E-06
P46412	Glutathione peroxidase 3	-1.677794	6.46E-06
Q8K182	Complement component C8 alpha chain	-1.675724	3.71E-13
Q9JUN5	Carboxypeptidase N catalytic chain	-1.410448	1.28E-06
Q9DBB9	Carboxypeptidase N subunit 2	-1.29884	3.70E-06
Q61508	Extracellular matrix protein 1	-1.207614	0.00331403
Q8BH61	Coagulation factor XIII A chain	-1.059634	0.02314028
P01592	Immunoglobulin J chain	-1.05555	0.00973218
P06683	Complement component C9	-1.048924	1.06E-05
O70362	Phosphatidylinositol-glycan-specific phospholipase D	-1.021162	0.00045605
sham vs 24hpi			
Q8CG14	Complement C1s-A	-1.525297	0.00243886
Q9QWK4	CD5 antigen-like	-1.0505985	0.02024458
sham vs 3dpi			
Q61646	Haptoglobin	-7.93895	4.36E-14
P06683	Complement component C9	-1.81387	4.46E-13
P63260	Actin	-1.541268	0.02493878
Q8K182	Complement component C8 alpha chain	-1.133236	4.46E-08
sham vs 10dpi			
P70389	Insulin-like growth factor-binding protein complex acid labile subunit	-1.894166	8.15E-07
P14847	C-reactive protein	-1.639714	1.28E-05
P63260	Actin	-1.452708	0.03770543
Q8K182	Complement component C8 alpha chain	-1.198056	1.67E-08
P49182	Heparin cofactor 2	-1.166788	0.02809606
Q9DBD0	Inhibitor of carbonic anhydrase	-1.061716	2.16E-07
P46412	Glutathione peroxidase 3	-1.050696	0.0040959
P98064	Mannan-binding lectin serine protease 1	-1.038332	0.02211326
sham vs 30dpi			
Q8BH61	Coagulation factor XIII A chain	-1.90996925	3.22E-06
P39039	Mannose-binding protein A	-1.75484225	2.22E-16
P01029	Complement C4-B	-1.5010925	5.00E-14
P13020	Gelsolin	-1.2672145	3.84E-10
P06684	Complement C5	-1.24668475	1.91E-13
Q07968	Coagulation factor XIII B chain	-1.182087	4.05E-06
Q61704	Inter-alpha-trypsin inhibitor heavy chain H3	-1.1793535	1.35E-07
P07758	Alpha-1-antitrypsin 1-1	-1.09278575	0.00084228
Q61703	Inter-alpha-trypsin inhibitor heavy chain H2	-1.0260855	1.77E-05
Q61129	Complement factor I	-1.0183035	3.89E-07

B.

Table 5.2: Proteins significantly changed in EVs after TBI. List of proteins (A) upregulated and (B) downregulated with p<0.05 but did not reach threshold of <-2 or > 2-fold change, respectively.

Together, our proteomic analysis unveiled time-dependent changes in the protein content of circulating EVs post injury. Among the identified proteins, SAA, CFD, CBG (upregulated), Hp, and VWF (downregulated) are particularly

interesting as potential novel biomarkers specific for the acute and chronic TBI phases.

5.6 Computational Evaluation of EVs Proteomics for identification of TBI-specific biomarkers

The proteomics data was further subjected to a computational machine learning process, Graph Neural Network (GNN)-based framework, to identify additional potential biomarkers for TBI. This network incorporated not only LFQ intensities, but also neurological associations, predicted protein-protein interactions, and database mining of previous experimental evidence for a more holistic interpretation of the proteomics data. We constructed a basal Protein-Protein Interaction (PPI) network using available databases from the STRING tool (Figure 4.15a) (SZKLARCZYK; GABLE; LYON; JUNGE *et al.*, 2019). The identification of potential biomarkers was formulated as a node classification problem, with node labels representing ranks from 1 (highest probability) to 6 (lowest probability). Using GNN-based learning techniques, we predicted the labels (i.e., probabilities of individual proteins being potential biomarkers) for all nodes in the network and generated networks with ranks for potential biomarkers for all time points compared to sham control (**Figure 5.16B**).

A number of apolipoproteins (Apo) and alpha-1-acid glycoproteins (Orm1 and Orm2) are well represented across the different time points in the network rankings. A potential reason why these proteins are prevalent may be attributed to their roles in BBB integrity and function for apolipoproteins, as well as acute inflammatory response for alpha-1-acid glycoproteins. Notably, serum amyloid

protein A (SAA) was ranked highly by computational analysis as potential biomarker for acute TBI phases, further confirming the potential utility of SAA as a TBI biomarker in clinical settings (**Table 5.3**).

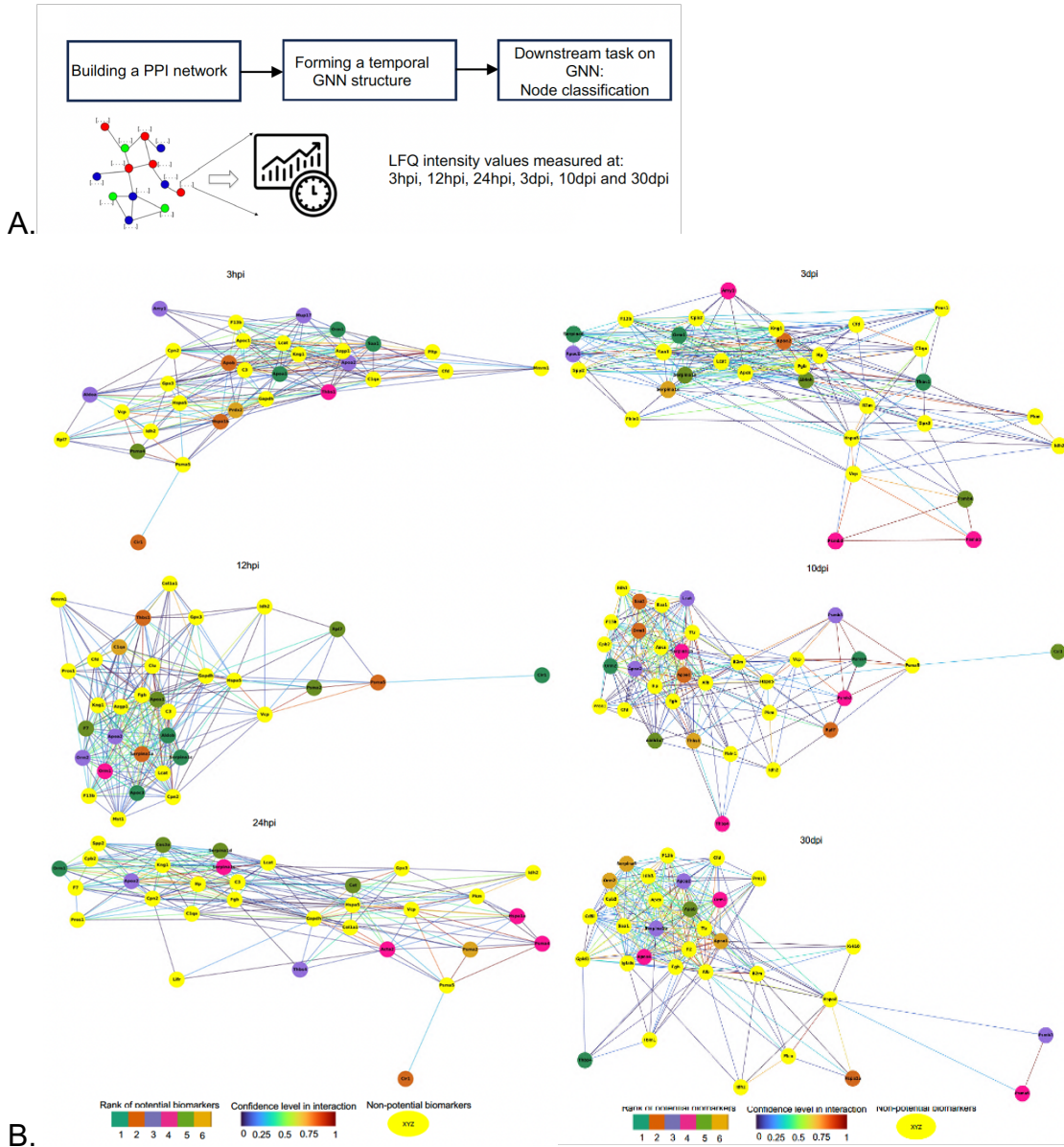


Figure 5.16: Computational analysis of EVs proteomics. (A) Analysis flow using STRING to build initial protein-protein interaction (PPI) network followed by Graph Neural Network (GNN)-based framework. (B) GNN enrichment analysis for potential biomarkers for each time point. Each protein is highlighted as a node with interactions between proteins represented as connections. Sliding color scale represents the confidence level of interaction between proteins as calculated from GNN. Rank of potential biomarkers are listed 1-6 with corresponding colors.

Rank	Time					
	3 hpi	12 hpi	24 hpi	3d pi	10 dpi	30 dpi
1	Orm1 Apoa1 Saa	Aldob Serpina1c Cir1 Apoc3	Orm1	Thbs1 Orm1 Serpina6	Orm2 Psm4	Thbs4
2	Apob Cir1 Hspa1b	Thbs1 Psm5 Serpina1a	Cir1	Apoa2	Apoa1 Orm1 Saa2 Rpl7	Hspa1a
3	Apoa2 C1sa Amy1 Aldoa Mup17	Orm2 Apoa2	Thbs4 Apoa2	Apoc2	Psm8 Apoa2 Lcat	Apoa2 Serpina1b Psm3
4	Thbs1	Orm1	Serpina1c Acta2 Psm4 Hspa1a	Amy1 Psm5 Psm3	Thbs4 Psm2 Serpina1b	Apoa4 Psm5 Orm1
5	Psm4	Apoa1 Psm2 F7 Rpl7	Cat Ces3a Serpina1d	Aldob Serpina1a Psm6	Cir1 Aldh1a7	Apob
6	Prdx2	C1qa	Psm2	Serpina1e	Thbs1	Apoa1 Orm2 Serpina6

Table 5.3: List of ranked potential biomarkers broken down per time point. Orm1, Alpha-1-acid glycoprotein 1; APOA1, Apolipoprotein A1; Saa, Serum Amyloid A; Aldob, Aldolase; Serpina, Alpha-1-Antitrypsin; Cir1, Corepressor Interacting With RBPJ; Apoc3, Apolipoprotein C-III; Thbs, Thrombospondin; Psm4, Proteasome 20S Subunit Alpha 4; Hspa, HSP70; Rpl7, Ribosomal Protein L7; C1, Complement C; Amy, Amylase; Mup, Major Urinary Protein; Lcat, Lecithin-Cholesterol Acyltransferase; Acta, Actin Alpha 2; F7, Coagulation Factor VII; Cat, Catalase; Ces3a, Carboxylesterase 3; Aldi, Aldehyde dehydrogenase; Prdx, Peroxiredoxin.

Our next step was to validate our potential proposed biomarkers. Because SAA, Hp, VWF, CFD, and CBG are highly abundant in the blood and not brain specific, it is possible that these proteins are enriched due to contamination of our EVs samples. To address this possibility, we performed additional Western blot analysis of SAA and CFD (upregulated at acute and chronic TBI phases, respectively) using 10x more EVs with 2 samples per experimental time point. SAA is a monomer with a molecular weight of 15kDa; our results showed a clear 15 kDa

SAA signal from the control mouse brain cortex sample, but absent in our EVs fractions (**Figure 5.17A**). However, we detected a higher molecular weight signal at the 30 kDa mark in both cortex extract and EVs fractions, suggesting the possibility of an SAA dimer (**Figure 5.17A**). Notably, the pattern of changes of this putative SAA dimer aligns with our proteomic and computational data indicating increased SAA levels in certain TBI phases. The presence of multimeric SAA forms have been reported in previous works (LU; YU; ZHU; CHENG *et al.*, 2014). In a similar fashion, CFD, a 25 kDa protein expressed mostly by adipose tissue and not brain cortex (STANTON; YATES; DEN HOLLANDER; SEDDON *et al.*, 2011), has not been reported to undergo multimerization, our Western analysis revealed a 60 kDa band, indicating the presence of a CFD dimer in EVs fractions (**Figure 5.17B**). Intriguingly, the highest putative 60 kDa CFD dimer was detected in EVs isolated during the chronic TBI phase, aligning with our proteomic and computational analyses. Although our results regarding possible multimerization of SAA and CFD is purely speculative and needs further testing, the absence of SAA and CFD monomers in EVs fractions may be simply attributed to their low abundance, below the detection limit of Western analysis. However, our validation analysis introduces another intriguing possibility regarding the nature of proteins in EVs, which have previously been assumed to be in their native form, but our data shows the potential for modified (posttranslational modifications, multimeric, truncated) proteins to be encapsulated. This opens new avenues for understanding their biological outcomes in the EVs space compared to their cellular origins.

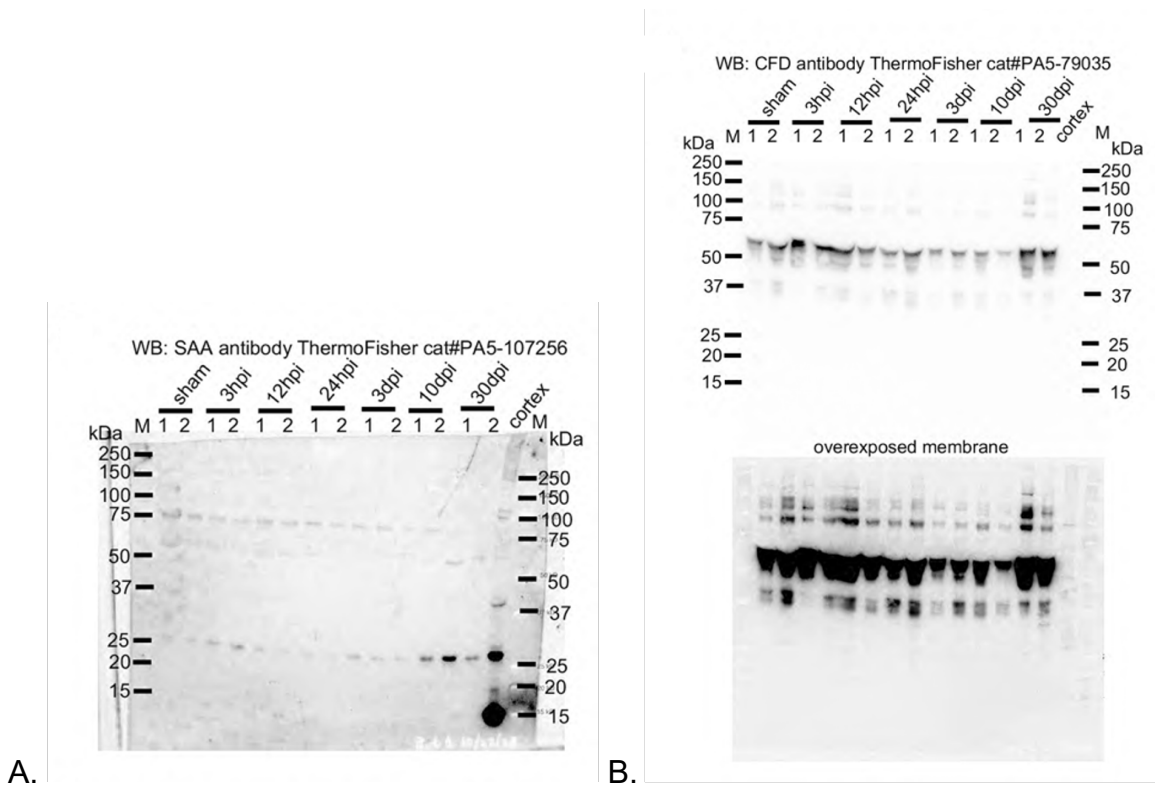


Figure 5.17: Validation of proposed SAA and CFD markers for TBI. EVs fractions were loaded with 10x more EVs (1 billion particles) along with 40 μ g of control mouse cortex sample and probed for A. SAA and B. CFD with short and longer exposure. The expected 15 kDa SAA signal was present in the control, but absent in EVs samples. However, the presence of a 30 kDa signal suggests SAA may be dimerized in EVs. Similarly, the 30 kDa CFD signal was only present in the control, but 60 kDa signals were present in the EVs. Experiments based on animals of N= 2/group.

5.7 Cultured neurons subjected to *in-vitro* model of TBI release EVs containing mtDNA

From our NTA (**Figure 5.4**) and qPCR (**Figure 5.8**) data, we observed the dynamic changes in biophysical properties of EVs across the different phases post injury along with the increased release of DNA, in particular mtDNA. Thus, we investigated whether neurons subjected to TBI can release EVs containing DNA. To mimic the shearing forces of a blunt force TBI, we used an *in-vitro* cell culture model of rat hippocampal neural stem cells (rHNSC). rHNSC cells generate a pure neuronal culture and has the ability to differentiate into neurons (MICCI;

KRISHNAN; BISHOP; ZHANG *et al.*, 2019). Rapid stretch injury (RSI) replicates the shearing forces of blunt TBI by rapidly stretching the cells via pressure applied by a vacuum. We examined the DNA content of EVs released by differentiated rHNSC neurons post RSI into the cell culture medium. Using qPCR primers located within the mitochondrial NAD1 and COXIII genes, we detected a significant 3 to 4-fold increase of mtDNA at the 1h post RSI acute phase (**Figure 5.18A**). In contrast, we did not detect any differences in the nuclear ACTB gene across all time points. Additionally, we analyzed the biophysical properties of EVs by NTA and noticed a marked increase in the number of EVs at 1h post RSI together with an increased mean diameter size of EVs (**Figure 5.18B**). Interestingly, the overall proportion of DNA in EVs was significantly skewed towards mtDNA with a 250-fold difference over nuDNA (**Figure 5.18C**). We further confirmed that RSI induced damaged mtDNA is released mainly through EVs by quantifying the amount of mtDNA within EVs versus their “free floating” form in the supernatant. Using qPCR, we confirmed that the majority of circulating mtDNA were present within EVs at 1h post RSI (**Figure 5.18D**). Together, this set of data shows that TBI induces acute EVs release from neurons and the majority of DNA contained within these particles are mtDNA.

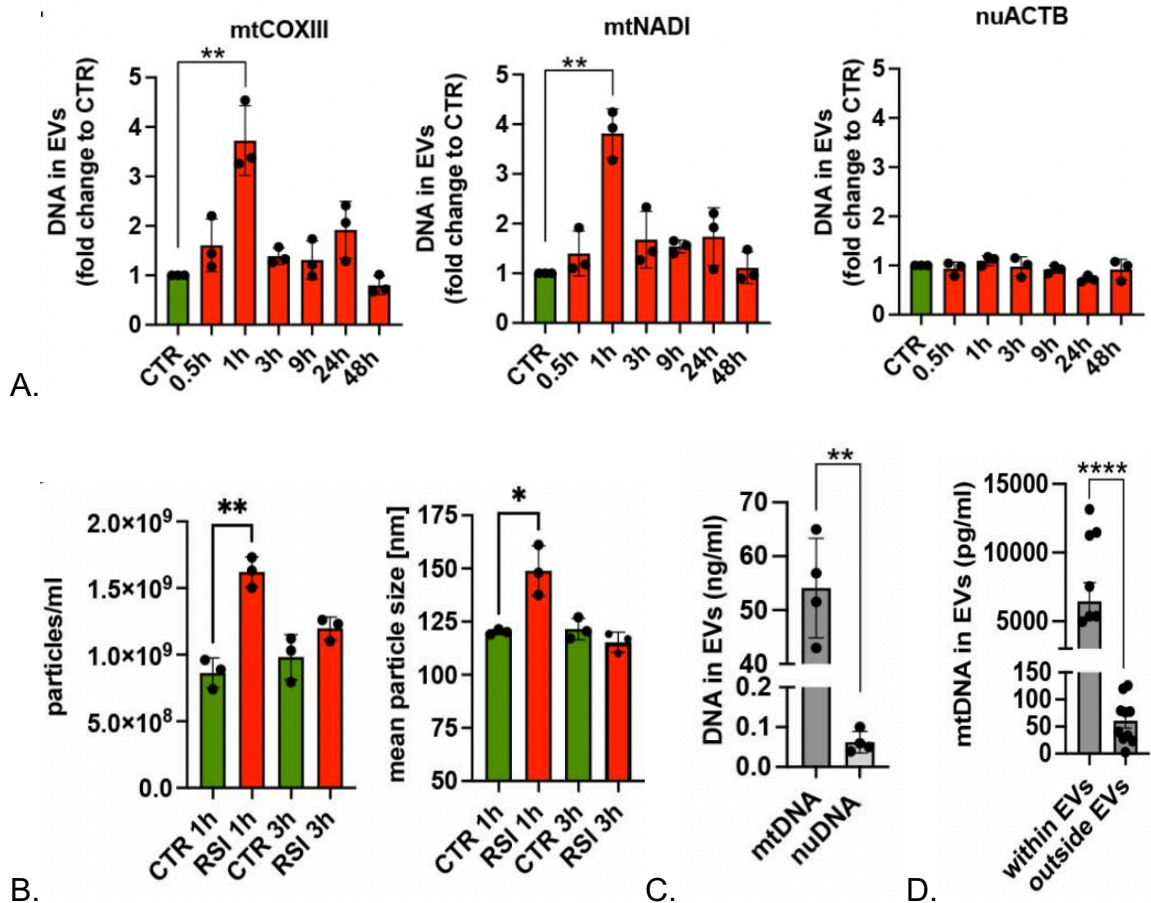


Figure 5.18: RSI causes acute mtDNA release in EVs from neurons. rHNSC differentiated into neurons were subjected to RSI and DNA content was quantified. A. mtDNA (COXIII and NADI), but not nuDNA, is significantly upregulated at 1h post RSI before returning to baseline levels at 3h. B. The number and size of EVs released post RSI shows a sharp increase only at the 1h time point as determined by NTA. C, D. The majority of DNA is encapsulated within EVs and of mitochondrial origin rather than nuclear. Data based on three independent experiments. * = $p < 0.05$, ** = $p < 0.01$, and **** = $p < 0.0001$. Kruskal-Wallis One-Way ANOVA test or t-Test for two group analysis. Data based on 3 independent experiments.

5.8 Analysis of DNA content in EVs released from glucose oxidase treatment of ARPE-19 cells

We have shown that TBI induces the increased release of DNA in EVs post injury (Figures 5.8 and 5.18). However, the properties of the mtDNA content remains warrants further investigation. Here, we investigated the sizes of mtDNA using an in-vitro model of age-related macular degeneration, the most common

type of RPE-initiated ocular pathology (SAADA; MCAULEY; MARCATTI; TANG *et al.*, 2022). We specifically used a non-neuronal model to prove the ubiquitous nature of mtDNA release in EVs from an insult or stressor. Glucose oxidase (GOx) enzymatically generates constant low levels of hydrogen peroxide (H₂O₂) over an extended period of time (WONG; WONG; CHEN, 2008). Previous experiments showed that 10 mU/mL of GOX generated 40 μM, 60 μM, and 100 μM of H₂O₂ within 1, 3 and 6 hours, respectively (SAADA; MCAULEY; MARCATTI; TANG *et al.*, 2022). Using a sublethal dose of 30 mU/mL of GOx, this compound was treated onto differentiated human ARPE-19 cells to mimic the low levels of oxidants that are suspected to drive the ocular pathologies. Similar to the rHNSC cells, treatment of GOx induced the release of EVs over the course of 24 hours with enhanced amounts of mtDNA. To investigate the mtDNA properties in EVs, we analyzed for sequence specificity and fragment sizes of these mtDNA by designing primers that amplified mtDNA fragments from 200 bp up to 6 kb covering the entire mitochondrial genome (**Figure 5.19A**). Using qPCR, we detected increased amounts of most of the mtDNA-encoded genes from EVs released by GOx treated ARPE-19 cells compared to non-treated controls (**Figure 5.19A**). Moreover, our results showed no enrichment of specific regions of the mitochondrial genome or fragment sizes, as we were able to amplify the majority of the mtDNA fragments, particularly in EVs derived from GOx-treated cells (**Figure 5.19B and 5.19C**). This set of data reinforces the idea that mtDNA is ubiquitously released in EVs in response to injury. Furthermore, the presence of various amplicon lengths may hint at the different sized EVs that are released and their cargo capacity.

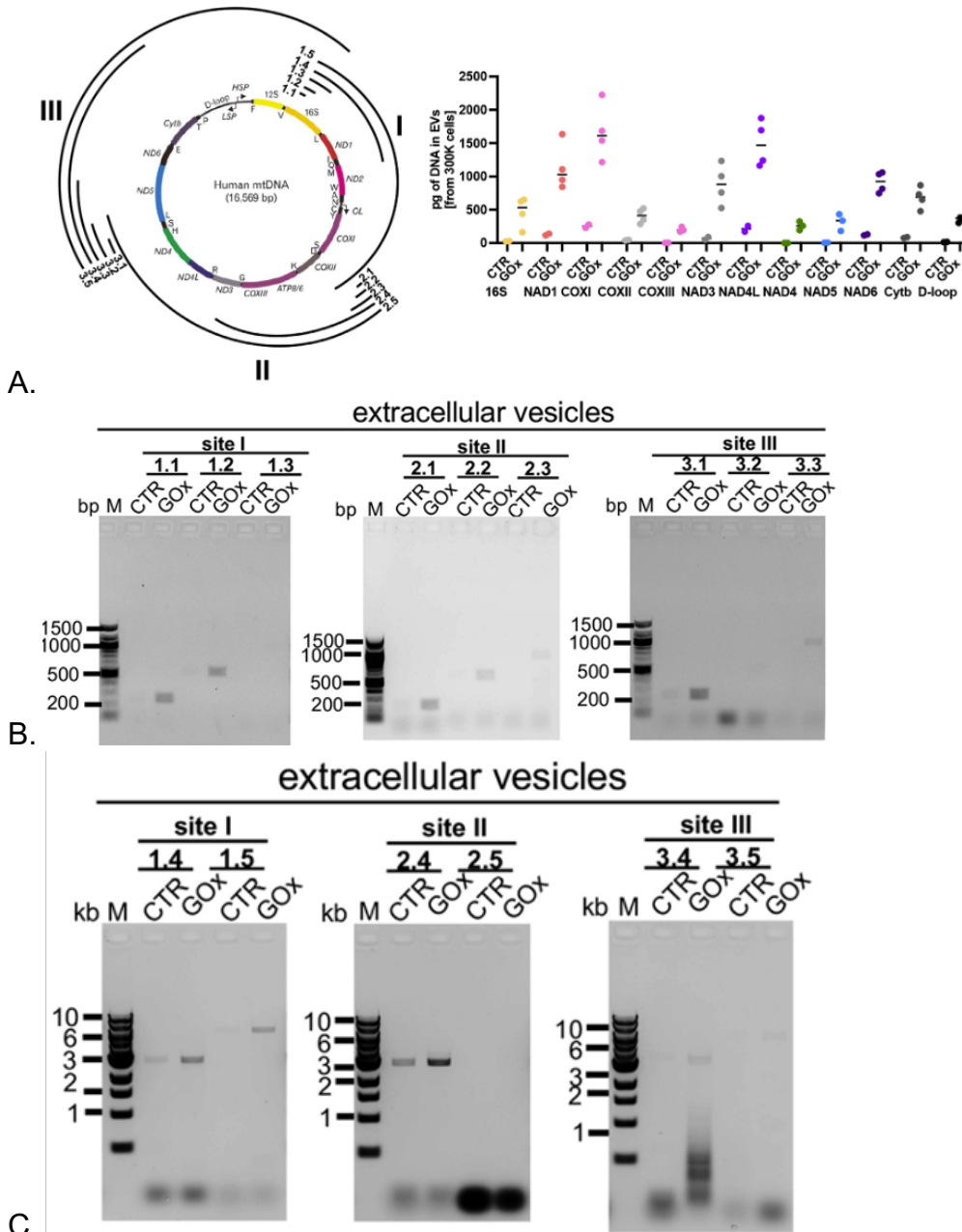


Figure 5.19: ARPE-19 derived EVs contain large fragments of mtDNA. A. schematic representation of human mtDNA together with primers used in analysis and all tested genes encoded by mtDNA are present in EVs released from GOx-treated ARPE-19 cells as measured by qPCR. Analysis of the mtDNA fragment size in EVs released at 24 h from the same number of CTR and GOx-treated ARPE-19 cells was performed. The amplicons of (B) 200 bp–1 kb and (C) 3–6 kb were analyzed. Representative images of N= 3 are shown (B and C). Please note enhanced amounts of amplicons in EVs isolated particularly from GOx-treated ARPE-19 cells

Chapter 6. Summary, Discussion, Limitations, and Future

Directions

6.1 Summary

In this study we comprehensively analyzed DNA and protein content of circulating EVs in blood as potential TBI biomarkers. Our findings highlight the presence of DNA, particularly mtDNA, and SAA within EVs circulating in plasma as novel, stable and reliable targets for TBI detection. Additionally, we validated NFL and GFAP, along with Iba1 as potentially promising emerging biomarkers of TBI. Furthermore, our investigation revealed the dynamic release of diverse subpopulations of EVs in TBI, including those originating from brain, as potential markers of detrimental processes occurring in brain post injury. Using in-vitro models of injury and stress, we confirmed the general release of different sized mtDNA fragments in EVs as a physiological stress response (SAADA; MCAULEY; MARCATTI; TANG *et al.*, 2022). Our study highlights the significance and potential of EVs as a valuable source of novel TBI biomarkers. Moreover, our study indicates that future diagnostic platforms should measure biophysical properties of EVs and incorporate combination of specific DNA and protein probes to fully assess TBI.

6.2 Discussion

The lack of comprehensive fluid-based biomarkers for the detection and assessment of TBI severity has compelled the urgent need to develop novel approaches to fill this gap in knowledge. The current diagnostic methods of GCS combined with imaging modalities are time consuming, cost-prohibitive, subjective, and fail to fully capture the complex pathophysiology of the phasic TBI disease

process. Ideally, diagnostic biomarkers should reflect the current disease status, predict the disease progression, rate the severity of injury, and be readily accessible in liquid biopsies. EVs have emerged as leading candidates in the field of both diagnostic markers and potential therapeutics across a plethora of diseases, including TBI. These biomolecules are ubiquitously released by all cell types, including neurological cells, into the extracellular space, where they are stable in the biofluid and protect their cargo from degradation. EVs carry a diverse range of cargo that reflect the current physiological and pathological status of their cellular origin, including proteins, nucleic acids, metabolites, and other biomolecules. Crucially, EVs can cross the BBB, facilitating the transfer of important information from the brain to the periphery. This unique feature makes EVs accessible in peripheral blood samples, allowing for non-invasive monitoring of TBI-induced changes. The dynamic alteration in EV cargo composition during TBI, such as changes in protein and DNA content, may provide valuable insights into the underlying pathophysiological processes in TBI progression. Most importantly, the inherent stability of EVs in biofluids offers promise for the development of sensitive and specific biomarkers, enabling early diagnosis, prognosis, and treatment monitoring for TBI patients. Additionally, changes in the biophysical properties (number, size) of EVs may provide additional valuable insights into the complex cellular responses following TBI, and may open new opportunities for developing EV-based biomarkers and therapeutics for TBI management, including cell specific damage in the secondary phase of injury. The

potential applications of EVs may open new avenues for developing EV-based biomarkers and therapeutics for TBI management.

In this study, we aimed to discover potential novel biomarkers by investigating changes in the biophysical properties of circulating EVs with their DNA and protein content across different phases of TBI using a preclinical weight drop mouse model. Our findings revealed significant alterations in the number and size of circulating EVs during the acute TBI phase, suggesting injury-specific changes within the EV subpopulations. Specifically, we observed a marked reduction in the number of EVs coinciding with an increase in their size at the 12 and 24 hpi acute phase (**Figure 5.4**) This significant difference corresponds with an enrichment of the exosomal marker CD63 (**Figure 5.6**). Furthermore, in both the acute and sub-acute TBI phases, we observed a dynamic increase in markers of microvesicles derived from microglia (CD11b) and astrocytes (ACSA-2) (**Figure 5.6**). These data highlight the dynamic release of specific EV subpopulations post-injury. However, there have been limited reports investigating the longitudinal changes in the biophysical properties of EVs in biofluids post-injury. In a mouse model of controlled cortical impact (CCI), the authors reported an increased number of EVs along with a decrease in their size up to 24 hpi (HAZELTON; YATES; DALE; ROODSELAAR *et al.*, 2018). Similarly, in a human CSF study, an increased number of EVs was detected at 1 dpi, but changes in their size were measured only after 4 dpi (KUHARIC; GRABUSIC; TOKMADZIC; STIFTER *et al.*, 2019). The apparent discrepancies between these findings and our study may be attributed to the differences in the TBI model used or the methods employed for

EVs detection. Further investigation is needed to compare and contrast these differences. However, our study agreed with previous reports of enhanced levels of microglia derived EVs in blood reported at 24 hpi in CCI mouse models (HAZELTON; YATES; DALE; ROODSELAAR *et al.*, 2018; KUMAR; STOICA; LOANE; YANG; ABULWERDI; KHAN; KUMAR *et al.*, 2017). To our knowledge, no previous studies have investigated the changes in astrocyte derived EVs in circulation post-injury. Nevertheless, our data supported by these reports underscore the critical importance of measuring the rapid dynamics of different EVs subpopulation release after TBI.

Mitochondrial dysfunction is a key feature of TBI. However, the quantification of extracellular mtDNA in bodily fluids, which is a powerful indicator of mitochondrial dysfunction (LIAO; CHEN; SONG; HE, 2022), has been relatively overlooked in TBI research. Studies have shown a significant increase in extracellular mtDNA levels in the blood during the acute phase of TBI in pigs (KILBAUGH; LVOVA; KARLSSON; ZHANG *et al.*, 2015), and in the CSF of pediatric patients (WALKO; BOLA; HONG; AU *et al.*, 2014). A general increase in circulating cell-free DNA (ccf-DNA), without discrimination between mtDNA and nuDNA, was observed in blood plasma of rats during the acute phase of TBI (OHAYON; BOYKO; SAAD; DOUVDEVANI *et al.*, 2012). This previous study is similar to our measurements of an increased amount of DNA, particularly mtDNA, in the acute phase (**Figure 5.8**). This data aligns with our recently reported study of increased amount of ccf-DNA in human serum samples immediately after injury (MARCATTI; SAADA; OKEREKE; WADE *et al.*, 2021). Furthermore, the increase

of extracellular mtDNA was predominantly encapsulated within EVs, as more than 90% of all ccf-mtDNA was detected from the isolated EV pelleted fraction compared to their “free-floating” counterpart form (**Figure 5.9**). This observation is crucial from a detection and stability perspective because blood plasma contains high levels of DNases I activity. The protective nature of circulating EVs allows for the detection of DNA in limited sample volumes, which allows for continuous monitoring of TBI progression. This can be accomplished by classical qPCR approach or the use of a novel fluorescent-based method that we have developed and validated (MARCATTI; SAADA; OKEREKE; WADE *et al.*, 2021).

Initially, brain-specific protein targets were explored along with biomarkers such as GFAP, NFs, S100B, NSE, UCH-L1, and Tau. However, assessing their levels in bodily fluids has limitations and yields conflicting results (CZEITER; AMREIN; GRAVESTIEN; LECKY *et al.*, 2020; GAN; STEIN; SWANSON; GUAN *et al.*, 2019; MARTINEZ; STABENFELDT, 2019; MONDELLO; SORINOLA; CZEITER; VAMOS *et al.*, 2018; THELIN; ZEILER; ERCOLE; MONDELLO *et al.*, 2017). Thus, alternative sources of biomarkers, such as EVs, have garnered attention in TBI research due to their intrinsic stability, ability to traverse the BBB, and cell-type specific content reflecting the cellular physiological and pathological states. Notably, levels of NFL and GFAP in EVs have been extensively studied (FLYNN; LEETE; SHAHIM; PATTINSON *et al.*, 2021; GUEDES; DEVOTO; LEETE; SASS *et al.*, 2020; KAWATA; MITSUHASHI; ALDRET, 2018; MONDELLO; GUEDES; LAI; CZEITER *et al.*, 2020; MONDELLO; SORINOLA; CZEITER; VAMOS *et al.*, 2018; WINSTON; ROMERO; ELLISMAN; NAUSS *et al.*, 2019).

Higher plasma NFL levels in exosomes isolated from moderate/severe TBI patients have been reported, highlighting the potential for these proteins as biomarkers. (GUEDES; LANGE; LIPPA; LAI *et al.*, 2022; MONDELLO; GUEDES; LAI; CZEITER *et al.*, 2020) and GFAP (MONDELLO; GUEDES; LAI; CZEITER *et al.*, 2020) Persistent GFAP increase has also been linked to long-term cognitive deficits in TBI veterans (PELTZ; KENNEY; GILL; DIAZ-ARRASTIA *et al.*, 2020; PUFFER; CUMBA GARCIA; HIMES; JUNG *et al.*, 2020). Interestingly, chronically elevated NFL levels in EVs were observed in military personnel with multiple mild TBIs (GUEDES; DEVOTO; LEETE; SASS *et al.*, 2020), while elevated GFAP levels (but not NFL) were found in the civilian population with TBI (FLYNN; LEETE; SHAHIM; PATTINSON *et al.*, 2021). The reasons for these differences whether related to the type and frequency of TBI or the presence of GFAP/NFL in different EVs subpopulations, remains unknown.

We employed two approaches, targeted immunoblotting, and global proteomics, to analyze the protein content of EVs in the blood. Consistent with previous findings, we observed a significant increase in the levels of NFL during the acute phase of TBI (**Figure 5.12**). Interestingly, NFL levels decreased during the sub-acute phase (3-10 dpi) but rebounded to an increase in the chronic phase (30 dpi). While the presence of microglia marker Iba1 in EVs has not been previously reported, in a similar fashion to NFL, it exhibited a marked increase during the acute TBI phase, followed by a reduction in the sub-acute phase and an enhancement in the chronic TBI phase (**Figure 5.12**). In contrast, the astrocyte marker GFAP displayed a different profile with a gradual increase to peak levels at

3 dpi with levels sustaining into the chronic phase (**Figure 5.12**). However, we were unable to detect the presence of S100 β , NSE, UCH-L1, and Tau in isolated EVs, despite their abundance in the mouse cortex (**Figure 5.11**). We speculate that these proteins may exist in a “free-floating form” in the blood, making them susceptible to proteolytic activity, thereby rendering their levels unstable and leading to variability in their detection in different studies due to sample processing. An alternative explanation may be their levels are below the detection limits of Western blot analysis. Therefore, it is no surprise that most studies focus on NFL and GFAP, as they are protected by EVs, providing more stable and reliable measurements. Nevertheless, additional studies are required to better understand these findings.

It is worth noting that various reports have used the terms “EVs” and “exosomes” interchangeably. This study used nomenclature in accordance with the latest guidelines from ISEV to specify the origins of exosomes and microvesicles, either derived from multivesicular bodies or plasma membrane blebbing, respectively (THERY; WITWER; AIKAWA; ALCARAZ *et al.*, 2018; WITWER; GOBERDHAN; O'DRISCOLL; THERY *et al.*, 2021). The isolated EVs in this study primarily consisted of small EVs, comprising a mixture of both exosomes and microvesicles. Our NTA and EVs markers data (CD63, CD11b, ACSA-2) support the theory of ongoing glial activation after the acute phase post-injury. Collectively, our data strongly indicate distinct dynamics in the release of various EVs subpopulations after TBI, offering additional valuable insights, which may closely reflect cell-type specific processes following TBI.

Our biostatistical and computational analysis of proteomics data revealed several proteins as potential biomarkers for TBI. Apolipoproteins (Apo), alpha-acid glycoproteins (Orm), thrombospondins (Thbs) and antitrypsin (Serpina) were the most abundantly present in circulating EVs, but their elevated levels could not be attributed to a specific time point. Notably, we identified significantly increased level of serum amyloid protein A (SAA), specifically at the acute TBI phase (**Figure. 5.15** and **Table 5.2**). SAA are small proteins with interesting associations with acute phase response to chronic inflammation (SACK, 2018). The increased level of SAA in serum was detected during infection (CHAE; AKSENTIJEVICH; KASTNER, 2009), rheumatoid arthritis (KURODA; TANABE; HASEGAWA; WAKAMATSU *et al.*, 2017), and COPD (BOZINOVSKI; HUTCHINSON; THOMPSON; MACGREGOR *et al.*, 2008). SAA have been previously identified as potential biomarkers for intracranial and extracranial clinical severity in TBI (CARABIAS; CASTANO-LEON; BLANCA NAVARRO; PANERO *et al.*, 2020) and have shown predictive value for the severity of injury (FARRE-ALINS; PALOMINO-ANTOLIN; NARROS-FERNANDEZ; LOPEZ-RODRIGUEZ *et al.*, 2021; WICKER; BENTON; GEORGE; FURLLOW *et al.*, 2019). However, none of these previous studies identified SAA within EVs. Thus, based on our data and supported by others, we propose that measuring the level of SAA in EVs present in circulation is a novel, independent readout for TBI identification. Finally, while there are significant overlaps in the proteins identified through biostatistical and computational analyses, we have observed some differences between them. These differences may be attributed to the fact that computational analysis incorporates additional

topological information such as Protein-Protein Interaction (PPI) network combined with Graph Neural Network (GNN). These features provide a more comprehensive and biologically relevant evaluation that is not present in biostatistical analysis. The effectiveness of both approaches can be improved upon with more extensive data. For example, utilizing a larger curated protein network to curate the PPI could aid in the subsequent training of GNN; in a similar fashion, a larger sample size may improve the confidence scores of the biostatistical approach.

Additionally, we examined the dynamics of mtDNA and its release in EVs after an insult or injury via in-vitro models. We induced rapid stretch injury (RSI) to pure neuronal cell cultures differentiated from rat hippocampal neural stem cells (rHNSC), as an accurate representation to the shearing forces of TBI. Our results revealed an increase in EVs numbers and sizes along with mtDNA levels in the acute phase immediately post injury (**Figure 5.18**). Furthermore, we confirmed that RSI induced damaged mtDNA is released mainly through EVs as compared to their “free floating” counterparts in the supernatant (**Figure 5.18**). Consequently, we investigated the sizes and sequence specificity of mtDNA fragments in EVs through glucose oxidase (GOx) treatment on human retinal epithelial cells (ARPE-19). We found that a chronic, low level of GOx-induced stress causes EVs release over the course of 24 hours with significant amounts of mtDNA detected within the particles. Our qPCR data suggests most of the mtDNA-encoded genes are detectable in EVs released by GOx treated ARPE-19 cells compared to the controls (**Figure 5.19**). Furthermore, our results suggest there is no enrichment of

specific regions of the mitochondrial genome or fragment sizes, as we were able to detect varying amplicon lengths ranging from 200 bp to 6 kb spanning the entire genome particularly in EVs derived from GOx treated cells (**Figure 5.19**). We specifically used a non-neuronal model to prove the ubiquitous nature of mtDNA release in EVs is not limited to TBI. Together, these data reinforces the theory that EVs are released as a stress response to an insult or injury, and mtDNA may be a potential marker for evaluating cellular damage.

Together, in this study we comprehensively analyzed DNA and protein content in circulating EVs in blood plasma as potential biomarkers after TBI. Our data highlights the levels of DNA, particularly mtDNA, and the protein SAA as novel, stable and reliable targets for TBI detection. We validated NFL, GFAP, and Iba1 as potentially promising emerging biomarkers. Furthermore, our study elucidated the dynamic release of diverse subpopulations of EVs post-injury, including those originating from the brain, as potential markers of detrimental processes occurring after TBI. Overall, our study highlights the significance and emphasizes the potential of EVs as a valuable source of TBI biomarkers. Our report promotes future diagnostic platforms should measure biophysical properties of EVs and incorporate specific DNA and protein probes to fully assess TBI severity.

6.3 Limitations

There are several limitations of the study, as our investigation only focused on one type of TBI. Our preclinical weight drop model replicates one of the most common types of TBI in motor vehicle accidents, accurately recapitulating the blunt

force trauma and rapid acceleration/deceleration of rotational energy of the unrestricted head and torso. However, other models like CCI, FPI and blast TBI replicate completely different injury mechanisms, thus resulting in potentially different protein biomarkers. There is also the limitation of specificity of our proposed protein biomarkers. Our study did not include an injured control group (i.e. orthopedic), thus we cannot definitively conclude whether the proposed biomarkers are general responses to injury or only specific to TBI. It is also worth noting that significant differences exist between mouse and human brains, which presents translational challenges moving forward. The timing, context, and pathophysiologies of the disease progression may differ across species, thus additional models of TBI, especially in larger animals (i.e. pig), are needed to validate the proposed biomarkers.

Another potential limitation is the use of only male mice in our study. To the best of our knowledge, there are no studies addressing sex specific TBI biomarkers, but previous studies have suggested sex-specific differences in TBI (GUPTE; BROOKS; VUKAS; PIERCE *et al.*, 2019). A meta-analysis examining outcomes, severity and possible pathophysiology reasons for these differences found contradictory evidence between sexes in humans versus animal models (GUPTE; BROOKS; VUKAS; PIERCE *et al.*, 2019). The study reports that while human females recover worse than their male counterparts, the exact opposite is true for females in animal models (GUPTE; BROOKS; VUKAS; PIERCE *et al.*, 2019). However, epidemiological studies have consistently reported males make up the majority of TBI cases (BIEGON, 2021; FROST; FARRER; PRIMOSCH;

HEDGES, 2013). Considering that our study adds to the growing body of knowledge for preclinical weight drop models and biomarkers, the potential for sex specific biomarkers creates an opportunity to advance the field with better treatment options and therapeutic strategies.

Last but not least, this study did not correlate EVs markers with motor or cognitive deficits induced by TBI. Additional behavioral testing could be a potential future direction that adds to the translational value of this study's results. Tracking the dynamics of various EVs markers with the manifestations of these deficits, combined with imaging diagnostics, would provide a more comprehensive assessment of TBI.

6.4 Future directions

As highlighted in the limitations, there are several topics that warrant further investigation. A direct follow up study should validate the potential biomarkers that have been proposed in our findings. Validation of targets would provide proof that our methodologies have merit in discovering new biomarkers in EVs for TBI. As part of the validation process, an important aspect to address is the specificity of these biomarkers to TBI, thus including one or more injured controls is necessary to determine the specificity of these markers. A partial, but more direct and faster, validation approach may be probing for these targets using targeted immunoblotting. However, technical considerations such as antibody sensitivity, amount of EVs used, and detection limits need to be considered. To potentially overcome these issues, ELISA-based methodologies may offer better sensitivity, although this technique will also come with its own set of challenges like false

positives, instability, and potential high cost of custom ELISA antibodies. Lastly, targeted proteomics of isolated EVs may be the most sensitive and comprehensive technique to profile the amount(s) of the marker in the particles. Validating the proposed proteins is a key next step to establishing EVs, SAA and the other targets as potential biomarkers.

Validation of the markers would add to the translatability of our results. Not only do the proposed biomarkers have to be sensitive enough to discriminate between the different forms, severity and frequency of TBI, but most importantly, the results must be applicable in the clinical settings. This calls for additional validation using another type of TBI model, larger animals to bridge the anatomical brain differences, and human clinical samples. As stated previously, the type and severity of TBI greatly affect the subsequent pathophysiology, thus potentially resulting in different fluid biomarkers. SAA and/or mtDNA levels may be specific to only blunt force TBI, but not CCI, FPI or bTBI. Also, our model induces a moderate/severe injury, but the majority of TBI cases are classified as mild; therefore, a future direction can be investigating a milder version of injury for biomarkers. Repetitive mild injuries that replicate repeated blows to the head indicative of violent sports collision or blast TBI in military personnel are also other categories of TBI worth exploring. Scaling to a pig or sheep model would help bridge the significant anatomical brain differences between the humans vs. rodents, thus providing more translational value. However, arguably the best samples would be collecting liquid biopsies directly from human subjects in clinics that have suffered a TBI. A whole new set of challenges arise when executing

clinical studies, such as sample volumes, timing of sample collection, and frequency of sampling are all factors that need to be accounted for, especially in longitudinal studies. The type of biofluid and volumes needed for subsequent experiments are crucial to patient enrollment and retention, as each subject may quit the study at any time. Furthermore, regulatory rules regarding consent, data privacy, and protocols are carefully scrutinized and subject to audits. Even with these challenges, human samples remain the best chance to discover highly accurate biomarkers for the assessment and monitoring of TBI. It is also worth noting any additional future study should include female animals or subjects to address any potential sex-specific differences in biomarkers.

In terms of technical adjustments, combining two or more techniques to purify or enrich for EVs may lead to novel discoveries. As stated previously, a potential limitation of this study is the use of only UC as the single method of EV isolation. While UC provides the highest yield in the most cost- and time-effective way to harvest EVs, it is often used in combination with another technique that offers more purity in the isolation process. For example, UC can be combined with affinity columns using antigens towards a specific plasma membrane marker (i.e., CD63, CD9, Annexin). In theory, using both these techniques should provide high yields of marker-specific fractions from the biofluid samples. These fractions can be further subdivided by SEC; the result would be marker-specific EVs sorted by their sizes. The number of isolation techniques can be combined and modified to the needs of the experimenter, but it should be cautioned that with each additional

technique, a portion of the EV fractions will be inevitably lost through technical steps (THÉRY; AMIGORENA; RAPOSO; CLAYTON, 2006).

Regarding the contents inside the EVs, it is worth exploring other types of cargo for possible targets. Namely, various RNA's and metabolites such as lipids, lipoproteins, and amino acids offer potential rich sources for additional biomarkers. Considering the extensive literature on RNA in EVs, the foundation is in place to compare and contrast RNA-based TBI biomarkers to other diseases. The plethora of different categories of RNAs also increases the likelihood that specific types or sequences of RNA may be associated with TBI pathophysiology (TURCHINOVICH; DRAPKINA; TONEVITSKY, 2019). It is worth noting that the kinds of biofluids, isolation methods, and sequencing techniques all greatly influence the results of the RNA study. For example, Nolte-'t Hoen et al.'s pioneer work characterizing immune cell EVs RNA content revealed predominantly small RNAs of <200 nucleotides. However, the exact opposite was true when the authors examined cellular RNA content (NOLTE-'T HOEN; BUERMANS; WAASDORP; STOORVOGEL *et al.*, 2012). The underrepresentation of miRNA compared to other RNA's in EVs has been noted in several other studies, suggesting a possible unknown mechanism of cells sequestering specific RNA species into EVs for release (BAGLIO; ROOIJERS; KOPPERS-LALIC; VERWEIJ *et al.*, 2015; BELLINGHAM; GUO; COLEMAN; HILL, 2012; JENJAROENPUN; KREMENSKA; NAIR; KREMENSKOY *et al.*, 2013; TOSAR; GÁMBARO; SANGUINETTI; BONILLA *et al.*, 2015). A comprehensive metabolomics study on the plethora of functional biomolecules in EVs may also prove useful. Previous studies have

highlighted the various roles of lipids, lipoproteins, and associated fatty acids in EVs biogenesis, cellular signaling, and receptor docking (DONOSO-QUEZADA; AYALA-MAR; GONZÁLEZ-VALDEZ, 2021; EGEA-JIMENEZ; ZIMMERMANN, 2020). Given the prevalence of apolipoproteins in our proteomics data set, it is unsurprising that lipid associated molecules play a role in many processes, including TBI recovery. The field of EV metabolomics is still relatively nascent with much untapped potential that would clearly benefit from additional studies. On the DNA side, it would be interesting to investigate if there are specific mtDNA fragment lengths or sequences that are more prevalent within the EVs. The possible bias of these features may suggest some sort of preferential packaging and sequester of damaged mitochondria for trafficking export.

With regards to the in-vitro RSI and ARPE-19 results, a possible direction to build upon the mtDNA angle may be to elucidate if there are particular EVs subpopulations released in response to injury that are enriched with damaged mtDNA. It is possible that different types of insults can trigger preferential release of specific subpopulations of EVs and consequently their cargos may also be different. Evaluating biomolecules that may be EVs-specific may provide valuable insight into the pathophysiology progress in an insult-specific context. These potential discoveries can be used as biomarkers for better assessment and treatment options.

The long-term goal is to translate our findings and develop a novel diagnostic tool for TBI. Ideally, we would like to create a portable, handheld device that combines microfluidics for EVs to detect and assess TBI severity and

progression. One challenge would be the sample processing and EVs isolation steps ahead of the microfluidic device sampling, as the challenges highlighted in the techniques, and more crucially, the processing times will drastically affect the accuracy, sensitivity, and overall general usefulness of this handheld device. As seen in the iSTAT-TBI plasma cartridge made by Abbott Laboratories, this device requires a separate platform, the iSTAT Alinity, in order to read the test, thus adding an extra cumbersome step. Furthermore, this device is not to be used as a point-of-care testing instrument, but rather to assist in the clinician's decision of ordering a CT scan following a suspected TBI case. Due to the complexities of TBI, the detection and monitoring of this disease by a single readout is not feasible, but rather requires a multiplexed platform to evaluate several targets, thus our results are useful in the development of such device. Our vision of the portable instrument aims to improve upon the existing platform by making the device a comprehensive tool that can immediately detect and assess TBI as a point-of-care diagnostic without the need of specialized equipment or training personnel. To achieve this lofty goal, collaborations with specialists across many disciplines are needed and many of the aforementioned follow up studies are required.

Bibliography

ABE, K.; SHIMADA, R.; OKADA, Y.; KIBAYASHI, K. Traumatic brain injury decreases serotonin transporter expression in the rat cerebrum. **Neurol Res**, 38, n. 4, p. 358-363, Apr 2016.

ACQUAH, C.; DANQUAH, M. K.; YON, J. L.; SIDHU, A. *et al.* A review on immobilised aptamers for high throughput biomolecular detection and screening. **Anal Chim Acta**, 888, p. 10-18, Aug 12 2015.

ADRIAN, H.; MÄRTEN, K.; SALLA, N.; LASSE, V. Biomarkers of Traumatic Brain Injury: Temporal Changes in Body Fluids. **eNeuro**, 3, n. 6, 2016.

AIRES, I. D.; RIBEIRO-RODRIGUES, T.; BOIA, R.; CATARINO, S. *et al.* Exosomes derived from microglia exposed to elevated pressure amplify the neuroinflammatory response in retinal cells. **Glia**, 68, n. 12, p. 2705-2724, Dec 2020.

AKAMATSU, Y.; HANAFY, K. A. Cell Death and Recovery in Traumatic Brain Injury. **Neurotherapeutics**, 17, n. 2, p. 446-456, Apr 2020.

ALAWIEH, A.; LANGLEY, E. F.; WEBER, S.; ADKINS, D. *et al.* Identifying the Role of Complement in Triggering Neuroinflammation after Traumatic Brain Injury. **J Neurosci**, 38, n. 10, p. 2519-2532, Mar 7 2018.

ALBERT-WEIßENBERGER, C.; VÁRRALLYAY, C.; RASLAN, F.; KLEINSCHNITZ, C. *et al.* An experimental protocol for mimicking pathomechanisms of traumatic brain injury in mice. **Exp Transl Stroke Med**, 4, p. 1, Feb 02 2012.

ALCARO, A.; HUBER, R.; PANKSEPP, J. Behavioral functions of the mesolimbic dopaminergic system: an affective neuroethological perspective. **Brain Res Rev**, 56, n. 2, p. 283-321, Dec 2007.

ALLURI, H.; SHAJI, C. A.; DAVIS, M. L.; THARAKAN, B. A Mouse Controlled Cortical Impact Model of Traumatic Brain Injury for Studying Blood-Brain Barrier Dysfunctions. **Methods Mol Biol**, 1717, p. 37-52, 2018.

AZONANO.COM. **Nanoparticle Tracking Analysis (NTA) Measurements**. 2015. Acesso em: 10/11/23.

BACHURSKI, D.; SCHULDNER, M.; NGUYEN, P. H.; MALZ, A. *et al.* Extracellular vesicle measurements with nanoparticle tracking analysis - An accuracy and repeatability comparison between NanoSight NS300 and ZetaView. **J Extracell Vesicles**, 8, n. 1, p. 1596016, 2019.

BAGLIO, S. R.; ROOIJERS, K.; KOPPERS-LALIC, D.; VERWEIJ, F. J. *et al.* Human bone marrow- and adipose-mesenchymal stem cells secrete exosomes enriched in distinctive miRNA and tRNA species. **Stem Cell Res Ther**, 6, n. 1, p. 127, Jul 01 2015.

BALAJ, L.; LESSARD, R.; DAI, L.; CHO, Y. J. *et al.* Tumour microvesicles contain retrotransposon elements and amplified oncogene sequences. **Nat Commun**, 2, p. 180, Feb 01 2011.

BALESTRERI, M.; CZOSNYKA, M.; CHATFIELD, D. A.; STEINER, L. A. *et al.* Predictive value of Glasgow Coma Scale after brain trauma: change in trend over the past ten years. **J Neurol Neurosurg Psychiatry**, 75, n. 1, p. 161-162, Jan 2004.

BARNES, D. E.; KAUP, A.; KIRBY, K. A.; BYERS, A. L. *et al.* Traumatic brain injury and risk of dementia in older veterans. **Neurology**, 83, n. 4, p. 312-319, Jul 22 2014.

BARTH, H. G.; BOYES, B. E.; JACKSON, C. Size exclusion chromatography. **Anal Chem**, 66, n. 12, p. 595R-620R, Jun 15 1994.

BATAGOV, A. O.; KUZNETSOV, V. A.; KUROCHKIN, I. V. Identification of nucleotide patterns enriched in secreted RNAs as putative cis-acting elements targeting them to exosome nano-vesicles. **BMC Genomics**, 12 Suppl 3, n. Suppl 3, p. S18, Nov 30 2011.

BATIUK, M. Y.; MARTIROSYAN, A.; WAHIS, J.; DE VIN, F. *et al.* Identification of region-specific astrocyte subtypes at single cell resolution. **Nat Commun**, 11, n. 1, p. 1220, Mar 5 2020.

BEARD, K.; YANG, Z.; HABER, M.; FLAMHOLZ, M. *et al.* Extracellular vesicles as distinct biomarker reservoirs for mild traumatic brain injury diagnosis. **Brain Commun**, 3, n. 3, p. fcab151, 2021.

BELLINGHAM, S. A.; GUO, B. B.; COLEMAN, B. M.; HILL, A. F. Exosomes: vehicles for the transfer of toxic proteins associated with neurodegenerative diseases? **Front Physiol**, 3, p. 124, 2012.

BERGER, M.; GRAY, J. A.; ROTH, B. L. The expanded biology of serotonin. **Annu Rev Med**, 60, p. 355-366, 2009.

BIEGON, A. Considering Biological Sex in Traumatic Brain Injury. **Front Neurol**, 12, p. 576366, 2021.

BLACK, K. L.; HANKS, R. A.; WOOD, D. L.; ZAFONTE, R. D. *et al.* Blunt versus penetrating violent traumatic brain injury: frequency and factors associated with secondary conditions and complications. **J Head Trauma Rehabil**, 17, n. 6, p. 489-496, Dec 2002.

BOGOSLOVSKY, T.; GILL, J.; JEROMIN, A.; DAVIS, C. *et al.* Fluid Biomarkers of Traumatic Brain Injury and Intended Context of Use. **Diagnostics (Basel)**, 6, n. 4, Oct 18 2016.

BORINUOLUWA, R.; AHMED, Z. Does Blast Mild Traumatic Brain Injury Have an Impact on PTSD Severity? A Systematic Review and Meta-Analysis. **Trauma Care**, 3, n. 1, p. 9-21, 2023.

BOZINOVSKI, S.; HUTCHINSON, A.; THOMPSON, M.; MACGREGOR, L. *et al.* Serum amyloid a is a biomarker of acute exacerbations of chronic obstructive pulmonary disease. **Am J Respir Crit Care Med**, 177, n. 3, p. 269-278, Feb 1 2008.

BRUNNER, A. D.; THIELERT, M.; VASILOPOULOU, C.; AMMAR, C. *et al.* Ultra-high sensitivity mass spectrometry quantifies single-cell proteome changes upon perturbation. **Mol Syst Biol**, 18, n. 3, p. e10798, Mar 2022.

BRZOZOWSKI, J. S.; JANKOWSKI, H.; BOND, D. R.; MCCAGUE, S. B. *et al.* Lipidomic profiling of extracellular vesicles derived from prostate and prostate cancer cell lines. **Lipids Health Dis**, 17, n. 1, p. 211, Sep 08 2018.

BURDA, J. E.; BERNSTEIN, A. M.; SOFRONIEW, M. V. Astrocyte roles in traumatic brain injury. **Exp Neurol**, 275 Pt 3, n. 0 3, p. 305-315, Jan 2016.

BUZAS, E. I. The roles of extracellular vesicles in the immune system. **Nat Rev Immunol**, 23, n. 4, p. 236-250, Apr 2023.

CALABRESI, P.; PICCONI, B.; TOZZI, A.; DI FILIPPO, M. Dopamine-mediated regulation of corticostriatal synaptic plasticity. **Trends Neurosci**, 30, n. 5, p. 211-219, May 2007.

CAMPOLO, M.; AHMAD, A.; CRUPI, R.; IMPELLIZZERI, D. *et al.* Combination therapy with melatonin and dexamethasone in a mouse model of traumatic brain injury. **J Endocrinol**, 217, n. 3, p. 291-301, Jun 2013.

CARABIAS, C. S.; CASTANO-LEON, A. M.; BLANCA NAVARRO, B.; PANERO, I. *et al.* Serum Amyloid A1 as a Potential Intracranial and Extracranial Clinical Severity Biomarker in Traumatic Brain Injury. **J Intensive Care Med**, 35, n. 11, p. 1180-1195, Nov 2020.

CERNAK, I.; NOBLE-HAEUSSLEIN, L. J. Traumatic brain injury: an overview of pathobiology with emphasis on military populations. **J Cereb Blood Flow Metab**, 30, n. 2, p. 255-266, Feb 2010.

CHAE, J. J.; AKSENTIJEVICH, I.; KASTNER, D. L. Advances in the understanding of familial Mediterranean fever and possibilities for targeted therapy. **Br J Haematol**, 146, n. 5, p. 467-478, Sep 2009.

CHANG, W. H.; CERIONE, R. A.; ANTONYAK, M. A. Extracellular Vesicles and Their Roles in Cancer Progression. **Methods Mol Biol**, 2174, p. 143-170, 2021.

CHAPUT, N.; THÉRY, C. Exosomes: immune properties and potential clinical implementations. **Semin Immunopathol**, 33, n. 5, p. 419-440, Sep 2011.

CHEN, J.; TAN, Q.; YANG, Z.; JIN, Y. Engineered extracellular vesicles: potentials in cancer combination therapy. **J Nanobiotechnology**, 20, n. 1, p. 132, Mar 15 2022.

CHEN, N.; WANG, J.; HU, Y.; CUI, B. *et al.* MicroRNA-410 reduces the expression of vascular endothelial growth factor and inhibits oxygen-induced retinal neovascularization. **PLoS One**, 9, n. 4, p. e95665, 2014.

CHEN, Y.; CONSTANTINI, S.; TREMBOVLER, V.; WEINSTOCK, M. *et al.* An experimental model of closed head injury in mice: pathophysiology, histopathology, and cognitive deficits. **J Neurotrauma**, 13, n. 10, p. 557-568, Oct 1996.

CHIRIACÒ, M. S.; BIANCO, M.; NIGRO, A.; PRIMICERI, E. *et al.* Lab-on-Chip for Exosomes and Microvesicles Detection and Characterization. **Sensors (Basel)**, 18, n. 10, Sep 20 2018.

CLINIC, M. **Traumatic Brain Injury**. 2021. Acesso em: 10/1/23.

CLISH, C. B. Metabolomics: an emerging but powerful tool for precision medicine. **Cold Spring Harb Mol Case Stud**, 1, n. 1, p. a000588, Oct 2015.

COLEMAN, M. L.; SAHAI, E. A.; YEO, M.; BOSCH, M. *et al.* Membrane blebbing during apoptosis results from caspase-mediated activation of ROCK I. **Nat Cell Biol**, 3, n. 4, p. 339-345, Apr 2001.

CORTEZ, S. C.; MCINTOSH, T. K.; NOBLE, L. J. Experimental fluid percussion brain injury: vascular disruption and neuronal and glial alterations. **Brain Res**, 482, n. 2, p. 271-282, Mar 20 1989.

COUCH, Y.; AKBAR, N.; ROODSELAAR, J.; EVANS, M. C. *et al.* Circulating endothelial cell-derived extracellular vesicles mediate the acute phase response and sickness behaviour associated with CNS inflammation. **Sci Rep**, 7, n. 1, p. 9574, Aug 29 2017.

COX, J.; MANN, M. MaxQuant enables high peptide identification rates, individualized p.p.b.-range mass accuracies and proteome-wide protein quantification. **Nat Biotechnol**, 26, n. 12, p. 1367-1372, Dec 2008.

CSUKA, E.; MORGANTI-KOSSMANN, M. C.; LENZLINGER, P. M.; JOLLER, H. *et al.* IL-10 levels in cerebrospinal fluid and serum of patients with severe traumatic brain injury: relationship to IL-6, TNF-alpha, TGF-beta1 and blood-brain barrier function. **J Neuroimmunol**, 101, n. 2, p. 211-221, Nov 15 1999.

CZEITER, E.; AMREIN, K.; GRAVESTEIJN, B. Y.; LECKY, F. *et al.* Blood biomarkers on admission in acute traumatic brain injury: Relations to severity, CT findings and care path in the CENTER-TBI study. **EBioMedicine**, 56, p. 102785, Jun 2020.

DADAS, A.; WASHINGTON, J.; DIAZ-ARRASTIA, R.; JANIGRO, D. Biomarkers in traumatic brain injury (TBI): a review. **Neuropsychiatr Dis Treat**, 14, p. 2989-3000, 2018.

DE RIVERO VACCARI, J. P.; BRAND, F.; ADAMCZAK, S.; LEE, S. W. *et al.* Exosome-mediated inflammasome signaling after central nervous system injury. **J Neurochem**, 136 Suppl 1, n. 0 1, p. 39-48, Jan 2016.

DE VLIENER, G.; MEYFROIDT, G. Kidney Dysfunction After Traumatic Brain Injury: Pathophysiology and General Management. **Neurocrit Care**, 38, n. 2, p. 504-516, Apr 2023.

DEFENSE, D. O. **Numbers for Traumatic Brain Injury Worldwide.** . 2022. Acesso em: 8/28/23.

DEVELOPMENT, N. I. O. C. H. A. H. **What are the common symptoms of traumatic brain injury (TBI)?** , 2020. Acesso em: 9/3/23.

DIAZ-ARRASTIA, R.; WANG, K. K.; PAPA, L.; SORANI, M. D. *et al.* Acute biomarkers of traumatic brain injury: relationship between plasma levels of ubiquitin C-terminal hydrolase-L1 and glial fibrillary acidic protein. **J Neurotrauma**, 31, n. 1, p. 19-25, Jan 01 2014.

DICKENS, A. M.; TOVAR-Y-ROMO, L. B.; YOO, S. W.; TROUT, A. L. *et al.* Astrocyte-shed extracellular vesicles regulate the peripheral leukocyte response to inflammatory brain lesions. **Sci Signal**, 10, n. 473, Apr 04 2017.

DISMUKE, W. M.; CHALLA, P.; NAVARRO, I.; STAMER, W. D. *et al.* Human aqueous humor exosomes. **Exp Eye Res**, 132, p. 73-77, Mar 2015.

DIXON, C. E.; CLIFTON, G. L.; LIGHTHALL, J. W.; YAGHMAI, A. A. *et al.* A controlled cortical impact model of traumatic brain injury in the rat. **J Neurosci Methods**, 39, n. 3, p. 253-262, Oct 1991.

DIXON, C. E.; LIGHTHALL, J. W.; ANDERSON, T. E. Physiologic, histopathologic, and cineradiographic characterization of a new fluid-percussion model of experimental brain injury in the rat. **J Neurotrauma**, 5, n. 2, p. 91-104, 1988.

DIXON, C. E.; LYETH, B. G.; POVLISHOCK, J. T.; FINDLING, R. L. *et al.* A fluid percussion model of experimental brain injury in the rat. **J Neurosurg**, 67, n. 1, p. 110-119, Jul 1987.

DONG, X.; DONG, J. F.; ZHANG, J. Roles and therapeutic potential of different extracellular vesicle subtypes on traumatic brain injury. **Cell Commun Signal**, 21, n. 1, p. 211, Aug 18 2023.

DONG, X.; LIU, W.; SHEN, Y.; HOUCK, K. *et al.* Anticoagulation targeting membrane-bound anionic phospholipids improves outcomes of traumatic brain injury in mice. **Blood**, 138, n. 25, p. 2714-2726, Dec 23 2021.

DONOSO-QUEZADA, J.; AYALA-MAR, S.; GONZÁLEZ-VALDEZ, J. The role of lipids in exosome biology and intercellular communication: Function, analytics and applications. **Traffic**, 22, n. 7, p. 204-220, Jul 2021.

DRAGOVIC, R. A.; GARDINER, C.; BROOKS, A. S.; TANNETTA, D. S. *et al.* Sizing and phenotyping of cellular vesicles using Nanoparticle Tracking Analysis. **Nanomedicine**, 7, n. 6, p. 780-788, Dec 2011.

EGEA-JIMENEZ, A. L.; ZIMMERMANN, P. Lipids in Exosome Biology. **Handb Exp Pharmacol**, 259, p. 309-336, 2020.

ELDER, G. A.; DORR, N. P.; DE GASPERI, R.; GAMA SOSA, M. A. *et al.* Blast exposure induces post-traumatic stress disorder-related traits in a rat model of mild traumatic brain injury. **J Neurotrauma**, 29, n. 16, p. 2564-2575, Nov 01 2012.

EMMANOUILIDOU, E.; MELACHROINOY, K.; ROUMELIOTIS, T.; GARBIS, S. D. *et al.* Cell-produced alpha-synuclein is secreted in a calcium-dependent manner by exosomes and impacts neuronal survival. **J Neurosci**, 30, n. 20, p. 6838-6851, May 19 2010.

ENNACEUR, A.; DELACOUR, J. A new one-trial test for neurobiological studies of memory in rats. 1: Behavioral data. **Behav Brain Res**, 31, n. 1, p. 47-59, Nov 01 1988.

ERWIG, L. P.; HENSON, P. M. Clearance of apoptotic cells by phagocytes. **Cell Death Differ**, 15, n. 2, p. 243-250, Feb 2008.

EYLEM, C. C.; YILMAZ, M.; DERKUS, B.; NEMUTLU, E. *et al.* Untargeted multi-omic analysis of colorectal cancer-specific exosomes reveals joint pathways of colorectal cancer in both clinical samples and cell culture. **Cancer Lett**, 469, p. 186-194, Jan 28 2020.

FARRE-ALINS, V.; PALOMINO-ANTOLIN, A.; NARROS-FERNANDEZ, P.; LOPEZ-RODRIGUEZ, A. B. *et al.* Serum Amyloid A1/Toll-Like Receptor-4 Axis, an Important Link between Inflammation and Outcome of TBI Patients. **Biomedicines**, 9, n. 6, May 25 2021.

FEENEY, D. M.; BOYESON, M. G.; LINN, R. T.; MURRAY, H. M. *et al.* Responses to cortical injury: I. Methodology and local effects of contusions in the rat. **Brain Res**, 211, n. 1, p. 67-77, Apr 27 1981.

FISHMAN, E. K.; JEFFREY, B. R. **Spiral CT: Principles, Techniques, and Clinical Applications**. Raven Press, 1995.

FLIERL, M. A.; STAHEL, P. F.; BEAUCHAMP, K. M.; MORGAN, S. J. *et al.* Mouse closed head injury model induced by a weight-drop device. **Nat Protoc**, 4, n. 9, p. 1328-1337, 2009.

FLYNN, S.; LEETE, J.; SHAHIM, P.; PATTINSON, C. *et al.* Extracellular vesicle concentrations of glial fibrillary acidic protein and neurofilament light measured 1 year after traumatic brain injury. **Sci Rep**, 11, n. 1, p. 3896, Feb 16 2021.

FROST, R. B.; FARRER, T. J.; PRIMOSCH, M.; HEDGES, D. W. Prevalence of traumatic brain injury in the general adult population: a meta-analysis. **Neuroepidemiology**, 40, n. 3, p. 154-159, 2013.

FRUGIER, T.; MORGANTI-KOSSMANN, M. C.; O'REILLY, D.; MCLEAN, C. A. In situ detection of inflammatory mediators in post mortem human brain tissue after traumatic injury. **J Neurotrauma**, 27, n. 3, p. 497-507, Mar 2010.

GADDAM, S. S.; BUELL, T.; ROBERTSON, C. S. Systemic manifestations of traumatic brain injury. **Handb Clin Neurol**, 127, p. 205-218, 2015.

GAN, Z. S.; STEIN, S. C.; SWANSON, R.; GUAN, S. *et al.* Blood Biomarkers for Traumatic Brain Injury: A Quantitative Assessment of Diagnostic and Prognostic Accuracy. **Front Neurol**, 10, p. 446, 2019.

GAO, X.; XIONG, Y.; LI, Q.; HAN, M. *et al.* Extracellular vesicle-mediated transfer of miR-21-5p from mesenchymal stromal cells to neurons alleviates early brain injury to improve cognitive function via the PTEN/Akt pathway after subarachnoid hemorrhage. **Cell Death Dis**, 11, n. 5, p. 363, May 13 2020.

GHANAM, J.; CHETTY, V. K.; BARTHEL, L.; REINHARDT, D. *et al.* DNA in extracellular vesicles: from evolution to its current application in health and disease. **Cell Biosci**, 12, n. 1, p. 37, Mar 28 2022.

GHARBI, T.; ZHANG, Z.; YANG, G. Y. The Function of Astrocyte Mediated Extracellular Vesicles in Central Nervous System Diseases. **Front Cell Dev Biol**, 8, p. 568889, 2020.

GILL, J.; MUSTAPIC, M.; DIAZ-ARRASTIA, R.; LANGE, R. *et al.* Higher exosomal tau, amyloid-beta 42 and IL-10 are associated with mild TBIs and chronic symptoms in military personnel. **Brain Inj**, 32, n. 10, p. 1277-1284, 2018.

GOETZL, E. J.; ELAHI, F. M.; MUSTAPIC, M.; KAPOGIANNIS, D. *et al.* Altered levels of plasma neuron-derived exosomes and their cargo proteins characterize acute and chronic mild traumatic brain injury. **FASEB J**, 33, n. 4, p. 5082-5088, Apr 2019.

GOETZL, E. J.; YAFFE, K.; PELTZ, C. B.; LEDREUX, A. *et al.* Traumatic brain injury increases plasma astrocyte-derived exosome levels of neurotoxic complement proteins. **FASEB J**, 34, n. 2, p. 3359-3366, Feb 2020.

GONZALES, P. A.; PISITKUN, T.; HOFFERT, J. D.; TCHAPYJNIKOV, D. *et al.* Large-scale proteomics and phosphoproteomics of urinary exosomes. **J Am Soc Nephrol**, 20, n. 2, p. 363-379, Feb 2009.

GRAW, J. A.; YU, B.; REZOAGLI, E.; WARREN, H. S. *et al.* Endothelial dysfunction inhibits the ability of haptoglobin to prevent hemoglobin-induced hypertension. **Am J Physiol Heart Circ Physiol**, 312, n. 6, p. H1120-H1127, Jun 1 2017.

GREEN, S. M. Cheerio, laddie! Bidding farewell to the Glasgow Coma Scale. **Ann Emerg Med**, 58, n. 5, p. 427-430, Nov 2011.

GUEDES, V. A.; DEVOTO, C.; LEETE, J.; SASS, D. *et al.* Extracellular Vesicle Proteins and MicroRNAs as Biomarkers for Traumatic Brain Injury. **Front Neurol**, 11, p. 663, 2020.

GUEDES, V. A.; LANGE, R. T.; LIPPA, S. M.; LAI, C. *et al.* Extracellular vesicle neurofilament light is elevated within the first 12-months following traumatic brain injury in a U.S military population. **Sci Rep**, 12, n. 1, p. 4002, Mar 7 2022.

GUESCINI, M.; GENEDANI, S.; STOCCHI, V.; AGNATI, L. F. Astrocytes and Glioblastoma cells release exosomes carrying mtDNA. **J Neural Transm (Vienna)**, 117, n. 1, p. 1-4, Jan 2010.

GUPTE, R.; BROOKS, W.; VUKAS, R.; PIERCE, J. *et al.* Sex Differences in Traumatic Brain Injury: What We Know and What We Should Know. **J Neurotrauma**, 36, n. 22, p. 3063-3091, Nov 15 2019.

GUSTAFSON, D.; VEITCH, S.; FISH, J. E. Extracellular Vesicles as Protagonists of Diabetic Cardiovascular Pathology. **Front Cardiovasc Med**, 4, p. 71, 2017.

HAMMAD, A.; WESTACOTT, L.; ZABEN, M. The role of the complement system in traumatic brain injury: a review. **J Neuroinflammation**, 15, n. 1, p. 24, Jan 22 2018.

HAMMOND, F. M.; BICKETT, A. K.; NORTON, J. H.; PERSHAD, R. Effectiveness of amantadine hydrochloride in the reduction of chronic traumatic brain injury irritability and aggression. **J Head Trauma Rehabil**, 29, n. 5, p. 391-399, 2014.

HARDING, C.; HEUSER, J.; STAHL, P. Endocytosis and intracellular processing of transferrin and colloidal gold-transferrin in rat reticulocytes: demonstration of a pathway for receptor shedding. **Eur J Cell Biol**, 35, n. 2, p. 256-263, Nov 1984.

HAROON, E.; FLEISCHER, C. C.; FELGER, J. C.; CHEN, X. *et al.* Conceptual convergence: increased inflammation is associated with increased basal ganglia glutamate in patients with major depression. **Mol Psychiatry**, 21, n. 10, p. 1351-1357, Oct 2016.

HAROON, E.; MILLER, A. H.; SANACORA, G. Inflammation, Glutamate, and Glia: A Trio of Trouble in Mood Disorders. **Neuropsychopharmacology**, 42, n. 1, p. 193-215, Jan 2017.

HAZELTON, I.; YATES, A.; DALE, A.; ROODSELAAR, J. *et al.* Exacerbation of Acute Traumatic Brain Injury by Circulating Extracellular Vesicles. **J Neurotrauma**, 35, n. 4, p. 639-651, Feb 15 2018.

HESSVIK, N. P.; LLORENTE, A. Current knowledge on exosome biogenesis and release. **Cell Mol Life Sci**, 75, n. 2, p. 193-208, Jan 2018.

- HICKMAN, S. E.; KINGERY, N. D.; OHSUMI, T. K.; BOROWSKY, M. L. *et al.* The microglial sensome revealed by direct RNA sequencing. **Nat Neurosci**, 16, n. 12, p. 1896-1905, Dec 2013.
- HICKS, R. R.; FERTIG, S. J.; DESROCHER, R. E.; KOROSHETZ, W. J. *et al.* Neurological effects of blast injury. **J Trauma**, 68, n. 5, p. 1257-1263, May 2010.
- HU, X.; XU, Y.; ZHANG, H.; LI, Y. *et al.* Role of necroptosis in traumatic brain and spinal cord injuries. **J Adv Res**, 40, p. 125-134, Sep 2022.
- HUANG, E. Y.; TSUI, P. F.; KUO, T. T.; TSAI, J. J. *et al.* Amantadine ameliorates dopamine-releasing deficits and behavioral deficits in rats after fluid percussion injury. **PLoS One**, 9, n. 1, p. e86354, 2014.
- HUANG, J.; ROTH, R.; HEUSER, J. E.; SADLER, J. E. Integrin alpha(v)beta(3) on human endothelial cells binds von Willebrand factor strings under fluid shear stress. **Blood**, 113, n. 7, p. 1589-1597, Feb 12 2009.
- HUANG, S.; GE, X.; YU, J.; HAN, Z. *et al.* Increased miR-124-3p in microglial exosomes following traumatic brain injury inhibits neuronal inflammation and contributes to neurite outgrowth. **FASEB J**, 32, n. 1, p. 512-528, Jan 2018.
- HUETTEL, S.; SONG, A.; MCCARTHY, G. **Functional Magnetic Resonance Imaging**. 2 ed. Massachusetts: 2009.
- HURLEY, J. H.; HANSON, P. I. Membrane budding and scission by the ESCRT machinery: it's all in the neck. **Nat Rev Mol Cell Biol**, 11, n. 8, p. 556-566, Aug 2010.
- IRION, U.; ST JOHNSTON, D. bicoid RNA localization requires specific binding of an endosomal sorting complex. **Nature**, 445, n. 7127, p. 554-558, Feb 01 2007.
- JARRAHI, A.; BRAUN, M.; AHLUWALIA, M.; GUPTA, R. V. *et al.* Revisiting Traumatic Brain Injury: From Molecular Mechanisms to Therapeutic Interventions. **Biomedicines**, 8, n. 10, Sep 29 2020.
- JENJAROENPUN, P.; KREMENSKA, Y.; NAIR, V. M.; KREMENSKOY, M. *et al.* Characterization of RNA in exosomes secreted by human breast cancer cell lines using next-generation sequencing. **PeerJ**, 1, p. e201, 2013.

JEPPESEN, D. K.; FENIX, A. M.; FRANKLIN, J. L.; HIGGINBOTHAM, J. N. *et al.* Reassessment of Exosome Composition. **Cell**, 177, n. 2, p. 428-445.e418, Apr 04 2019.

KAHLERT, C.; MELO, S. A.; PROTOPOPOV, A.; TANG, J. *et al.* Identification of double-stranded genomic DNA spanning all chromosomes with mutated KRAS and p53 DNA in the serum exosomes of patients with pancreatic cancer. **J Biol Chem**, 289, n. 7, p. 3869-3875, Feb 14 2014.

KALIMON, O. J.; SULLIVAN, P. G. Sex Differences in Mitochondrial Function Following a Controlled Cortical Impact Traumatic Brain Injury in Rodents. **Front Mol Neurosci**, 14, p. 753946, 2021.

KANG, G. Y.; BANG, J. Y.; CHOI, A. J.; YOON, J. *et al.* Exosomal proteins in the aqueous humor as novel biomarkers in patients with neovascular age-related macular degeneration. **J Proteome Res**, 13, n. 2, p. 581-595, Feb 07 2014.

KARIMI, N.; CVJETKOVIC, A.; JANG, S. C.; CRESCITELLI, R. *et al.* Detailed analysis of the plasma extracellular vesicle proteome after separation from lipoproteins. **Cell Mol Life Sci**, 75, n. 15, p. 2873-2886, Aug 2018.

KAWATA, K.; MITSUHASHI, M.; ALDRET, R. A Preliminary Report on Brain-Derived Extracellular Vesicle as Novel Blood Biomarkers for Sport-Related Concussions. **Front Neurol**, 9, p. 239, 2018.

KENNEY, K.; QU, B. X.; LAI, C.; DEVOTO, C. *et al.* Higher exosomal phosphorylated tau and total tau among veterans with combat-related repetitive chronic mild traumatic brain injury. **Brain Inj**, 32, n. 10, p. 1276-1284, 2018.

KERR, N. A.; DE RIVERO VACCARI, J. P.; ABBASSI, S.; KAUR, H. *et al.* Traumatic Brain Injury-Induced Acute Lung Injury: Evidence for Activation and Inhibition of a Neural-Respiratory-Inflammasome Axis. **J Neurotrauma**, 35, n. 17, p. 2067-2076, Sep 01 2018.

KHALIN, I.; JAMARI, N. L.; RAZAK, N. B.; HASAIN, Z. B. *et al.* A mouse model of weight-drop closed head injury: emphasis on cognitive and neurological deficiency. **Neural Regen Res**, 11, n. 4, p. 630-635, Apr 2016.

KILBAUGH, T. J.; LVOVA, M.; KARLSSON, M.; ZHANG, Z. *et al.* Peripheral Blood Mitochondrial DNA as a Biomarker of Cerebral Mitochondrial Dysfunction

following Traumatic Brain Injury in a Porcine Model. **PLoS One**, 10, n. 6, p. e0130927, 2015.

KINNUNEN, K. M.; GREENWOOD, R.; POWELL, J. H.; LEECH, R. *et al.* White matter damage and cognitive impairment after traumatic brain injury. **Brain**, 134, n. Pt 2, p. 449-463, Feb 2011.

KNAPP, S. **Glasgow Coma Scale**. 2020. Acesso em: 10/1/23.

KO, J.; HEMPHILL, M.; YANG, Z.; BEARD, K. *et al.* Multi-Dimensional Mapping of Brain-Derived Extracellular Vesicle MicroRNA Biomarker for Traumatic Brain Injury Diagnostics. **J Neurotrauma**, 37, n. 22, p. 2424-2434, Nov 15 2020.

KOBEISSY, F. H. Brain Neurotrauma: Molecular, Neuropsychological, and Rehabilitation Aspects. *In*, 2015.

KODAM, S. P.; ULLAH, M. Diagnostic and Therapeutic Potential of Extracellular Vesicles. **Technol Cancer Res Treat**, 20, p. 15330338211041203, 2021.

KONSTANTINIDOU, A.; MOUGIOS, V.; SIDOSSIS, L. S. Acute Exercise Alters the Levels of Human Saliva miRNAs Involved in Lipid Metabolism. **Int J Sports Med**, 37, n. 7, p. 584-588, Jun 2016.

KOROTKOV, A.; PUHAKKA, N.; GUPTA, S. D.; VUOKILA, N. *et al.* Increased expression of miR142 and miR155 in glial and immune cells after traumatic brain injury may contribute to neuroinflammation via astrocyte activation. **Brain Pathol**, 30, n. 5, p. 897-912, Sep 2020.

KORTHAUER, K.; KIMES, P. K.; DUVALLET, C.; REYES, A. *et al.* A practical guide to methods controlling false discoveries in computational biology. **Genome Biol**, 20, n. 1, p. 118, Jun 4 2019.

KOSTYUK, V. A.; POTAPOVICH, A. I. Mechanisms of the suppression of free radical overproduction by antioxidants. **Front Biosci (Elite Ed)**, 1, n. 1, p. 179-188, Jun 01 2009.

KOWAL, J.; TKACH, M.; THÉRY, C. Biogenesis and secretion of exosomes. **Curr Opin Cell Biol**, 29, p. 116-125, Aug 2014.

KROEMER, G.; GALLUZZI, L.; VANDENABEELE, P.; ABRAMS, J. *et al.* Classification of cell death: recommendations of the Nomenclature Committee on Cell Death 2009. **Cell Death Differ**, 16, n. 1, p. 3-11, Jan 2009.

KUHARIC, J.; GRABUSIC, K.; TOKMADZIC, V. S.; STIFTER, S. *et al.* Severe Traumatic Brain Injury Induces Early Changes in the Physical Properties and Protein Composition of Intracranial Extracellular Vesicles. **J Neurotrauma**, 36, n. 2, p. 190-200, Jan 15 2019.

KUMAR, A.; STOICA, B. A.; LOANE, D. J.; YANG, M. *et al.* Microglial-derived microparticles mediate neuroinflammation after traumatic brain injury. **J Neuroinflammation**, 14, n. 1, p. 47, Mar 15 2017.

KUMAR, A.; STOICA, B. A.; LOANE, D. J.; YANG, M. *et al.* Microglial-derived microparticles mediate neuroinflammation after traumatic brain injury. **J Neuroinflammation**, 14, n. 1, p. 47, Mar 15 2017.

KURIAKOSE, M.; SKOTAK, M.; MISISTIA, A.; KAHALI, S. *et al.* Tailoring the Blast Exposure Conditions in the Shock Tube for Generating Pure, Primary Shock Waves: The End Plate Facilitates Elimination of Secondary Loading of the Specimen. **PLoS One**, 11, n. 9, p. e0161597, 2016.

KURODA, T.; TANABE, N.; HASEGAWA, E.; WAKAMATSU, A. *et al.* Significant association between renal function and area of amyloid deposition in kidney biopsy specimens in both AA amyloidosis associated with rheumatoid arthritis and AL amyloidosis. **Amyloid**, 24, n. 2, p. 123-130, Jun 2017.

LAN, Y. L.; LI, S.; LOU, J. C.; MA, X. C. *et al.* The potential roles of dopamine in traumatic brain injury: a preclinical and clinical update. **Am J Transl Res**, 11, n. 5, p. 2616-2631, 2019.

LANE, R. E.; KORBIE, D.; HILL, M. M.; TRAU, M. Extracellular vesicles as circulating cancer biomarkers: opportunities and challenges. **Clin Transl Med**, 7, n. 1, p. 14, May 31 2018.

LEI, J.; GAO, G.; FENG, J.; JIN, Y. *et al.* Glial fibrillary acidic protein as a biomarker in severe traumatic brain injury patients: a prospective cohort study. **Crit Care**, 19, p. 362, Oct 12 2015.

LEVIN, H. S., SHUM, D., CHAN, R.C. Understanding traumatic brain injury: current research and future directions. New York (NY): Oxford University Press 2013.

LEWIS, R. G.; FLORIO, E.; PUNZO, D.; BORRELLI, E. The Brain's Reward System in Health and Disease. **Adv Exp Med Biol**, 1344, p. 57-69, 2021.

LI, D.; HUANG, S.; YIN, Z.; ZHU, J. *et al.* Increases in miR-124-3p in Microglial Exosomes Confer Neuroprotective Effects by Targeting FIP200-Mediated Neuronal Autophagy Following Traumatic Brain Injury. **Neurochem Res**, 44, n. 8, p. 1903-1923, Aug 2019.

LI, P.; NIJHAWAN, D.; BUDIARDJO, I.; SRINIVASULA, S. M. *et al.* Cytochrome c and dATP-dependent formation of Apaf-1/caspase-9 complex initiates an apoptotic protease cascade. **Cell**, 91, n. 4, p. 479-489, Nov 14 1997.

LI, Y.; SUN, M.; WANG, X.; CAO, X. *et al.* Dental stem cell-derived extracellular vesicles transfer miR-330-5p to treat traumatic brain injury by regulating microglia polarization. **Int J Oral Sci**, 14, n. 1, p. 44, Sep 05 2022.

LIAO, S.; CHEN, L.; SONG, Z.; HE, H. The fate of damaged mitochondrial DNA in the cell. **Biochim Biophys Acta Mol Cell Res**, 1869, n. 5, p. 119233, May 2022.

LINDQUIST, L. K.; LOVE, H. C.; ELBOGEN, E. B. Traumatic Brain Injury in Iraq and Afghanistan Veterans: New Results From a National Random Sample Study. **J Neuropsychiatry Clin Neurosci**, 29, n. 3, p. 254-259, 2017.

LIP, G. Y.; BLANN, A. von Willebrand factor: a marker of endothelial dysfunction in vascular disorders? **Cardiovasc Res**, 34, n. 2, p. 255-265, May 1997.

LONG, X.; YAO, X.; JIANG, Q.; YANG, Y. *et al.* Astrocyte-derived exosomes enriched with miR-873a-5p inhibit neuroinflammation via microglia phenotype modulation after traumatic brain injury. **J Neuroinflammation**, 17, n. 1, p. 89, Mar 19 2020.

LU, J.; YU, Y.; ZHU, I.; CHENG, Y. *et al.* Structural mechanism of serum amyloid A-mediated inflammatory amyloidosis. **Proc Natl Acad Sci U S A**, 111, n. 14, p. 5189-5194, Apr 08 2014.

LUEPTOW, L. M. Novel Object Recognition Test for the Investigation of Learning and Memory in Mice. **J Vis Exp**, n. 126, Aug 30 2017.

LYDIC, T. A.; TOWNSEND, S.; ADDA, C. G.; COLLINS, C. *et al.* Rapid and comprehensive 'shotgun' lipidome profiling of colorectal cancer cell derived exosomes. **Methods**, 87, p. 83-95, Oct 01 2015.

MAC DONALD, C. L.; JOHNSON, A. M.; WIERZECHOWSKI, L.; KASSNER, E. *et al.* Outcome Trends after US Military Concussive Traumatic Brain Injury. **J Neurotrauma**, 34, n. 14, p. 2206-2219, Jul 15 2017.

MANEK, R.; MOGHIEB, A.; YANG, Z.; KUMAR, D. *et al.* Protein Biomarkers and Neuroproteomics Characterization of Microvesicles/Exosomes from Human Cerebrospinal Fluid Following Traumatic Brain Injury. **Mol Neurobiol**, 55, n. 7, p. 6112-6128, Jul 2018.

MANUKONDA, R.; ATTEM, J.; YENUGANTI, V. R.; KALIKI, S. *et al.* Exosomes in the visual system: New avenues in ocular diseases. **Tumour Biol**, 44, n. 1, p. 129-152, 2022.

MARCATTI, M.; SAADA, J.; OKEREKE, I.; WADE, C. E. *et al.* Quantification of Circulating Cell Free Mitochondrial DNA in Extracellular Vesicles with PicoGreen in Liquid Biopsies: Fast Assessment of Disease/Trauma Severity. **Cells**, 10, n. 4, Apr 6 2021.

MARMAROU, A.; FODA, M. A.; VAN DEN BRINK, W.; CAMPBELL, J. *et al.* A new model of diffuse brain injury in rats. Part I: Pathophysiology and biomechanics. **J Neurosurg**, 80, n. 2, p. 291-300, Feb 1994.

MAROTO, R.; ZHAO, Y.; JAMALUDDIN, M.; POPOV, V. L. *et al.* Effects of storage temperature on airway exosome integrity for diagnostic and functional analyses. **J Extracell Vesicles**, 6, n. 1, p. 1359478, 2017.

MARTINDALE, S. L.; ORD, A. S.; RULE, L. G.; ROWLAND, J. A. Effects of blast exposure on psychiatric and health symptoms in combat veterans. **J Psychiatr Res**, 143, p. 189-195, Nov 2021.

MARTINEZ, B. I.; STABENFELDT, S. E. Current trends in biomarker discovery and analysis tools for traumatic brain injury. **J Biol Eng**, 13, p. 16, 2019.

MASEL, B. E.; DEWITT, D. S. Traumatic brain injury: a disease process, not an event. **J Neurotrauma**, 27, n. 8, p. 1529-1540, Aug 2010.

MCCOMBIE, W. R.; MCPHERSON, J. D.; MARDIS, E. R. Next-Generation Sequencing Technologies. **Cold Spring Harb Perspect Med**, 9, n. 11, Nov 01 2019.

MEHTA, D.; AHKAMI, A. H.; WALLEY, J.; XU, S. L. *et al.* The incongruity of validating quantitative proteomics using western blots. **Nat Plants**, 8, n. 12, p. 1320-1321, Dec 2022.

MELO, S. A.; LUECKE, L. B.; KAHLERT, C.; FERNANDEZ, A. F. *et al.* Glypican-1 identifies cancer exosomes and detects early pancreatic cancer. **Nature**, 523, n. 7559, p. 177-182, Jul 09 2015.

MICCI, M. A.; KRISHNAN, B.; BISHOP, E.; ZHANG, W. R. *et al.* Hippocampal stem cells promotes synaptic resistance to the dysfunctional impact of amyloid beta oligomers via secreted exosomes. **Mol Neurodegener**, 14, n. 1, p. 25, Jun 14 2019.

MLECZKO, A. M.; CELICHOWSKI, P.; BAŁKOWSKA-ŻYWICKA, K. Transfer RNA-derived fragments target and regulate ribosome-associated aminoacyl-transfer RNA synthetases. **Biochim Biophys Acta Gene Regul Mech**, Jun 06 2018.

MONDELLO, S.; GUEDES, V. A.; LAI, C.; CZEITER, E. *et al.* Circulating Brain Injury Exosomal Proteins following Moderate-To-Severe Traumatic Brain Injury: Temporal Profile, Outcome Prediction and Therapy Implications. **Cells**, 9, n. 4, Apr 15 2020.

MONDELLO, S.; SORINOLA, A.; CZEITER, E.; VAMOS, Z. *et al.* Blood-Based Protein Biomarkers for the Management of Traumatic Brain Injuries in Adults Presenting to Emergency Departments with Mild Brain Injury: A Living Systematic Review and Meta-Analysis. **J Neurotrauma**, Jul 2 2018.

MURPHY, D. E.; DE JONG, O. G.; BROUWER, M.; WOOD, M. J. *et al.* Extracellular vesicle-based therapeutics: natural versus engineered targeting and trafficking. **Exp Mol Med**, 51, n. 3, p. 1-12, Mar 15 2019.

MÖBIUS, W.; OHNO-IWASHITA, Y.; VAN DONSELAAR, E. G.; OORSCHOT, V. M. *et al.* Immunoelectron microscopic localization of cholesterol using

biotinylated and non-cytolytic perfringolysin O. **J Histochem Cytochem**, 50, n. 1, p. 43-55, Jan 2002.

NAJAFI, S.; MAJIDPOOR, J.; MORTEZAEI, K. Extracellular vesicle-based drug delivery in cancer immunotherapy. **Drug Deliv Transl Res**, 13, n. 11, p. 2790-2806, Nov 2023.

NATHAN, C.; CUNNINGHAM-BUSSEL, A. Beyond oxidative stress: an immunologist's guide to reactive oxygen species. **Nat Rev Immunol**, 13, n. 5, p. 349-361, May 2013.

NELL, V.; YATES, D. W.; KRUGER, J. An extended Glasgow Coma Scale (GCS-E) with enhanced sensitivity to mild brain injury. **Arch Phys Med Rehabil**, 81, n. 5, p. 614-617, May 2000.

NG, S. Y.; LEE, A. Y. W. Traumatic Brain Injuries: Pathophysiology and Potential Therapeutic Targets. **Front Cell Neurosci**, 13, p. 528, 2019.

NISHIMURA, K.; CORDEIRO, J. G.; AHMED, A. I.; YOKOBORI, S. *et al.* Advances in Traumatic Brain Injury Biomarkers. **Cureus**, 14, n. 4, p. e23804, Apr 2022.

NOLTE-'T HOEN, E. N.; BUERMANS, H. P.; WAASDORP, M.; STOOORVOGEL, W. *et al.* Deep sequencing of RNA from immune cell-derived vesicles uncovers the selective incorporation of small non-coding RNA biotypes with potential regulatory functions. **Nucleic Acids Res**, 40, n. 18, p. 9272-9285, Oct 2012.

NONAKA, T.; MASUDA-SUZUKAKE, M.; ARAI, T.; HASEGAWA, Y. *et al.* Prion-like properties of pathological TDP-43 aggregates from diseased brains. **Cell Rep**, 4, n. 1, p. 124-134, Jul 11 2013.

O'NEIL, M. E.; CARLSON, K.; STORZBACH, D.; BRENNER, L. *et al.* Complications of Mild Traumatic Brain Injury in Veterans and Military Personnel: A Systematic Review. *In*, 2013.

OHAYON, S.; BOYKO, M.; SAAD, A.; DOUVDEVANI, A. *et al.* Cell-free DNA as a marker for prediction of brain damage in traumatic brain injury in rats. **J Neurotrauma**, 29, n. 2, p. 261-267, Jan 20 2012.

OKONKWO, D. O.; YUE, J. K.; PUCCIO, A. M.; PANCZYKOWSKI, D. M. *et al.* GFAP-BDP as an acute diagnostic marker in traumatic brain injury: results from

the prospective transforming research and clinical knowledge in traumatic brain injury study. **J Neurotrauma**, 30, n. 17, p. 1490-1497, Sep 01 2013.

OSIER, N.; DIXON, C. E. The Controlled Cortical Impact Model of Experimental Brain Trauma: Overview, Research Applications, and Protocol. **Methods Mol Biol**, 1462, p. 177-192, 2016.

OSTROWSKI, M.; CARMO, N. B.; KRUMEICH, S.; FANGET, I. *et al.* Rab27a and Rab27b control different steps of the exosome secretion pathway. **Nat Cell Biol**, 12, n. 1, p. 19-30; sup pp 11-13, Jan 2010.

PADILLA, A.; MOAKE, J. L.; BERNARDO, A.; BALL, C. *et al.* P-selectin anchors newly released ultralarge von Willebrand factor multimers to the endothelial cell surface. **Blood**, 103, n. 6, p. 2150-2156, Mar 15 2004.

PAN, B. T.; TENG, K.; WU, C.; ADAM, M. *et al.* Electron microscopic evidence for externalization of the transferrin receptor in vesicular form in sheep reticulocytes. **J Cell Biol**, 101, n. 3, p. 942-948, Sep 1985.

PELTZ, C. B.; KENNEY, K.; GILL, J.; DIAZ-ARRASTIA, R. *et al.* Blood biomarkers of traumatic brain injury and cognitive impairment in older veterans. **Neurology**, 95, n. 9, p. e1126-e1133, Sep 1 2020.

PERETS, N.; HERTZ, S.; LONDON, M.; OFFEN, D. Intranasal administration of exosomes derived from mesenchymal stem cells ameliorates autistic-like behaviors of BTBR mice. **Mol Autism**, 9, p. 57, 2018.

PESONEN, A.; BEN-HAMOUDA, N.; SCHNEIDER, A. Acute kidney injury after brain injury: does it exist? **Minerva Anestesiol**, 87, n. 7, p. 823-827, Jul 2021.

PHAM LE KHANH, H.; NEMES, D.; RUSZNYÁK, Á.; UJHELYI, Z. *et al.* Comparative Investigation of Cellular Effects of Polyethylene Glycol (PEG) Derivatives. **Polymers (Basel)**, 14, n. 2, Jan 11 2022.

PREVENTION, C. F. D. C. A. **TBI: Get the facts.** 2019a. Acesso em: 8/28/23.

PREVENTION, C. F. D. C. A. **TBI: Potential effects.**, 2019b. Acesso em: 8/28/23.

PREVENTION, C. F. D. C. A. **What is a concussion?** , 2019c. Acesso em: 8/28/23.

PREVENTION, C. F. D. C. A. **Injury prevention and control: traumatic brain injury and concussion.** 2020. Acesso em: 8/28/23.

PRINZ, M.; PRILLER, J.; SISODIA, S. S.; RANSOHOFF, R. M. Heterogeneity of CNS myeloid cells and their roles in neurodegeneration. **Nat Neurosci**, 14, n. 10, p. 1227-1235, Sep 27 2011.

PUFFER, R. C.; CUMBA GARCIA, L. M.; HIMES, B. T.; JUNG, M. Y. *et al.* Plasma extracellular vesicles as a source of biomarkers in traumatic brain injury. **J Neurosurg**, 134, n. 6, p. 1921-1928, Jul 24 2020.

RAGHAV, A.; ASHRAF, H.; JEONG, G. B. Engineered Extracellular Vesicles in Treatment of Type 1 Diabetes Mellitus: A Prospective Review. **Biomedicines**, 10, n. 12, Nov 25 2022.

RAGHAV, A.; JEONG, G. B. A systematic review on the modifications of extracellular vesicles: a revolutionized tool of nano-biotechnology. **J Nanobiotechnology**, 19, n. 1, p. 459, Dec 30 2021.

RAGHAV, A.; SINGH, M.; JEONG, G. B.; GIRI, R. *et al.* Extracellular vesicles in neurodegenerative diseases: A systematic review. **Front Mol Neurosci**, 15, p. 1061076, 2022.

RAIBORG, C.; STENMARK, H. The ESCRT machinery in endosomal sorting of ubiquitylated membrane proteins. **Nature**, 458, n. 7237, p. 445-452, Mar 26 2009.

RAJENDRAN, L.; HONSHO, M.; ZAHN, T. R.; KELLER, P. *et al.* Alzheimer's disease beta-amyloid peptides are released in association with exosomes. **Proc Natl Acad Sci U S A**, 103, n. 30, p. 11172-11177, Jul 25 2006.

RAPOSO, G.; STOORVOGEL, W. Extracellular vesicles: exosomes, microvesicles, and friends. **J Cell Biol**, 200, n. 4, p. 373-383, Feb 18 2013.

RATAJCZAK, J.; MIEKUS, K.; KUCIA, M.; ZHANG, J. *et al.* Embryonic stem cell-derived microvesicles reprogram hematopoietic progenitors: evidence for horizontal transfer of mRNA and protein delivery. **Leukemia**, 20, n. 5, p. 847-856, May 2006.

RISDALL, J. E.; MENON, D. K. Traumatic brain injury. **Philos Trans R Soc Lond B Biol Sci**, 366, n. 1562, p. 241-250, Jan 27 2011.

ROME, S. Use of miRNAs in biofluids as biomarkers in dietary and lifestyle intervention studies. **Genes Nutr**, 10, n. 5, p. 483, Sep 2015.

ROMINE, J.; GAO, X.; CHEN, J. Controlled cortical impact model for traumatic brain injury. **J Vis Exp**, n. 90, p. e51781, Aug 05 2014.

SAADA, J.; MCAULEY, R. J.; MARCATTI, M.; TANG, T. Z. *et al.* Oxidative stress induces Z-DNA-binding protein 1-dependent activation of microglia via mtDNA released from retinal pigment epithelial cells. **J Biol Chem**, 298, n. 1, p. 101523, Jan 2022.

SACK, G. H., JR. Serum amyloid A - a review. **Mol Med**, 24, n. 1, p. 46, Aug 30 2018.

SALMINEN, L. E.; PAUL, R. H. Oxidative stress and genetic markers of suboptimal antioxidant defense in the aging brain: a theoretical review. **Rev Neurosci**, 25, n. 6, p. 805-819, 2014.

SAMAN, S.; KIM, W.; RAYA, M.; VISNICK, Y. *et al.* Exosome-associated tau is secreted in tauopathy models and is selectively phosphorylated in cerebrospinal fluid in early Alzheimer disease. **J Biol Chem**, 287, n. 6, p. 3842-3849, Feb 03 2012.

SAVINA, A.; VIDAL, M.; COLOMBO, M. I. The exosome pathway in K562 cells is regulated by Rab11. **J Cell Sci**, 115, n. Pt 12, p. 2505-2515, Jun 15 2002.

SCHNEIDER, A.; SIMONS, M. Exosomes: vesicular carriers for intercellular communication in neurodegenerative disorders. **Cell Tissue Res**, 352, n. 1, p. 33-47, Apr 2013.

SCOTLAND, N. **Scottish Acquired Brain Injury Network**. 2023. Acesso em: 9/1/23.

SHINODA, J.; YANO, H.; NAKAYAMA, N. Altered biphasic serotonin discharge hypothesis in mild traumatic brain injury. **Concussion**, 6, n. 3, p. CNC94, Sep 2021.

SIMON, D. W.; MCGEACHY, M. J.; BAYIR, H.; CLARK, R. S. B. *et al.* The far-reaching scope of neuroinflammation after traumatic brain injury. **Nat Rev Neurol**, 13, n. 9, p. 572, Sep 2017.

SINAI, C. **CT Brain with or without contrast**. 2023. Acesso em: 10/1/23.

SKOTLAND, T.; HESSVIK, N. P.; SANDVIG, K.; LLORENTE, A. Exosomal lipid composition and the role of ether lipids and phosphoinositides in exosome biology. **J Lipid Res**, 60, n. 1, p. 9-18, Jan 2019.

SKOTLAND, T.; SANDVIG, K.; LLORENTE, A. Lipids in exosomes: Current knowledge and the way forward. **Prog Lipid Res**, 66, p. 30-41, Apr 2017.

SMITH-BINDMAN, R.; MIGLIORETTI, D. L.; JOHNSON, E.; LEE, C. *et al.* Use of diagnostic imaging studies and associated radiation exposure for patients enrolled in large integrated health care systems, 1996-2010. **JAMA**, 307, n. 22, p. 2400-2409, Jun 13 2012.

STANTON, C. M.; YATES, J. R.; DEN HOLLANDER, A. I.; SEDDON, J. M. *et al.* Complement factor D in age-related macular degeneration. **Invest Ophthalmol Vis Sci**, 52, n. 12, p. 8828-8834, Nov 11 2011.

STOLER, D. D. R. **Dr. Diane Brain Health**. 2021. Acesso em: 9/3/23.

STROKE, N. I. O. N. D. A. **Traumatic brain injury: Hope through research**. 2020. Acesso em: 9/3/23.

STÅHL, A. L.; JOHANSSON, K.; MOSSBERG, M.; KAHN, R. *et al.* Exosomes and microvesicles in normal physiology, pathophysiology, and renal diseases. **Pediatr Nephrol**, 34, n. 1, p. 11-30, Jan 2019.

SUBRA, C.; LAULAGNIER, K.; PERRET, B.; RECORD, M. Exosome lipidomics unravels lipid sorting at the level of multivesicular bodies. **Biochimie**, 89, n. 2, p. 205-212, Feb 2007.

SZKLARCZYK, D.; GABLE, A. L.; LYON, D.; JUNGE, A. *et al.* STRING v11: protein-protein association networks with increased coverage, supporting functional discovery in genome-wide experimental datasets. **Nucleic Acids Res**, 47, n. D1, p. D607-D613, Jan 8 2019.

TABER, K. H.; WARDEN, D. L.; HURLEY, R. A. Blast-related traumatic brain injury: what is known? **J Neuropsychiatry Clin Neurosci**, 18, n. 2, p. 141-145, 2006.

TAKAHASHI, A.; OKADA, R.; NAGAO, K.; KAWAMATA, Y. *et al.* Exosomes maintain cellular homeostasis by excreting harmful DNA from cells. **Nat Commun**, 8, p. 15287, May 16 2017.

TAO, L.; ZHOU, J.; YUAN, C.; ZHANG, L. *et al.* Metabolomics identifies serum and exosomes metabolite markers of pancreatic cancer. **Metabolomics**, 15, n. 6, p. 86, May 30 2019.

TAYLOR, R. C.; CULLEN, S. P.; MARTIN, S. J. Apoptosis: controlled demolition at the cellular level. **Nat Rev Mol Cell Biol**, 9, n. 3, p. 231-241, Mar 2008.

THAKUR, B. K.; ZHANG, H.; BECKER, A.; MATEI, I. *et al.* Double-stranded DNA in exosomes: a novel biomarker in cancer detection. **Cell Res**, 24, n. 6, p. 766-769, Jun 2014.

THARMARATNAM, T.; ISKANDAR, M. A.; TABOBONDUNG, T. C.; TOBBIA, I. *et al.* Chronic Traumatic Encephalopathy in Professional American Football Players: Where Are We Now? **Front Neurol**, 9, p. 445, 2018.

THELIN, E. P.; ZEILER, F. A.; ERCOLE, A.; MONDELLO, S. *et al.* Serial Sampling of Serum Protein Biomarkers for Monitoring Human Traumatic Brain Injury Dynamics: A Systematic Review. **Front Neurol**, 8, p. 300, 2017.

THERY, C.; WITWER, K. W.; AIKAWA, E.; ALCARAZ, M. J. *et al.* Minimal information for studies of extracellular vesicles 2018 (MISEV2018): a position statement of the International Society for Extracellular Vesicles and update of the MISEV2014 guidelines. **J Extracell Vesicles**, 7, n. 1, p. 1535750, 2018.

THÉRY, C.; AMIGORENA, S.; RAPOSO, G.; CLAYTON, A. Isolation and characterization of exosomes from cell culture supernatants and biological fluids. **Curr Protoc Cell Biol**, Chapter 3, p. Unit 3.22, Apr 2006.

THÉRY, C.; WITWER, K. W.; AIKAWA, E.; ALCARAZ, M. J. *et al.* Minimal information for studies of extracellular vesicles 2018 (MISEV2018): a position statement of the International Society for Extracellular Vesicles and update of the MISEV2014 guidelines. **J Extracell Vesicles**, 7, n. 1, p. 1535750, 2018.

TIAN, Y.; SALSBERY, B.; WANG, M.; YUAN, H. *et al.* Brain-derived microparticles induce systemic coagulation in a murine model of traumatic brain injury. **Blood**, 125, n. 13, p. 2151-2159, Mar 26 2015.

TOSAR, J. P.; GÁMBARO, F.; SANGUINETTI, J.; BONILLA, B. *et al.* Assessment of small RNA sorting into different extracellular fractions revealed by high-throughput sequencing of breast cell lines. **Nucleic Acids Res**, 43, n. 11, p. 5601-5616, Jun 23 2015.

TRAJKOVIC, K.; HSU, C.; CHIANTIA, S.; RAJENDRAN, L. *et al.* Ceramide triggers budding of exosome vesicles into multivesicular endosomes. **Science**, 319, n. 5867, p. 1244-1247, Feb 29 2008.

TRAMS, E. G.; LAUTER, C. J.; SALEM, N.; HEINE, U. Exfoliation of membrane ecto-enzymes in the form of micro-vesicles. **Biochim Biophys Acta**, 645, n. 1, p. 63-70, Jul 06 1981.

TSENER, J.; BENI-ADANI, L.; ASSAF, Y.; ALEXANDROVICH, A. G. *et al.* Dynamic changes in the recovery after traumatic brain injury in mice: effect of injury severity on T2-weighted MRI abnormalities, and motor and cognitive functions. **J Neurotrauma**, 25, n. 4, p. 324-333, Apr 2008.

TURCHINOVICH, A.; DRAPKINA, O.; TONEVITSKY, A. Transcriptome of Extracellular Vesicles: State-of-the-Art. **Front Immunol**, 10, p. 202, 2019.

TYANOVA, S.; TEMU, T.; SINITCYN, P.; CARLSON, A. *et al.* The Perseus computational platform for comprehensive analysis of (prote)omics data. **Nat Methods**, 13, n. 9, p. 731-740, Sep 2016.

VALADI, H.; EKSTRÖM, K.; BOSSIOS, A.; SJÖSTRAND, M. *et al.* Exosome-mediated transfer of mRNAs and microRNAs is a novel mechanism of genetic exchange between cells. **Nat Cell Biol**, 9, n. 6, p. 654-659, Jun 2007.

VAN BREGT, D. R.; THOMAS, T. C.; HINZMAN, J. M.; CAO, T. *et al.* Substantia nigra vulnerability after a single moderate diffuse brain injury in the rat. **Exp Neurol**, 234, n. 1, p. 8-19, Mar 2012.

VAN NIEL, G.; D'ANGELO, G.; RAPOSO, G. Shedding light on the cell biology of extracellular vesicles. **Nat Rev Mol Cell Biol**, 19, n. 4, p. 213-228, Apr 2018.

VANDER HEIDEN, M. G.; CANTLEY, L. C.; THOMPSON, C. B. Understanding the Warburg effect: the metabolic requirements of cell proliferation. **Science**, 324, n. 5930, p. 1029-1033, May 22 2009.

VEZIROGLU, E. M.; MIAS, G. I. Characterizing Extracellular Vesicles and Their Diverse RNA Contents. **Front Genet**, 11, p. 700, 2020.

VLAHOS NICHOLAS, T. R. **TBI by Pattern: Penetrating, Nonpenetrating, and Blast Injury**. Elsevier, 2021. (*Brain Injury Medicine*).

VORHEES, C. V.; WILLIAMS, M. T. Morris water maze: procedures for assessing spatial and related forms of learning and memory. **Nat Protoc**, 1, n. 2, p. 848-858, 2006.

WALKO, T. D., 3RD; BOLA, R. A.; HONG, J. D.; AU, A. K. *et al*. Cerebrospinal fluid mitochondrial DNA: a novel DAMP in pediatric traumatic brain injury. **Shock**, 41, n. 6, p. 499-503, Jun 2014.

WANG, J.; XIE, X.; WU, Y.; ZHOU, Y. *et al*. Brain-Derived Extracellular Vesicles Induce Vasoconstriction and Reduce Cerebral Blood Flow in Mice. **J Neurotrauma**, 39, n. 11-12, p. 879-890, Jun 2022.

WANG, S.; CESCO, F.; LOERS, G.; SCHWEIZER, M. *et al*. Synapsin I is an oligomannose-carrying glycoprotein, acts as an oligomannose-binding lectin, and promotes neurite outgrowth and neuronal survival when released via glia-derived exosomes. **J Neurosci**, 31, n. 20, p. 7275-7290, May 18 2011.

WEBER, J. A.; BAXTER, D. H.; ZHANG, S.; HUANG, D. Y. *et al*. The microRNA spectrum in 12 body fluids. **Clin Chem**, 56, n. 11, p. 1733-1741, Nov 2010.

WEI, Z.; BATAGOV, A. O.; SCHINELLI, S.; WANG, J. *et al*. Coding and noncoding landscape of extracellular RNA released by human glioma stem cells. **Nat Commun**, 8, n. 1, p. 1145, Oct 26 2017.

WHITHAM, M.; PARKER, B. L.; FRIEDRICHSEN, M.; HINGST, J. R. *et al*. Extracellular Vesicles Provide a Means for Tissue Crosstalk during Exercise. **Cell Metab**, 27, n. 1, p. 237-251.e234, Jan 09 2018.

WICKER, E.; BENTON, L.; GEORGE, K.; FURLOW, W. *et al*. Serum Amyloid A Protein as a Potential Biomarker for Severity and Acute Outcome in Traumatic Brain Injury. **Biomed Res Int**, 2019, p. 5967816, 2019.

WIKIPEDIA. **Magnetic resonance imaging of the brain**. 2023. Acesso em: 10/1/23.

WINSTON, C. N.; ROMERO, H. K.; ELLISMAN, M.; NAUSS, S. *et al.* Assessing Neuronal and Astrocyte Derived Exosomes From Individuals With Mild Traumatic Brain Injury for Markers of Neurodegeneration and Cytotoxic Activity. **Front Neurosci**, 13, p. 1005, 2019.

WITWER, K. W.; GOBERDHAN, D. C.; O'DRISCOLL, L.; THERY, C. *et al.* Updating MISEV: Evolving the minimal requirements for studies of extracellular vesicles. **J Extracell Vesicles**, 10, n. 14, p. e12182, Dec 2021.

WOLF, P. The nature and significance of platelet products in human plasma. **Br J Haematol**, 13, n. 3, p. 269-288, May 1967.

WONG, C. M.; WONG, K. H.; CHEN, X. D. Glucose oxidase: natural occurrence, function, properties and industrial applications. **Appl Microbiol Biotechnol**, 78, n. 6, p. 927-938, Apr 2008.

WU, Y.; LIU, W.; ZHOU, Y.; HILTON, T. *et al.* von Willebrand factor enhances microvesicle-induced vascular leakage and coagulopathy in mice with traumatic brain injury. **Blood**, 132, n. 10, p. 1075-1084, Sep 06 2018.

WUBBOLTS, R.; LECKIE, R. S.; VEENHUIZEN, P. T.; SCHWARZMANN, G. *et al.* Proteomic and biochemical analyses of human B cell-derived exosomes. Potential implications for their function and multivesicular body formation. **J Biol Chem**, 278, n. 13, p. 10963-10972, Mar 28 2003.

XIN, H.; LI, Y.; CUI, Y.; YANG, J. J. *et al.* Systemic administration of exosomes released from mesenchymal stromal cells promote functional recovery and neurovascular plasticity after stroke in rats. **J Cereb Blood Flow Metab**, 33, n. 11, p. 1711-1715, Nov 2013.

XIONG, Y.; MAHMOOD, A.; CHOPP, M. Emerging treatments for traumatic brain injury. **Expert Opin Emerg Drugs**, 14, n. 1, p. 67-84, Mar 2009.

XIONG, Y.; MAHMOOD, A.; CHOPP, M. Animal models of traumatic brain injury. **Nat Rev Neurosci**, 14, n. 2, p. 128-142, Feb 2013.

YANG, D.; ZHANG, W.; ZHANG, H.; ZHANG, F. *et al.* Progress, opportunity, and perspective on exosome isolation - efforts for efficient exosome-based theranostics. **Theranostics**, 10, n. 8, p. 3684-3707, 2020.

YANG, Q.; XU, J.; GU, J.; SHI, H. *et al.* Extracellular Vesicles in Cancer Drug Resistance: Roles, Mechanisms, and Implications. **Adv Sci (Weinh)**, 9, n. 34, p. e2201609, Dec 2022.

YANG, Y.; YE, Y.; KONG, C.; SU, X. *et al.* MiR-124 Enriched Exosomes Promoted the M2 Polarization of Microglia and Enhanced Hippocampus Neurogenesis After Traumatic Brain Injury by Inhibiting TLR4 Pathway. **Neurochem Res**, 44, n. 4, p. 811-828, Apr 2019.

YIN, Z.; HAN, Z.; HU, T.; ZHANG, S. *et al.* Neuron-derived exosomes with high miR-21-5p expression promoted polarization of M1 microglia in culture. **Brain Behav Immun**, 83, p. 270-282, Jan 2020.

YÁÑEZ-MÓ, M.; SILJANDER, P. R.; ANDREU, Z.; ZAVEC, A. B. *et al.* Biological properties of extracellular vesicles and their physiological functions. **J Extracell Vesicles**, 4, p. 27066, 2015.

ZETTERBERG, H.; SMITH, D. H.; BLENNOW, K. Biomarkers of mild traumatic brain injury in cerebrospinal fluid and blood. **Nat Rev Neurol**, 9, n. 4, p. 201-210, Apr 2013.

ZHANG, Y.; CHOPP, M.; MENG, Y.; KATAKOWSKI, M. *et al.* Effect of exosomes derived from multipotent mesenchymal stromal cells on functional recovery and neurovascular plasticity in rats after traumatic brain injury. **J Neurosurg**, 122, n. 4, p. 856-867, Apr 2015.

ZHANG, Z. G.; BULLER, B.; CHOPP, M. Exosomes - beyond stem cells for restorative therapy in stroke and neurological injury. **Nat Rev Neurol**, 15, n. 4, p. 193-203, Apr 2019.

ZHAO, H.; YANG, L.; BADDOUR, J.; ACHREJA, A. *et al.* Tumor microenvironment derived exosomes pleiotropically modulate cancer cell metabolism. **Elife**, 5, p. e10250, Feb 27 2016.

ZHAO, Y.; JAMALUDDIN, M.; ZHANG, Y.; SUN, H. *et al.* Systematic Analysis of Cell-Type Differences in the Epithelial Secretome Reveals Insights into the

Pathogenesis of Respiratory Syncytial Virus-Induced Lower Respiratory Tract Infections. **J Immunol**, 198, n. 8, p. 3345-3364, Apr 15 2017.

ZHAO, Y.; TIAN, B.; SUN, H.; ZHANG, J. *et al.* Pharmacoproteomics reveal novel protective activity of bromodomain containing 4 inhibitors on vascular homeostasis in TLR3-mediated airway remodeling. **J Proteomics**, 205, p. 103415, Aug 15 2019.

ZHAO, Z.; WANG, M.; TIAN, Y.; HILTON, T. *et al.* Cardiolipin-mediated procoagulant activity of mitochondria contributes to traumatic brain injury-associated coagulopathy in mice. **Blood**, 127, n. 22, p. 2763-2772, Jun 02 2016.

ZHAO, Z.; ZHOU, Y.; TIAN, Y.; LI, M. *et al.* Cellular microparticles and pathophysiology of traumatic brain injury. **Protein Cell**, 8, n. 11, p. 801-810, Nov 2017.

ZHENG, W.; LIU, A.; XIA, N.; CHEN, N. *et al.* How the Innate Immune DNA Sensing cGAS-STING Pathway Is Involved in Apoptosis. **Int J Mol Sci**, 24, n. 3, Feb 03 2023.

ZHOU, Y.; DANBOLT, N. C. Glutamate as a neurotransmitter in the healthy brain. **J Neural Transm (Vienna)**, 121, n. 8, p. 799-817, Aug 2014.

Vita

Tony Zifeng Tang is a highly motivated and skilled professional with 10+ years of scientific training. He is an expert neuroscientist with a strong background in biomarker discovery and validation, extracellular vesicles, experimental design, data analysis and presentation. Tony is a driven scientist seeking breakthrough into the biotech and pharmaceutical industry space focusing on drug development and clinical trials after graduating from the University of Texas Medical Branch at Galveston

Tony received his Bachelor of Science in Microbiology from the University of California at Davis in 2012. After working for 3 years for Bayer CropScience in West Sacramento, California, he decided to pursue higher education by moving to Oklahoma State University for a Master's in Science degree in Nutritional Sciences, graduating in 2017. It was at Stillwater where Tony was first exposure to neuroscience research. With a new interest in neuroscience, he decided to apply for UTMB's graduate program and was accepted in 2019.

In his PhD training, Tony earned a perfect 4.0 GPA with numerous internal and external awards each year, highlighted by winning UTMB Department of Neurobiology's top prize of the Fisher Award for Excellence in Neuroscience. Furthermore, he has contributed to several publications along with multiple poster and oral presentations across various conferences.

Tony earned his PhD in Neuroscience from UTMB in February 2024. This dissertation was prepared by Tony (Zifeng) Tang.